Università degli Studi di Napoli Federico II

DEPARTMENT OF CHEMICAL, MATERIALS, AND INDUSTRIAL PRODUCTION ENGINEERING

(DICMAPI)

PHD IN INDUSTRIAL PRODUCTS AND PROCESSES ENGINEERING

XXXVI CYCLE

An immunocompetent 3D-Human Dermal Equivalent model to unravel the complexities of wound healing and scar formation

Supervisor

Prof. Paolo Antonio Netti

Coordinator

Prof. Andrea D'Anna

Advisors

Dr. Giorgia Imparato

Prof. Francesco Urciuolo

Dr. Costantino Casale

PhD student Roberta Passariello

2020/2024

Table of Contents

List of Figures and Tables

Acronyms list (alphabetic order)

Abbreviation	Expanded form
ANOVA	Analysis of variance
BSA	Bovine Serum Albumin
CAD	Computer-Aided Design
CAM	Computer-Aided Manufacturing
COI	Collagen Orientation Index
CS	Chondroitin Sulphate
CT	Closure Time
CTF	Corrected Total Fluorescence
DAMPs	Damage-Associated Molecular Patterns
DAPI	4' 6-DiAmidino-2-PhenylIndole
DED	Decellularized Dermis
DS	Dermatan Sulphate
ECM	Extracellular Matrix
EDA	Extra Domain A
EDTA	Ethylenediaminetetraacetic Acid
EGF	Epidermal Growth Factor
ELISA	Enzyme-Linked Immunosorbent Assay
E-MEM	Eagle's BSS Minimum Essential Medium
FBS	Fetal Bovine Serum
FFT	Fast Fourier Transform
FGF	Fibroblast Growth Factor
GAG	Glycosaminoglycan
H&E	Haematoxylin and Eosin
HA	Hyaluronic Acid
HD-µTP	Human Dermal Microtissue Precursor
HDE	Human Dermal Equivalent
HDF	Human Dermal Fibroblast
HEPES	4-(2-hydroxyethyl)-1-piperazineethanesulfonic acid
HSE	Human Skin Equivalent
IFN-γ	Interferon-gamma
IGF	Insulin-like Growth Factor
IL	Interleukin
KGF	Keratinocyte Growth Factor
LMWHA	Low Molecular Weight fragments of HA
$MgCl_2$	Magnesium Chloride
MMP	Matrix Metalloproteinase
NETs	Neutrophil Extracellular Traps
O/W/O	Oil/Water/Oil
OsO_4	Osmium tetroxide
PBS	Phosphate Buffered Saline
PDGF	Platelet-Derived Growth Factor

PDMS	Polydimethylsiloxane
PIV	Particle Image Velocimetry
PMA	Phorbol 12-Myristate 13-Acetate
PMMA	Poly(Methyl Methacrylate)
ROI	Region Of Interest
ROS	Reactive Oxygen Species
RPMI	Roswell Park Memorial Institute Medium
RT	Room Temperature
SEM	Standard Error of the Mean (in Statistical Analysis)
SEM	Scanning Electron Microscopy
SHG	Second Harmonic Generation
STAT6	Signal Transducers and Activators of Transcription 6
TFM	Traction Force Microscopy
TGF-β	Transforming Growth Factor-beta
TH1	T-Helper cell type 1
TH2	T-Helper cell type 2
TIMP	Tissue Inhibitor of Metalloproteinase
TNF-α	Tumour Necrosis factor-alpha
UV	Ultraviolet
VEGF	Vascular Endothelial Growth Factor
vWF	von Willebrand Factor
α-SMA	alpha-Smooth Muscle Actin

Abstract

The skin isolates and protects the body from external agents, and in case of injury, it initiates a natural biological phenomenon, known as wound healing, during which the body blocks the bleeding, heals, and closes the wound. The damaged tissue is then rebuilt, and the injury is repaired.

It is during the repair process of such injuries that the mechanism of formation of a crippling scar occurs. In this phase, it may occur that the fibrous connective tissue, which fills empty spaces, follows the pattern of the tissue but in a disorganized way and loses elasticity. Fibrotic tissue formation is characterized by excessive growth and hardening of various tissues due to the disproportionate deposition of components of the ECM, especially type I collagen. Of the latter, a microscopically reticulated network is created, which not only causes a mechanical restriction, but also the thickened tissue is weak and hypoxic[1].

The diversity of the lesion produces different scars. Some are not even noticeable and do not cause discomfort, while others can be painful, unsightly, real disfigurements, and therefore disabling to the point of causing relational problems, especially if they affect the face[2–5]. Other scars can create movement limitations and adhesions[6].

The entire biological complex process is strongly influenced and regulated by the inflammatory response triggered by both tissue-resident and circulating cells of the immune system[7]. Although inflammation occurs almost immediately after the injury, this strictly regulates the final stages of healing. In particular, the mediators released by M2 macrophages stimulate fibroblasts towards the production of scar tissue and, consequently, give shape to the final repair result[8].

Hence, the manipulation of immune elements emerges as an appealing strategy in the field of regenerative medicine, as the widespread efficacy of stem cell and growth factor interventions in clinical settings remains to be conclusively demonstrated.

To accomplish these tasks, this study employs innovative 3D-HDE models to delve into the detailed mechanisms of wound healing and scar formation. By producing controlled injuries in these models, we aim to comprehensively analyse cellular

responses and ECM dynamics during the wound closure process. The focus is on understanding the intricate interplay between fibroblasts and the ECM, crucial for guiding the wound repair process. Additionally, our investigation extends to exploring microenvironmental changes and matrix remodelling in response to simulated immunocompetence, emphasizing the integration of endogenous matrices with immune system components, especially M2 macrophages. Our research has demonstrated that the 3D-HDE models replicate some aspects of the complexity of the human dermis, offering a valuable platform for simulating and studying wound healing and scar formation processes. The comprehensive analysis of cellular and matrix-level interactions has allowed us to identify the specific molecular and cellular events that lead to the formation of scars.

Chapter 1: Introduction

1.1 Context and Motivations of the Research

Wounds and scar formation represent complex biological processes of considerable scientific and clinical interest. An in-depth understanding of such phenomena is crucial, as they can have a significant impact on the physical and emotional well-being of people, especially in the case of severe or deforming injuries.

Wound healing is an intricate biological process aimed at restoring the structure and functionality of damaged tissue. This mechanism involves a variety of cells, cytokines, growth factors, and other elements that interact to restore the architecture of the injured site[9]. Fibroblasts, as crucial stromal cells, play a key role in the production of a new ECM, replacing the damaged one and thus facilitating the healing process[10]. These cells, in response to stimuli, move in a coordinated and massive way[11], contributing to the synthesis and the remodelling of the matrix. Simultaneously, the ECM influences the motility and directionality of cells in response to deformation gradients, highlighting a dynamic of reciprocal interaction between fibroblasts and ECM[12].

In addition, in the context of wound healing, the immune system plays a fundamental role, orchestrating molecular and cellular responses that modulate the fate of scarring. The immune response is triggered by the loss of tissue barrier, with the involvement of cells such as neutrophils, lymphocytes and macrophages that act in the removal of cellular debris and the prevention of infections[7]. Macrophages of type M2, with their ability to modulate inflammation and promote ECM synthesis, play a key role in defining the outcome of scarring[13].

Scar formation is a common result of this process and occurs when the normal healing process is impaired, leading to tissue composition and function that differ significantly from the surrounding tissue. It represents a quick and adaptive compromise to repair the tissue but often at the expense of its original structure and function. Although a natural response to wound healing, scarring can result in several problems that go beyond the aesthetic aspect. Hypertrophic scars, keloids or other complications can cause pain, functional limitations, and psychological impacts[14].

Among the organs to be examined to deepen the understanding of these processes, the skin, particularly the dermis, emerges as a subject of particular interest to researchers. The skin, the largest organ of the body, plays a critical role in protecting it from the external environment. The dermis, the skin layer that contains most of the cells and the ECM involved in the formation of scars, is a fundamental focus of the investigation.

An in-depth understanding of wound healing processes and scar formation is imperative to improve existing therapeutic strategies and develop new modes of intervention. The deepening of these mechanisms will provide a stronger scientific basis to address scar issues, improving the quality of life of patients and reducing associated clinical burdens. Strengthening the molecular and cellular understanding of how the immune system, especially M2 macrophages, affects the fate of scarring is crucial to developing more precise and effective therapeutic strategies.

Conventional models[15] used in the study of wound healing have inherent limitations, often resulting from their inability to fully recreate the tissue microenvironment *in vivo*. Models based on cell cultures or animals may lack representativeness, especially with respect to endogenous interactions crucial to the healing process.

In this context, tissue engineering, which uses cells grown within three-dimensional scaffolds, reduces the gap between flat cell cultures and physiological tissues and preserves tissue-specific differentiated phenotype. These exogenous matrices are valuable tools for conducting rapid studies of phenomena that occur during the closing process but, at the same time, do not completely replicate the native context.

In contrast, the adoption of endogenous models, based on matrices self-produced by the same cells, offers a unique opportunity to study physiological dynamics more accurately, strengthening the validity and clinical relevance of observations.

Compared to exogenous matrices, the model based on the use of an endogenous ECM revealed the ability to replicate *in vitro* crucial phenomena related to ECM functions such as morphogenesis, neo-synthesis and assembly of the ECM or modification of the architecture of the ECM during a pathological state.

1.2 Objectives of the Thesis

This research aims to comprehensively explore the wound healing processes and scar formation, employing an innovative approach based on a three-dimensional endogenous model of HDE.

The primary objectives of the thesis are twofold.

Firstly, the intent is to conduct a thorough analysis of the healing dynamics in a 3D-HDE after a secondary healing wound. This involves the investigation of cellular responses and ECM synthesis during the wound closure process. The wound is induced at the centre of the 3D-HDE tissue using a punch biopsy, allowing the monitoring of the healing process over time. A crucial focus is placed on the interaction between fibroblasts and the ECM, recognizing the fundamental role of this interaction in guiding the wound repair process. The analysis extends to the migration of fibroblasts at the wound closure, examining their directionality and cooperative motility in response to common stimuli. Additionally, it is evaluated how the dynamics of ECM remodelling directly influence the direction and speed of *en mass* migration of fibroblasts. Activation of fibroblasts and the reconstruction of the ECM, with the transition to myofibroblasts and the expression of key proteins such as α-SMA, fibronectin, tenascin-C, and collagen, are fundamental elements of the research.

Secondly, the research focuses on microenvironmental changes and matrix remodelling in a 3D-HDE in response to simulated immunocompetence. The importance of endogenous matrices integrated with macrophages in scar formation is thoroughly explored. Through detailed research, the integration of endogenous matrices with the immune system, particularly M2 macrophages, is examined, highlighting their crucial role in modulating the ECM during tissue repair. The versatility and functional plasticity of macrophages are investigated, revealing their fundamental contribution to creating a conducive microenvironment for healing. The interactive dynamics between macrophages, fibroblasts, and key molecules of the ECM are explored in the context of supporting tissue homeostasis, initiating the healing process, and maturing the ECM. The positive role of macrophages in activating fibroblasts into myofibroblasts is emphasized, supported by the significant secretion and arrangement of ECM components (such as tenascin, fibronectin, collagen, and HA), resembling an *in vivo* scar.

Ultimately, a further objective is to enhance the credibility of endogenous 3D-HDE models by substantiating the resemblances in the structural and organizational aspects of collagen fibres when compared to *in vivo* murine models. This effort aims to strengthen the authenticity and efficacy of these models in accurately simulating the process of scar formation.

Chapter 2: Literature Review

2.1 Wound healing and Scar formation processes

The biology of wound healing

Wound healing is a complex mechanism that spans over different temporal and spatial scales and aims to restore the architecture, morphology, and functionality of the injured tissue. Starting from the regeneration of residual undamaged cells, the healing cascade will end up in the deposition of new connective tissue that eventually becomes a scar[16]. To accomplish this task, the precise recruitment and coordination of different cell populations are of paramount importance[17], occurring through mechanical and biochemical regulatory networks during four distinct but overlapping phases (Figure 1).

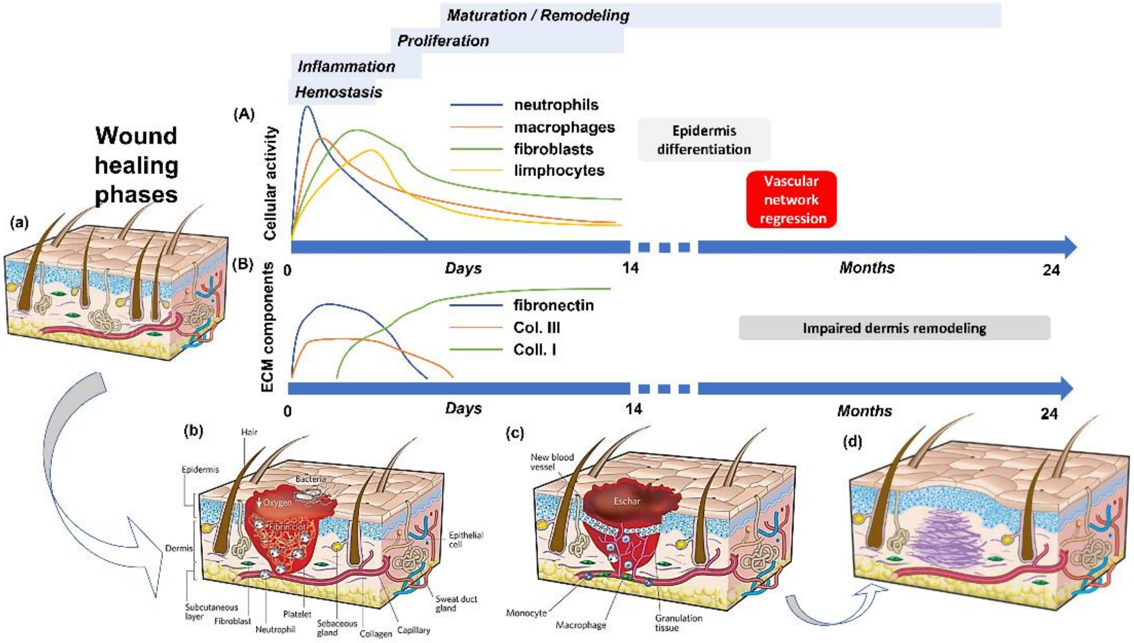

Figure 1– Schematic representation of wound healing phases: (A)-(B) Temporal evolution of cell-mediated wound healing and relative ECM components synthesis, (a) Undamaged skin, (b) Haemostatic phase and immune cells invasion in the wound bed, (c) Proliferation phase characterized by keratinocytes, fibroblasts and endothelial cells migration and proliferation for angiogenesis, collagen deposition, granulation tissue formation, re-epithelialization, and wound contraction to occur, (d) Maturation phase consisting in collagen remodelling (from type III to type I) and wound closure. Reprinted from Gurtner GC, Werner S, Barrandon Y et al. Wound repair and regeneration. Nature 2008;453:314–21.

Upon injury, the tissue barrier properties are lost, thus initiating the finely tuned and controlled cascade of wound healing stages regulated by a sequence of biologically active species (growth factors, cytokines, chemokines) [18]. These factors activate the different cell types and are released by the cells themselves to produce effects that are essential for the correct restoration of the complex three-dimensional architecture of any tissue (Table 1). This biological process begins with the haemostatic phase in which blood and lymphatic vessels undergo vasoconstriction to reduce blood and lymph loss. In addition, a new fibrin cap is formed, providing early wound coverage and a simple scaffold for subsequent cell infiltration and migration. As the wound extends to the endothelium, circulating platelets are activated thanks to the adhesion to the underlying collagen fibres. Once activated, they begin to secrete the content of their cytoplasmic granules: coagulation factors that form the intrinsic and extrinsic pathways leading to a stable fibrin clot development, and a plethora of growth factors that enhance the chemotaxis and the division of the cells which are part of the other stages of wound healing[16,17,19,20]. The first to respond to the platelets'-releasing chemotactic factors call are immune system cells that mount an inflammatory response as soon as they penetrate inside the wound site. This second phase, characterized by the presence of erythema, heat, oedema, and pain, has the main objective of preventing infection and cleaning up the wound thanks to the destruction of any pathogens as well as cellular and matrix debris. As a fundamental part of innate immunity, neutrophils are the first to appear and are mainly responsible for invasion management and phagocytosis of microorganisms, capturing them through NETs and destroying them through the secretion of ROS and antimicrobial peptides and proteases. Apoptotic neutrophils, additionally, produce important chemotactic cytokines and growth factors, such as IL-17 and VEGF, thus allowing the entrance of monocytes from the blood stream, which will later differentiate into macrophages[1]. In wound healing investigations, specifically, those concerning the role of the inflammatory response, both monocyte-derived and tissue-resident macrophages have been widely studied since they are considered to be the key players in this complex repair mechanism. In response to microenvironmental signals, macrophages change their phenotype, making their presence crucial: they switch from a pro-inflammatory (M1) to an anti-inflammatory (M2) state mediating the entire wound healing process. Soon after the injury, the recruited macrophages switch to the M1 configuration to create a more inflammatory, pathogen-killing environment by releasing pro-inflammatory molecules such as IFN-γ, IL-1, IL-6, IL-12, IL-23, and TNF-α. In addition, they remove cell fragments, degrade the broken matrix by synthesizing several MMPs and digest neutrophils to avoid non-specific tissue degradation and incessant inflammation. In the last part, factors such as FGF-2, PDGF, and VEGF are released, which are responsible for more immune cells settling in and promoting the proliferation of endothelial cells, fibroblasts, and epithelial cells. At this stage, a new provisional tissue begins to form inducing an alternative activation of macrophages, the M2 phenotype. M2 macrophages are anti-inflammatory macrophages that with the help of TGF-β1, VEGF, FGF, and PDGF support inflammation suppression and drive new ECM synthesis, wound contraction, and angiogenesis[7,21]. Continuous studies attempt to find an explanation for the presence of T lymphocytes even when no suspicious contamination is present[1,7,22]. Their role in wound healing is still defined as unknown or irrelevant but recent studies have shown that they are important for tissue remodelling and infection resolution. As with macrophages, it has been seen that the TH1 / TH2 paradigm and, therefore, the dual nature of this cell type, contributes both to the formation of a phlogistic environment and the replacement of injured tissue with new tissue[23]. Regarding the first aspect, IFN-γ produced by M1 macrophages controls CD4+ TH1 polarization, which promotes the preliminary pro-inflammatory wound microenvironment. As with the M2 phenotype, there is a specific subset of CD4+ T cells, TH2 cells, that have the potential to shift the overall balance of inflammatory factors in a wound towards a more regenerative or fibrotic outcome. This type of helper T cells is primarily activated by molecules released from dying cells due to damage, known as DAMPs, and contributes to the final stages of wound healing through the release of IL-4 and IL- 13, which support the proliferation of fibroblasts and the deposition of ECM[24]. Once the inflammatory phase is over, healing continues with the final two phases, which involve the formation and remodelling of a new ECM. These stages are largely dependent on the anti-inflammatory cells of the immune system (M2 macrophages and TH2 cells) as a prominent source of cytokines (IL-4, IL-13) and growth factors (TGF-β1) that promote matrix deposition and differentiation of fibroblasts into myofibroblasts, angiogenesis, and re-epithelialization.

The proliferative phase, as the name suggests, involves the recruitment and proliferation of the cells necessary for the formation of new tissue. As a platform for the adhesion and movement of fibroblasts, endothelial and epithelial cells, the granulation tissue, so-called because of its high cellular content, is preliminarily reproduced. This new tissue is generated by the synthesis and deposition of the components of the ECM by fibroblasts. Also in this case, both the fibroblasts deriving from the differentiation of fibrocytes, and undamaged fibroblasts present in the tissue migrate and proliferate in the injured tissue and are positioned in layered planes, parallel to the surface of the epithelium. In the same configuration, type I and type III collagen fibres are released, allowing the matrix to be easily contracted, thus reducing the exposed wound volume. Subsequently, the fibroblasts differentiate into myofibroblasts, which can be recognized by the expression of α-SMA and cause the contraction of the wound by grasping the flaps of the same[1,25] and are also capable of multiplying and secreting ECM proteins such as collagens I and III and fibronectin. Fibronectin is a key mediator of cell migration in wound healing and participates in the organization and stabilization of the ECM. At the proliferation stage, fibronectin assembles into a complex 3D structure on the cell surface, which provides tissue architecture and regulates cell adhesion, migration, proliferation, and apoptosis during skin wound healing. It is believed that the formation of further collagen networks depends on the initial structure of fibronectin, through mechanisms involving integrins. Stimulation of the proliferative activity of fibroblasts through TGF-β depends on the preliminary assembly of the fibronectin matrix[26].

Another unique component that plays a role in the regeneration of skin wounds is tenascin-C. The expression of this protein in intact tissues is minimal. Expression increases with tissue damage and regulates cell adhesion and therefore affects the functionality of the dermis during wound healing[26].

The highest increases in tenascin-C and TGF-β occur in response to skin damage and an increase in MMP expression in the wound, but it has been shown to up-regulate type I collagen expression and down-regulate MMP-1 expression in fibroblasts[27].

HA emerges as a crucial player in the wound healing process, playing a fundamental role in promoting tissue repair and regeneration. Throughout the various stages of healing, HA actively engages in homeostasis, inflammation, proliferation, migration, and remodelling processes[28].

Participating in a feedback loop with cytokines and LMWHA, HA facilitates the inflammatory response by stimulating fibroblast migration and proliferation. Additionally, HA contributes to the production of KGF, promoting the proliferation and migration of keratinocytes.

Following its initial deposition, there is a temporary decrease[29] in elevated levels of HA, triggering the production of CS and DS proteoglycans[28]. These proteoglycans play a crucial role in collagen polymerization, essential for wound closure and scar formation[28].

However, in fibrotic conditions such as pulmonary and hepatic fibrosis, an excessive accumulation of HA is observed[30,31]. This accumulation contributes to the excessive deposition of ECM components, promoting scarring and fibrosis. HA is implicated in fibroblast activation, myofibroblast differentiation, and the production of pro-inflammatory cytokines, further accentuating tissue fibrotic remodelling[30,31].

Once a stroma equivalent has formed, it requires the supply of oxygen and nutrients hence new blood vessels need to be formed. In response to hypoxia and high lactic acid concentration, platelets and macrophages release growth factors, such as VEGF, which stimulate endothelial cells to proliferate and form new capillaries[1,32]. Lastly, the wound completely closes as a result of the re-epithelialization process conducted by the epithelial cells, present at the edges of the lesion. In the presence of EGF released by platelets and TGF-α released by both macrophages and platelets, a phenotypic change occurs. This leads to the abandonment of desmosomes and hemidesmosomes and to the expression of actin filaments that allow cell detachment and subsequent migration. This process is facilitated by plasmin which removes the fibrin clot, and collagenase, which digests damaged stroma[20,33]. At this point, the granulation tissue enters the remodelling phase, which can take years to reach equilibrium. Initially, the development of new tissue stops with the apoptosis of cells that are no longer needed, as well as the pruning of non-functional vessels. Moreover, overly produced ECM components get degraded by the action of collagenase and MMPs secreted by fibroblasts, macrophages, endothelial and epithelial cells. During tissue maturation, type III collagen is completely replaced by type I collagen; the collagen fibres align along tension lines and water is reabsorbed to facilitate filaments approach and cross-link. This type of collagen is aligned in small parallel bundles and is, therefore, different from collagen that is randomly arranged in healthy tissue[1,20]. In humans, due to the lack of regenerative capacity, this process can end with the formation of scar tissue that cannot replicate either the function or the structure of the normal tissue.

It is important to add that the presence of the immune system, particularly the pro-fibrotic phenotype of M2 macrophages, plays a crucial role in this process. M2 macrophages overstimulate fibroblasts through the secretion of TGF-β1. Fibroblasts, in response to this growth factor, transform into myofibroblasts, active cells that contract the wound and produce ECM components to replace the previously damaged tissue.

This is largely due to the rapid intrinsic nature of the reparative response because the immune system aims to expedite the repair process to limit the exposure of the wound to the external environment and reduce the risk of infections, at the expense of perfect but slower morphological and functional regeneration.

However, the excessive production of TGF-β1 by M2 macrophages can lead fibroblasts to generate an excessive amount of matrix, resulting in a scar that, while fulfilling the repair function, may significantly differ in structure and function from normal tissue. In particular, scar differs from healthy tissue in terms of composition, mechanical properties, colour, vascularity, and formation of dermal, epithelial, and vascular adnexa. Additionally, the scar can only replicate 80% of the tensile strength of healthy tissue. This phenomenon, however, does not occur in foetal tissue which instead follows a predominantly regenerative path. Healing dynamics studies of foetal tissue have shown how the failure to assemble an adequate inflammatory response, due to the absence of immune cells and, therefore, also of the factors that normally secrete, results in perfectly regenerated tissue, capable of forming the intricate dermal and epidermal adnexa and scarless[34]. The only human compartment that resembles this behaviour is the oral mucosa. The wounds of the oral mucosa are characterized by an extremely reduced secretion of pro-inflammatory cytokines, and this generates an unfavourable environment for the infiltration of the immune system cells. The main consequence of this phenomenon is the reduction of fibroblast activity and, consequently, a non-excessive deposition of collagen fibres[35]. As described in this section, the inflammatory response plays a leading role in the coordination of the different healing phases. In particular, macrophages make a huge contribution both in the initial part to prevent the onset of infection and in the final part by manoeuvring the steps that lead to the generation of new tissue. For this reason, a thorough characterization is needed, making use of a 3D model that can better recapitulate the complex architecture found *in vivo*. Indeed, tissue damage is something that concerns the extra cellular components and their assembly, not just the cellular aspect. Tissue remodelling and scarring are biological processes, triggered by the trauma and inflammation, occurring at the ECM level. This must first be reconstituted and, subsequently, regain its role as a modulator of cell-cell and cell-matrix communication to ensure that the repair algorithm proceeds in a controlled and well-organized manner.

Table 1: Main cells and molecules involved in the wound healing process.

Cell type	**Activated by**	**Molecules released**	**Effects**

PLATELETS [1]	Exposure to the underlying collagen and vWF after blood vessel rupture	PDGF, TGF-β, bFGF, KGF, EGF, IGF	Fibrin clot (scab) formation; enhance neutrophils, macrophages, fibroblasts and endothelial cells chemotaxis and infiltration
ENDOTHELIAL CELLS (HEMOSTASIS PHASE) [1]	Blood vessel injury	Prostaglandins, Leukotrienes	Vasodilation and platelets disassembly; increase in vascular permeability and leukocytes chemotaxis and adhesion
ENDOTHELIAL CELLS (PROLIFERATION PHASE) [1]	Tissue hypoxia, bFGF, KGF, VEGF, TNF-α, TGF-β, thrombin	Proteolytic enzymes, matrix MMP	Angiogenesis
DERMAL MAST CELLS [1]	Complement system (C3a and C5a), physical stimuli (heat or mechanical injury)	Histamine, TNF-α, IL-1, TGF-β, PDGF, serine protease, chymase, tryptase, Prostaglandins, Leukotrienes	More leaky and permeable blood vessels; breakdown of the ECM to pave the way for fibroblast and endothelial cells proliferation
NEUTROPHILS [7]	Factor released by platelets, by-products of bacterial degradation	ROS, Nitric oxide, antimicrobial peptides, antimicrobial proteases, IL-17, VEGF	Phagocytosis; antimicrobial function; wound debridement
MACROPHAGES (M1 PHENOTYPE – PRO-INFLAMMATORY) [7]	Derived from chemotaxis of migrating monocytes activated by bacterial products, complement degradation products (C5a) and factor released by platelets and neutrophils	Proteinases, antimicrobial peptides, and proteases, TNF-α, TGF-β, IL-1, IL-8	Phagocytosis; antimicrobial function; wound debridement
MACROPHAGES (M2 PHENOTYPE – ANTI-INFLAMMATORY) [7]		Proteinases, TGF-β, EGF, PDGF, TNF-α, IL-1, IFN-γ, IGF, IL-6, Fibronectin, bFGF, VEGF	Matrix synthesis regulation; cell recruitment and activation; angiogenesis

T LYMPHOCYTES [24]	IFN-γ released by macrophages	IL-2, IFN-γ, IL-4, IL-10, TGF-β, TNF-α, FGF	Macrophages production and differentiation regulation; synthesis and proliferation of fibroblast
EPITHELIAL CELLS/KERATINOCYTES [1]	Mainly, EGF, secreted by platelets and TGF- α produced by macrophages, platelets, and keratinocytes	bFGF, VEGF, TNF-α	Re-epithelization
FIBROBLASTS/MYOFIBROBLASTS [1]	PDGF, TGF-β, FGF, EGF, IGF released by platelets and macrophages	Collagen type I and III, elastin, GAGs, adhesive glycoproteins	Matrix components synthesis; wound contraction

Types of wounds and scars

Wounds can be classified based on their depth and the severity of tissue damage. Superficial wounds involve only the outer layer of the skin, known as the epidermis, while deep wounds affect deeper layers such as the dermis and may even extend into the subcutaneous tissue and beyond[36].

Superficial wounds, like abrasions (Figure 2) or light cuts, primarily involve the epidermis. Typically, the healing of these wounds is faster and carries fewer risks of complications. The healing process begins with wound cleaning, blood clotting, and inflammation. Skin cells multiply to close the wound, and scar formation is often minimal or almost imperceptible. Superficial wounds tend to have a simpler healing process and can even heal without leaving visible scars[37].

Figure 2 - Examples of superficial wounds: an abrasion is a superficial skin injury caused by friction or rubbing against a hard or rough surface. This type of wound primarily involves the outermost layer of the skin, the epidermis, and may result in redness, scraping, or the removal of the superficial layer of skin.

Deep wounds, such as more extensive cuts or penetrating injuries, involve deeper layers of the skin. These wounds can be more challenging to manage and require greater attention during the healing process. When deep wounds heal, the scarring process may involve the formation of granulation tissue, collagen production, and vascular regeneration to strengthen the wound[38]. However, due to the increased structural complexity involved, deep wounds are more prone to leaving visible scars[37]. In some cases, surgical intervention or specific treatments may be necessary to reduce the risk of scarring and promote optimal healing[39].

In general, three modes[40] of wound healing have been identified: primary intention, secondary intention or tertiary intention (Figure 3), where the intention ideally refers to the path the wound follows to heal.

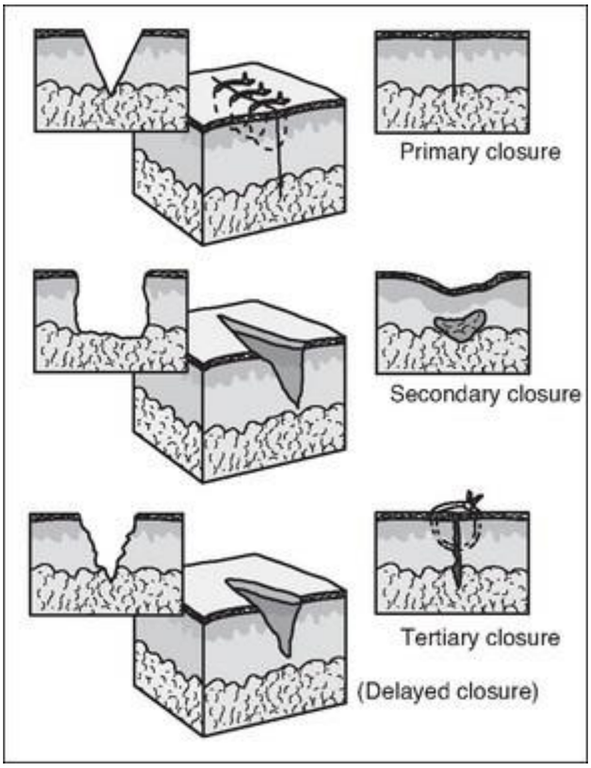

Figure 3 – Visualization of Wound Healing types. Primary Intention: Clean, well-aligned wounds with immediate closure; Secondary Intention: Wounds left open, undergoing granulation tissue formation; Tertiary Intention: Delayed closure after observation, combining aspects of both primary and secondary intention healing.

It is important to emphasize that these modes differ primarily in the extent of reparative phenomena but share fundamentally the same mechanisms involved. Primary intention healing is by far more favourable: the wound is clean (non-infected), with clear, close, and juxtaposed margins, and minimal loss of substance[41]. In the case of sutured surgical or accidental wounds, the margins are carefully apposed using stitches (Figure 4), a procedure that further facilitates repair[41].

Figure 4 - Example of healing by primary intention: a surgical wound, closed by sutures.

Secondary intention healing is typical of wounds characterized by extensive loss of substance (Figure 5A) or bacterial infections. In this case, an intense inflammatory response is evoked, and there is a massive production of granulation tissue to repair the extensive loss of substance[42].

Both of these phenomena profoundly alter the normal reparative process and result in significant scarring outcomes[43] as shown in Figure 5B.

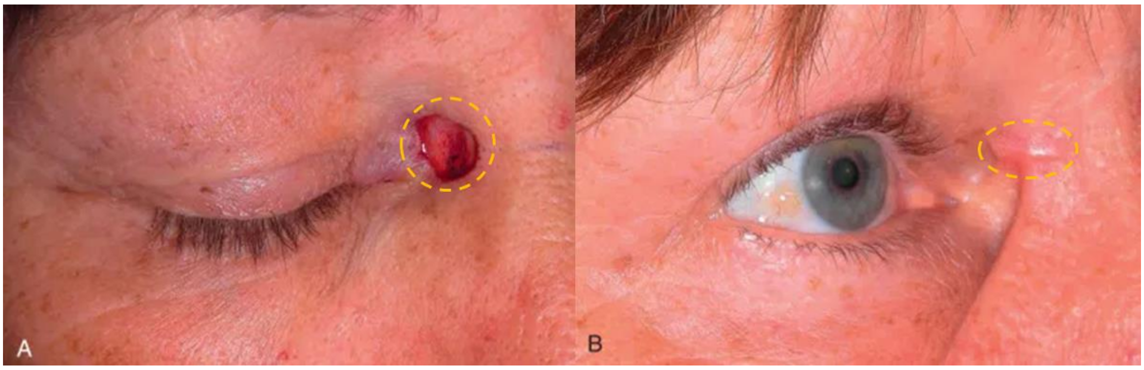

Figure 5 – Example of healing by secondary intention: (A) Small wound from surgery in the concave medial canthus. The wound was left to heal by second intention. (B) Two months after the surgery, her wound has healed with a hypertrophic scar. Yellow circular shapes delineate respectively the wounded and the scarred areas.

Occasionally, wounds, particularly surgical ones, may experience partial or complete dehiscence during the postoperative course[41]. This complication is typically addressed through a healing known as delayed primary closure, which involves a combination of primary and secondary intention healing[44]. In the event of wound dehiscence, the standard approach involves complete reopening of the wound, meticulous cleaning, removal of necrotic areas, and appropriate dressing[45]. Subsequently, after assessing the local situation and confirming the absence of infection, the wound edges can be re-sutured. This process, referred to as healing by tertiary intention, aims to promote effective healing and reduce the risk of infection.

Generally, wounds less than 2 mm deep do not scar[46] but larger wounds generally do scar.

There are different types of scars, and their nature depends on various factors, including the depth of the wound, the location on the body, individual genetics, and wound care[47]. Here are some of the main types of scars:

- Normal or linear scar (Figure 6) is flat, thin, and similar in colour to the surrounding skin. It forms when the wound heals without significant issues and is often the result of surgical wounds or clean cuts[48].

Figure 6 - Linear scar resulting from a surgical procedure on the abdomen.

- Keloid scars (Figure 7 left) occur when scar tissue grows beyond the edges of the original wound. They are often thicker and more noticeable than the original injury and can be itchy and sometimes painful[2]. They are more common in individuals with a genetic predisposition and may occur more frequently in people with darker skin[49].
- Hypertrophic scars (Figure 7 right), similar to keloid scars, are thick and raised but stay within the boundaries of the original wound[2]. They can be red or dark and may cause itching or discomfort[50].

Figure 7 – Keloid scar on the left: highlighted by swelling and a darker colour, this scar is characterized by excessive growth of scar tissue. A hypertrophic scar on the right: featuring a more restrained swelling compared to keloid, it represents a normal response to excessive skin healing.

- Atrophic scars (Figure 8) are characterized by a loss of tissue, resulting in a depression or indentation in the skin. These scars form when there is a lack of collagen during the wound healing process[3]. Collagen is a key structural protein in the skin, and its deficiency in the healing tissue can lead to the sunken appearance of atrophic scars. Acne scars[4] are a common example of atrophic scars.

Figure 8 – Atrophic acne scars show indentations and depressions, these scars result from the loss of tissue during the healing process.

- Contracture scars (Figure 9) are scars that result from the skin tightening during the healing process. These scars can extend deeper into the skin and may affect underlying muscles and tissues[51]. Contracture scars are often associated with burns, where the heat causes damage to the deeper layers of the skin[5]. This type of scar can limit the range of motion in specific areas of the body[52].

Figure 9 - Persistent neck contracture despite multiple surgical interventions: showcasing tightness and restricted movement, these scars often arise from burns or injuries, causing the skin to tighten and potentially affecting mobility.

- Adhesions (Figure 10) are formations of scar tissue that occur when two layers of tissue abnormally join during the healing process[53]. These adhesions can develop in various contexts, such as after surgeries, between internal organs, or between the skin and underlying tissues[54]. They can lead to functional problems and painful symptoms, restricting the mobility of the affected organs[54]. The formation of adhesions is often associated with more severe wounds or surgical interventions involving tissue manipulation. When the surfaces of internal tissues stick together during healing, they can create unwanted connections that compromise the normal functionality of the involved organ[55].

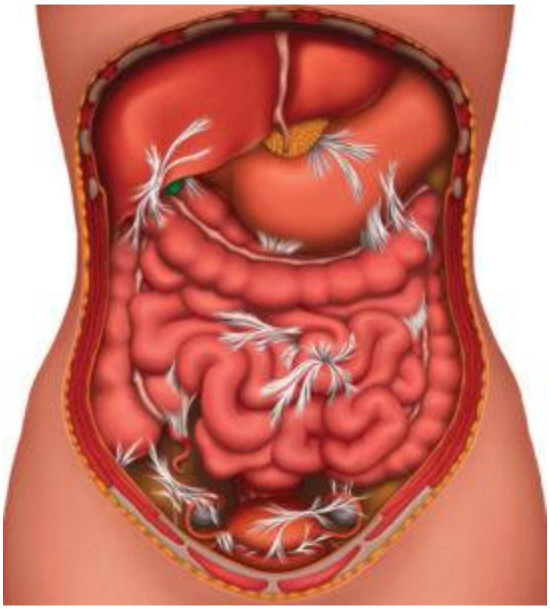

Figure 10 – Representation of abdominal adhesions that may arise when the body heals from an accident, fall, surgery, infection, inflammation, trauma, radiation therapy, or endometriosis.

2.2 Regenerative Medicine and Tissue engineering

Tissue engineering is an interdisciplinary discipline that aims to apply the principles of engineering and biomedical sciences to develop advanced solutions for the repair, replacement, or enhancement of biological tissues[56].

Tissue engineering has deep roots in the pilot stages of regenerative medicine, dating back to the 1990s when scientists began experimenting with cell culture and the construction of three-dimensional supports to facilitate tissue growth *in vitro*[57].

However, it is in recent decades that it has become increasingly important thanks to developments in biotechnology and new knowledge in cellular biology. Its mission is to address the challenges related to the lack of functional tissues caused by disease, ageing, or trauma.

Its central objective is the creation of biological constructs capable of replicating the anatomical and functional characteristics of natural tissues; this is generally achieved through the synergistic integration of three-dimensional scaffolds, cells, and biochemical signals[58].

The three-dimensional scaffold, often made from biocompatible polymers and hydrogel, provides the basic structure and substrate essential for tissue growth and development[59].

Cells, also an integral part of the process, interact with the scaffold, proliferate, and differentiate to form the desired functional tissue. At the same time, the intake of growth factors or biophysical stimuli plays a crucial role in driving cell growth and differentiation within the scaffold, providing crucial signals to target the process of tissue formation and maturation[60].

This harmonious combination creates an environment conducive to the formation of three-dimensional tissue constructs, representing a key approach in tissue engineering.

Tissue engineering applications range from the regeneration of complex organs such as the liver and heart to the repair of tissues such as skin, bone and cartilage[61]. Advances in this field have opened new frontiers for regenerative medicine, offering customized and targeted solutions for the treatment of chronic diseases and irreparable injuries.

In pursuing the objectives of tissue engineering, the creation of functional three-dimensional constructs requires the application of several innovative techniques. The traditional approach was cell culture on static scaffolds, but in recent years new strategies have emerged to improve the accuracy and effectiveness of tissue formation, such as bioreactor culture and biological 3D printing.

The implementation of bioreactive cultures[62–64] (Figure 11) in tissue engineering represents a significant step towards more accurate simulation of the physiological environment, promoting optimal cell growth and improving tissue organization. These bioreactors are devices designed to provide a dynamic and controlled environment, introducing mechanical, hydrodynamic, and biochemical stimuli to modulate cellular response and improve the quality of tissue produced.

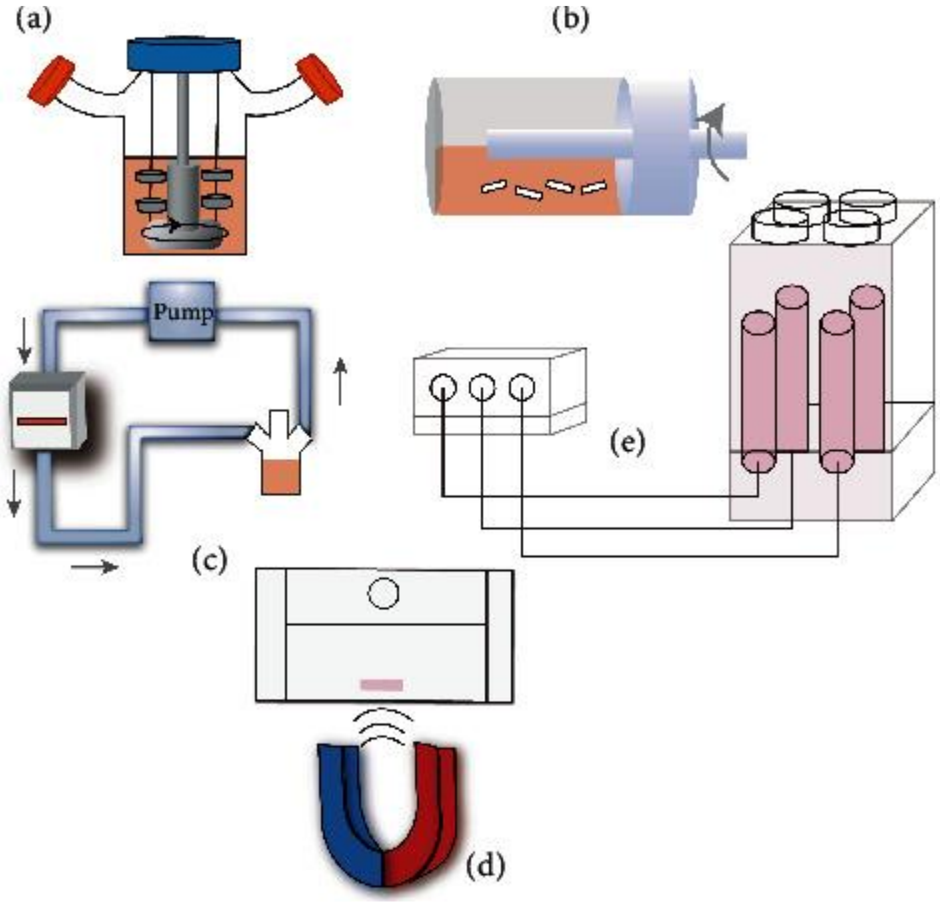

Figure 11 - Common bioreactors used in tissue engineering. (a) Spinner flask bioreactor. (b) Rotating wall vessel. (c) Direct perfusion. (d) Magnetic bioreactor. (e) Ultrasonic bioreactors.

At the same time, organic 3D printing[65–68] has taken a revolutionary role in tissue engineering. This innovative technology allows the precise deposition of cells, scaffold materials and growth factors (Figure 12) in three-dimensional space, creating intricate and sophisticated tissue structures. What makes this methodology extraordinary is its extraordinary flexibility, allowing for design of customized tissue constructs.

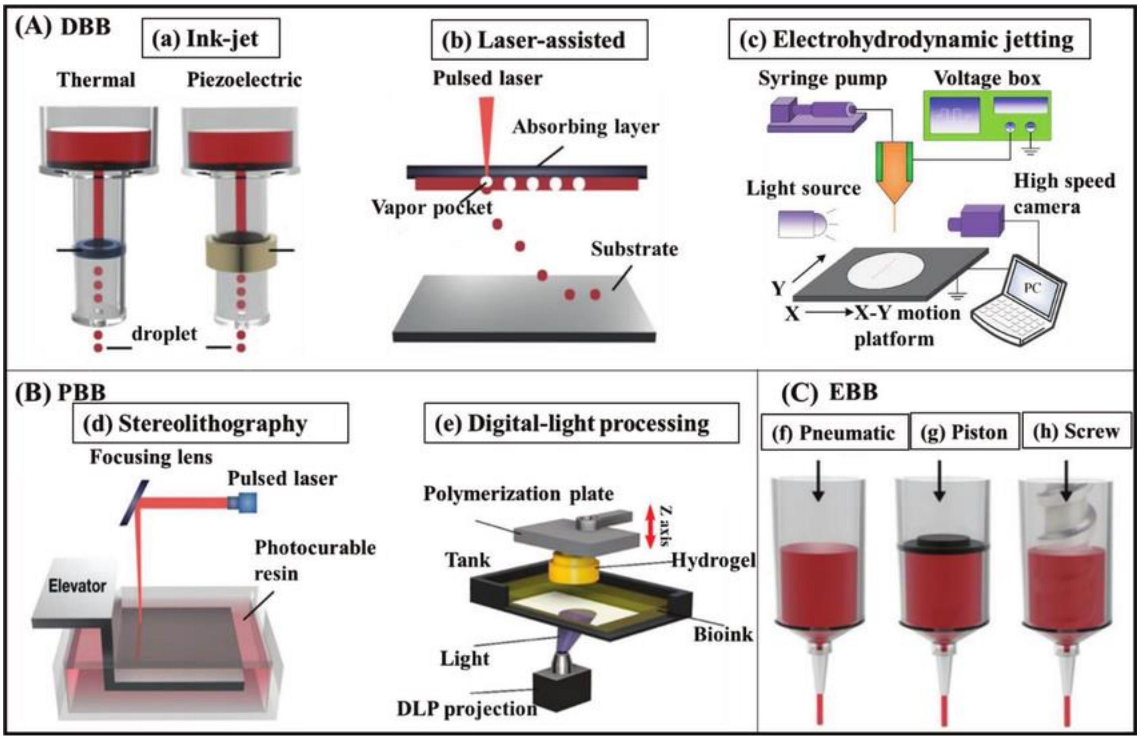

Figure 12 - Schematic illustration of 3D bioprinting systems. (A) Droplet-assisted bioprinting (DBB) including (a) inkjet, (b) laser-assisted, and (c) electrohydrodynamic jetting. (B) Photocuring-based bioprinting (PBB) including (d) stereolithography and (e) digital-light processing. (C) Extrusion-based bioprinting (EBB), which may be (f) pneumatic, (g) piston, and (h) screw.

For the recapitulation of functional three-dimensional anatomical constructs, tissue engineering adopts two distinct approaches (Figure 13), known as **top-down** and **bottom-up**, which have established themselves as complementary methodologies for the creation of new organs or tissues *in vitro*.

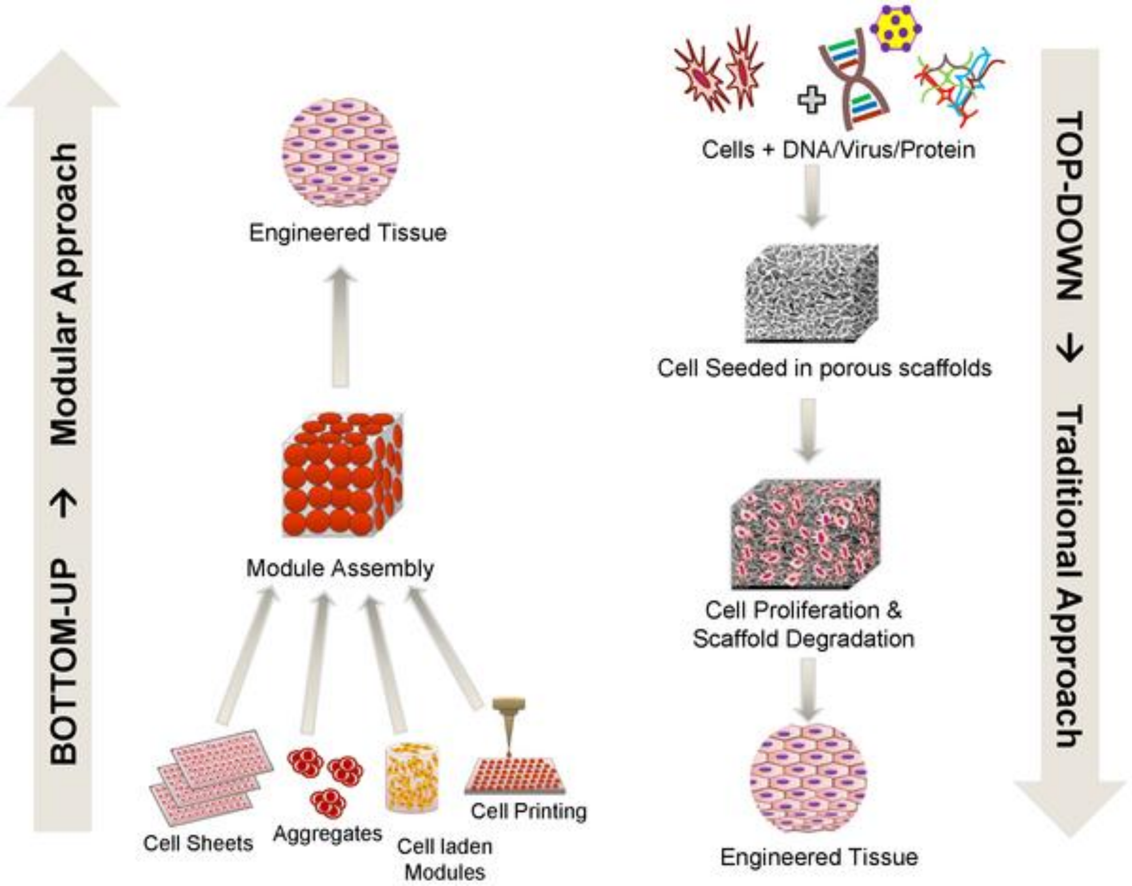

Figure 13 - In the traditional, top-down approach (on the right), cells are seeded into full-sized porous scaffolds to create tissue constructs. Conversely, the modular or bottom-up approach (on the left) involves assembling small, non-diffusion-limited, cell-lad.

The top-down approach is based on reducing larger tissue structures into smaller, functional constructs. This strategy often involves the decellularization of natural tissues, eliminating host cells and preserving the three-dimensional architecture and composition of the ECM[69]. The result is a biological scaffold that can be repopulated with the patient's cells, facilitating the regeneration of the original tissue.

The bottom-up approach, on the contrary, focuses on the gradual construction of tissue constructs starting from basic components. This approach offers greater precision in tissue design, allowing the creation of custom constructs[70].

While the top-down approach preserves native tissue architecture, the bottom-up approach provides detailed control over tissue design.

Regardless of the approach, it is essential, however, to distinguish between exogenous and endogenous constructs since this distinction plays a key role in determining the effectiveness and physiology of the tissues generated.

Exogenous constructs derive from synthetic or biological materials in which cells are seeded[71]. Common examples are three-dimensional scaffolds created in the laboratory through techniques such as 3D printing or cell culture on pre-existing matrices. Although these constructs can significantly contribute to tissue regeneration, their physiology may differ from that of natural tissues, leading to challenges such as graft integration and immune response[72].

In addition, the generated matrix may differ from that of natural tissues, leading to a certain heterogeneity in structure and function.

When we refer, instead, to endogenous constructs, we mean an approach in which the tissue matrix is produced directly by the cells themselves, under targeted and controlled conditions[73].

This process can be stimulated through the use of specific biochemical signals, growth factors or the application of controlled forces. Cells, in response to these stimuli, generate a three-dimensional ECM that acts as a structural support for cell growth and the formation of new tissues and represents a more faithful imitation of native physiology.

The endogenous approach with a self-produced matrix plays a fundamental role in promoting more physiological and integrated tissue healing. The matrix generated by the cells themselves is in tune with the surrounding biological environment, facilitating the optimal interaction between the cells and their microenvironment. This process more faithfully reflects the natural dynamics of tissue formation and contributes to the structural and functional homogeneity of the regenerated tissue. The physiological importance of endogenous constructs lies in their ability to respect and exploit natural biological processes. These constructs allow you to explore in detail cellular interactions, differentiation, and response to environmental signals under more realistic conditions.

In addition, the locally produced matrix facilitates better integration, reducing the risk of adverse reactions, and promotes the formation of more homogeneous and functional tissues, in tune with the intrinsic healing dynamics of the body. This endogenous approach, therefore, leads to more adherent results to natural physiology.

The recreation of an endogenous environment *in vitro* improves the validity and relevance of the experimental results, allowing a better understanding of tissue dynamics and paving the way for more effective applications within tissue engineering.

For these reasons, endogenous tissue emerges as a versatile and representative platform to explore a wide range of human conditions and pathologies in the laboratory. This approach allows us to recreate, in a controlled way, the microenvironmental conditions that characterize specific pathologies, offering a more physiological model than the traditional exogenous constructs[74–77].

In vitro endogenous constructs allow to replicate the complexity of the tissue microenvironment, facilitating the simulation of more realistic physiological conditions. This is particularly relevant when exploring pathologies involving complex interactions between cells, ECM, and biochemical signals such as wound healing and fibrosis.

In this way, it is possible to study in detail the cellular responses and changes in the ECM associated with different conditions. This is crucial for understanding the molecular and cellular bases of pathologies and for developing targeted therapeutic strategies.

In vitro endogenous constructs studies provide fertile ground for evaluating the effectiveness of drugs and therapies. The ability to model specific pathological conditions allows you to assess the impact of potential treatments in a more realistic context, facilitating a smoother transition from basic research to clinical trials.

2.3 Bioengineered dermis models for wound healing and scar tissue studies

The skin is the most extensive tissue exposed to the external environment, which means that it is vulnerable and more susceptible to injury and trauma. For this reason, the integumentary system is often the one most reproduced *in vitro* to analyse its wound healing dynamics. Currently, numerous models both *in vitro* and *in vivo* have been developed for this study and to conduct several tests of new therapeutic strategies capable of manipulating tissue repair. These include 2D cell cultures, animal models, and 3D exogenous models. Despite the benefits they have brought in understanding the different key pathophysiological mechanisms, these models have some limitations.

Today, animal testing is the main preclinical step in drug discovery and is still crucial in predicting pharmacokinetics and providing information on the efficacy or toxicity of drug candidates.

Current attention to the so-called "3Rs principles" in all research fields (reduction, refinement, and replacement of animal testing), supports the need for advanced *in vitro* approaches as alternatives to animal models[78].

Moreover, although mice and humans have almost the same types of cells, murine models do not summarize human physiopathology following a predominantly regenerative rather than reparative pathway[79].

Most of the wound healing experiments were based on a 2D culture of cells belonging to the tissue being studied, mainly keratinocytes and fibroblasts.

Due to the simplicity and low cost of these tests, mechanical, electrical, thermal, and optical damage has been inflicted and studied (Figure 14).

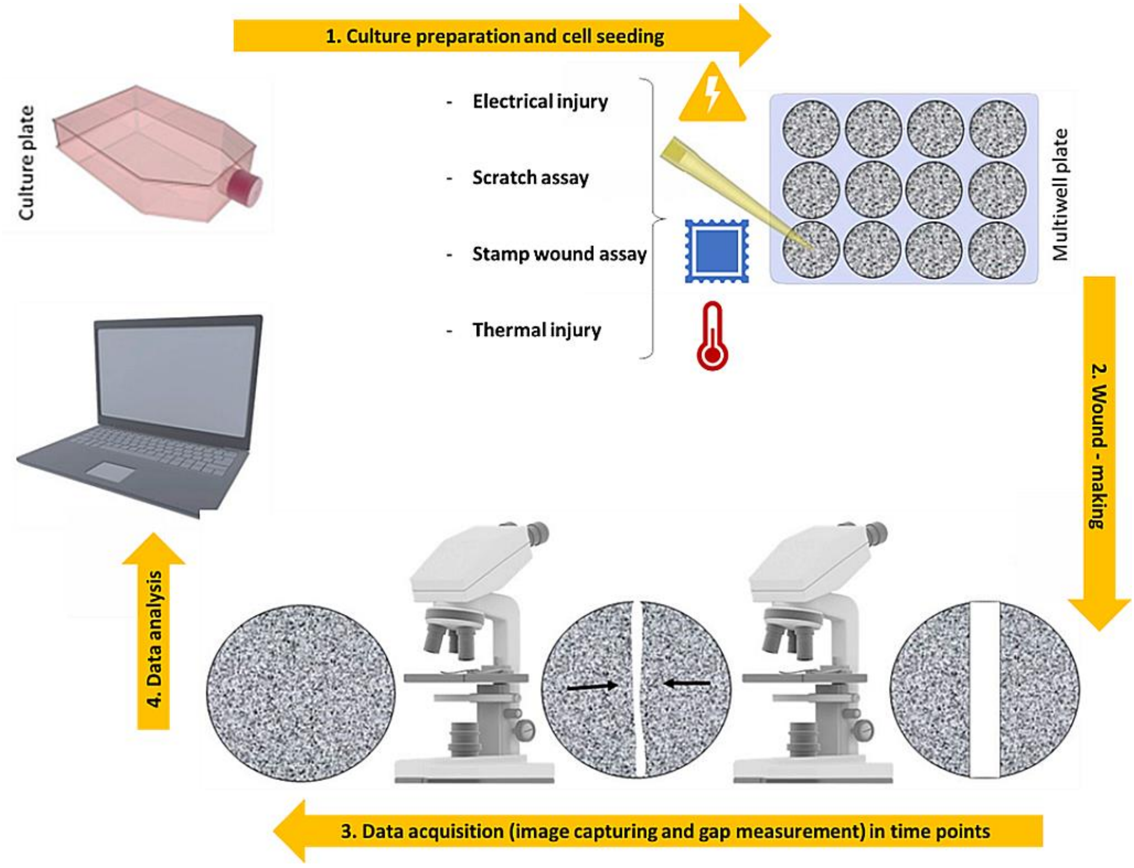

Figure 14 - 2D scratch-assay steps: ***(1)*** *Cell culture preparation and cell seeding into a plastic-bottomed multiwell tissue culture plates,* ***(2)*** *Cells confluent monolayer scratching with a pipette tip,* ***(3)*** *Time-lapse brightfield image acquisition of wounds up to gap closure,* ***(4)*** *Data analysis for mean cells migration rate estimation.*

Despite the advantages and ease-of-use for the study of cell migration and proliferation, essential for understanding the processes of angiogenesis[80] and re-epithelialization[81], *in vitro* 2D assays cannot summarize the complex conditions of a wound.

Both for the absence of other important cell lineages and, more importantly, because 2D studies do not summarize the exact microenvironment of a wound. 2D cell cultures are characterized by cells seeded on flat and hard substrates, not representative of the cellular environment. The biggest problem is that 2D cultures lack the scaffolding ECM, which establishes intercellular signals or networks and external dynamic stimuli that mimic the microenvironment *in vivo* and instruct cells to grow, migrate, and differentiate[82].

Advanced 3D culture hosting systems are essential as they facilitate the intricate biological processes of tissue remodelling and scarring. These processes are triggered by trauma and inflammation, impacting the ECM. Reconstituting the matrix is crucial to reinstating its function as a regulator for cell-cell and cell-matrix communication, thereby ensuring a well-controlled and organized repair mechanism. The tissue engineering approach, aiming to reproduce a functional and structural dermal substitute, relies on the creation of three-dimensional scaffolds as an ECM analogue to guide cell adhesion, growth, and differentiation.

Regardless of their origin, synthetic or natural, the scaffolds used to replicate the human dermis can be divided into two main categories: exogenous or endogenous. In an exogenous dermis, a pre-existing scaffold is used to accommodate human fibroblasts. Synthetic[83] and natural biopolymers[84], as well as human DED[85–87] fall into this approach. On the contrary, if the fabrication process of the dermis is based on established bioengineering processes able to induce human fibroblasts in synthesizing and assembling their own ECM, the resulting dermis is considered an endogenous engineered dermis. In this category fall engineered dermis obtained by both cell-sheet engineering[88] and dermal microtissue assembly approaches[73,89,90].

2.3.1 Wound healing models based on exogenous tissue equivalents.

Exogenous scaffolds[91] have been used to build full-thickness models subjected to different wounding methods: mechanical, thermal or laser-induced damage (Table 2)[92–94]. Early works by Falanga et al.[95] reported the use of bilayer skin models, with the dermal component made of reconstructed rat tail collagen containing human fibroblasts. After a mechanical injury obtained by using a skin mesher, the wounded region was investigated *in vitro* for up to 6 days in terms of keratinocytes migration, proliferation, re-epithelization, and inflammatory response. During the culture period, it was observed a complete re-epithelization and closure of the defect; in addition, the expression of acute proinflammatory cytokines was detected with a peak 24 h post-injury. Other groups have used human DED populated with human fibroblasts[96,97]. These models have been used to study the effect of both biopolymers (i.e., fibrin) and growth factors on wound closure. Geer et al.[96], used a full-thickness model consisting of DED and keratinocytes to investigate the role of fibrin in the closure of partial wounds, highlighting its beneficial role in promoting the re-epithelization process. In another work by Xie et al.[97] (Figure 15), a bilayer skin model based on DED was injured with a punch biopsy, creating a 4 mm wound that extended through both the epidermis and dermis. The wounded area was filled with a biomimetic hydrogel to mimic the formation of the fibrin clot; furthermore, re-epithelization and dermis closure were studied by using histological and immunostaining techniques. Although these systems represent an advance in the field, compared with 2D approaches, the authors recognized crucial limitations of the models, such as the lack of immune response and the absence of other cell types (e.g., melanocytes, Langerhans' cells, microvascular endothelial cells). Moreover, the importance of reliable and robust 3D wound healing models have also pushed the development of standardized wound healing models by using 3D printing technology as well as computer-assisted mechanical wounds[88]. Nevertheless, most models that replicate the full-thickness wound healing process, are used as *in vitro* platforms to screen molecules able to speed-up the re-epithelization step, by using the dermis as a supporting 3D matrix for the epidermis. The presence of the dermis should allow the study of more complex phenomena underlying skin regeneration, such as the formation of the fibrotic scar. Indeed, wound closure is not just a cellular phenomenon: together with inflammation and immune response, it is necessary to consider the complex machinery involving different cell types, ECM remodelling and cell-ECM crosstalk. In this direction, several studies have been performed to investigate the interactions between fibroblasts, immune cells and endothelial cells and the force distribution and ECM remodelling during the closure of deep wounds (Figure 16)[98–102].

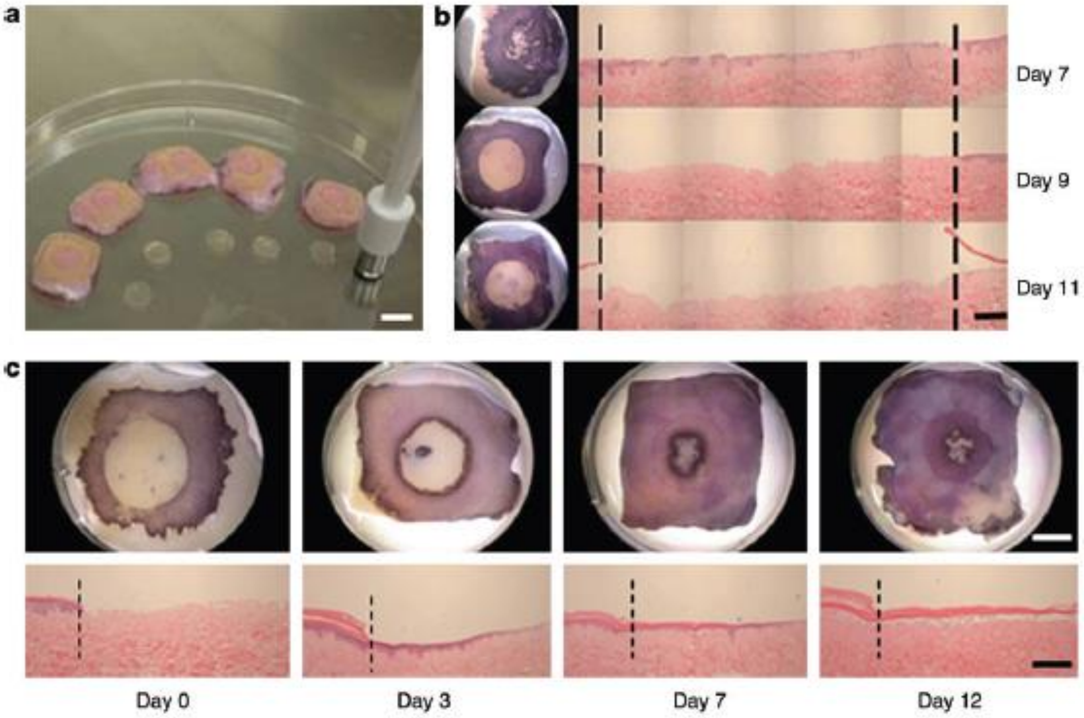

Figure 15 - Development and validation of a 6mm diameter superficial-thickness DED-HSE wound model. (a) Photograph of the technique used to create the superficial-thickness wound in the DED-HSE. A wound was created using a 6mm punch biopsy, followed by the removal of a central portion of the epidermis with forceps. (b) Methylthiazol tetrazolium (MTT) (left panels) and histological analysis (right panels). A 6mm superficial-thickness wound was created in individual DED-HSE after culture at the air-liquid interface for 7, 9, and 11 days. Dashed lines indicate the wound boundaries. (c) Representative images of MTT and haematoxylin and eosin-stained DED-HSEs during repair. Samples were cultured with Full Green's (FG) medium for 3, 7, and 12 days after superficial-thickness wounds were created. Dashed lines indicate the wound boundaries.

More detailed investigations reporting mechanistic studies and ECM remodelling have been obtained by inducing a cut in rat tail collagen gels containing either fibroblasts alone[101] of fibroblast and endothelial cells[99]. Sakar et al.[101], developed an optically accessible device hosting rat tail collagen microtissues populated with 3T3 fibroblasts injured by an incision to simulate a deep wound occurring in the dermis. The study was conducted in the absence of the epidermis layer since the attention was focused on the mechanistic aspects that occur during wound closure at the dermis level. Tensile force microscopy, time-lapse imaging and immunostaining revealed that fibroblasts closed the gap by means of a coordinated action of force-dependent contraction involving the entire tissue. Also, circumferential fibroblast migration around the edges of the wound and a concomitant assembling of fibronectin around the wound edges was observed as the mechanism by which the cells restored tissue integrity. Advancement of this model was proposed by Tefft et al.[99], in which the engineered dermis was populated by a co-culture of fibroblasts and endothelial cells. After cut, the authors found remarkable differences between their 3D model and 2D wound healing model. Indeed, while the latter showed fast migration of endothelial cells after the wound, the dynamic in the 3D environment was quite different. It was observed that fibroblasts were engaged in the closure and in the deposition of new ECM components (i.e., fibronectin and collagen type III); the vessel structures, on the other hand, were primarily restricted to the wound periphery, and movement of the vascular structures was associated with tissue contraction of the initial matrix, adding a new perspective to the understanding of blood vessel dynamics in early stages of healing. In this context, tissue engineering, using cells growing within 3D supports, reduces the gap between flat cell cultures and physiological tissues and preserve the differentiated tissue-specific phenotype. Although 3D exogenous matrices do not fully mimic the native context, they are valuable tools to conduct fast studies on mechanistic phenomena occurring during the closure process.

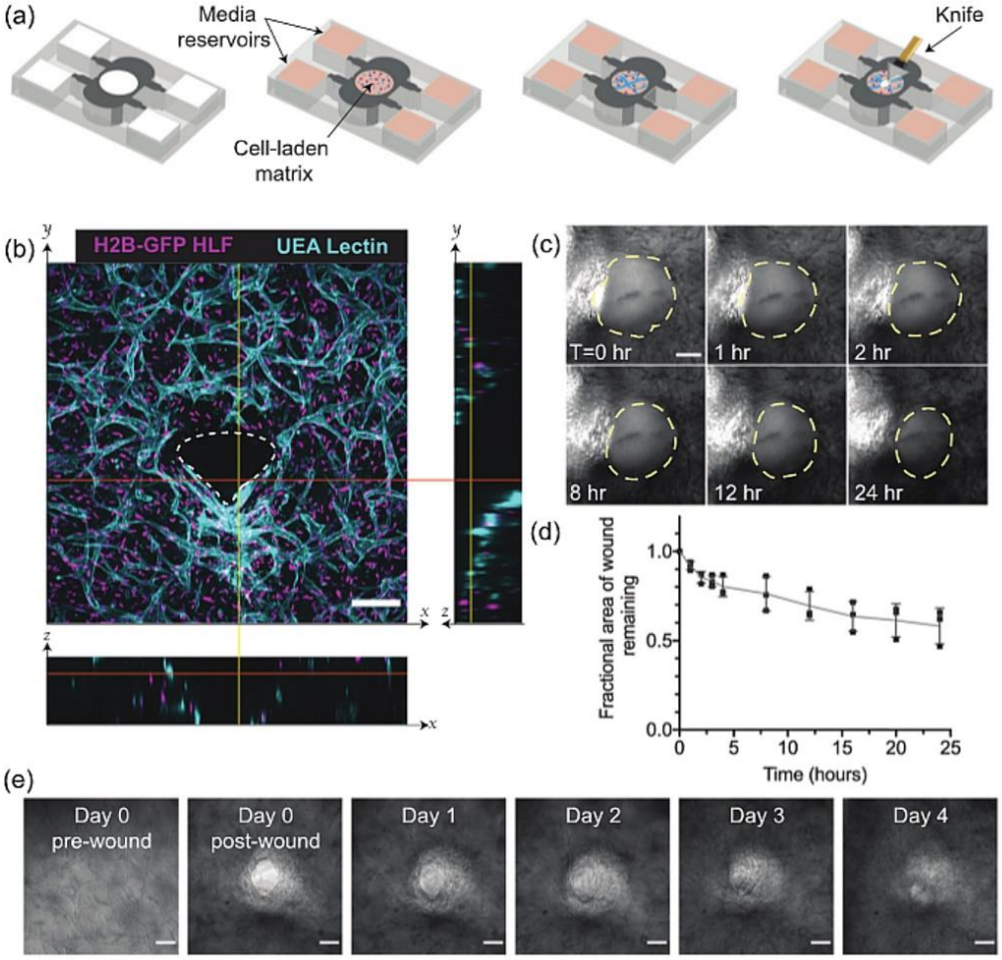

Figure 16 - Damaged 3D exogenous dermis equivalent: (a) Schematic representation of the experimental design: endothelial cells and fibroblasts embedded in a fibrin gel are inserted in a PDMS device. The 3D vascularized tissue is allowed to mature for 3 days before cutting with a diamond knife, (b) Immunofluorescence image of the wounded vascularized tissue one day after cutting. Z-projection, both in x-z and y-z coordinated, indicates the wound depth and white dotted lines delineate wound boundaries, (c) 24 h-brightfield time-lapse acquisitions with wound borders highlighted by yellow dotted lines, (d) Quantification of wound area reduction over 1 day, (e) Brightfield images of the tissue up to wound closure day (day4).

Table 2 - Common 3D models used for three-dimensional wound healing assays.

3D models	Aim	Ref
Exogenous skin wound models		
Fibroblasts-populated Rat tail Collagen I + keratinocytes	Besides new tissue formation, these *in vitro* platforms enable us to screen molecules able to speed-up the re-epithelization step	[92,95]
Fibroblasts in DED + keratinocytes		[96,97]
Exogenous dermal wound models		

Fibroblasts-populated Rat tail Collagen I	Reproduction of the complex processes concerning ECM remodelling and cell-ECM crosstalk	[101]
Fibroblast and endothelial cells embedded in Rat tail Collagen I and fibrinogen		[99]
Endogenous dermal wound model		
Fibroblasts embedded in their own ECM	Able to replicate *in vitro* morphogenesis, neo-synthesis, assembly, ECM turnover and modification of ECM composition/architecture during a pathological state.	[75,103,104]

2.3.2 Wound healing models based on endogenous tissue equivalents.

As discussed so far, the dynamics involving the dermis during the closure process, play a crucial role in understanding the phenomena underlying the closure of deep wounds. It is well accepted that the inflammatory process and the pro-inflammatory agents released during this step, strongly affect the neo-ECM remodelling leading to the formation of the fibrotic scar. In this perspective, an ideal engineered dermis should be able to replicate, not only the cellular events, but also the complex ECM dynamics involved during the morphogenesis of the dermis: the synthesis and 3D assembling of the neo-ECM components (e.g., collagen, elastin, hyaluronic acid, and fibronectin). In this context, the exogenous matrices provide partial information about the ECM dynamics. Although interesting phenomena such as cell differentiation, migration and mechanical signalling can be studied, different limitations appear. For instance, from a mechanical point of view, the 3D context generated by the exogenous matrices is quite different in terms of local stiffness and hydration from the native one. Also, exogenous matrices do not contain all the ECM components that are able to provide the native regulatory context useful for the correct maintenance of fibroblasts. The lack of both correct mechanical and compositional microenvironment makes the exogenous matrices an over simplified 3D context, as the fibroblast receptors are not properly engaged in physiological interactions with their own ECM. This can result in aberrant responses. Moreover, exogenous matrices are unable to modify their composition/architecture during the progression of a pathological status as the native ECM does [105]. In fact, compared to the exogenous matrices, the model based on the use of an endogenous ECM has revealed the ability to replicate *in vitro* crucial phenomena related to the ECM functionalities: (i) morphogenesis, neo-synthesis, assembly and ECM turnover [106], (ii) modification of ECM composition/architecture during a pathological state[75,104,107], (iii) correct dermis/epidermis crosstalk via the spontaneous formation of both rete ridge profile and hair follicle-like structures[73]. Lombardi et al.[103], used an endogenous 3D-HDE obtained by inducing fibroblasts to synthesize and assemble their own ECM (Figure 17). The dermis model was surprisingly indistinguishable from the native one in terms of composition, architecture, and mechanical properties, being collagen, elastin, fibronectin, and hyaluronic acid correctly assembled in the extracellular space during the formation process. Once the dermis was correctly assembled, the engineered tissue was cut, and the closure was observed for up to 3 weeks. During the closure steps, in addition to observing cellular events such as fibroblasts invasion and differentiation, relevant ECM dynamics were also detected. A provisional matrix of fibronectin and hyaluronic acid was deposited in the gap in the first week, followed by the deposition and assembly of a collagen matrix in the successive weeks. Furthermore, the collagen network assembled in a scar-like architecture that showed an orientation of the collagen fibres orthogonal to the cut direction. Finally, the composition of the neo formed ECM differed from that of the undamaged tissue. Overall, the spatiotemporal cellular and extracellular events occurring during the closure resembled those that occur during the formation of a scar tissue in the native dermis. These data suggested that, even in absence of an acute inflammatory response, adult fibroblasts engage in a repair process instead of a regenerative one. Moreover, the use of endogenous engineered dermis allows *in vivo*-like studies after the application of different damaging sources which share with the mechanical wounds the remodelling of the ECM. For instance, in a study of Casale et al.[104], a HSE was presented, consisting of a dermis made up entirely of fibroblasts embedded in their own ECM on which epidermal cells were seeded. HSEs were subjected to UV-A rays' exposure and the results obtained showed that, as a result of damage, these skin equivalents were not only able to replicate the complex cells-ECM interactions but provided evidence of the reorganization of the collagen network after the photodamage.

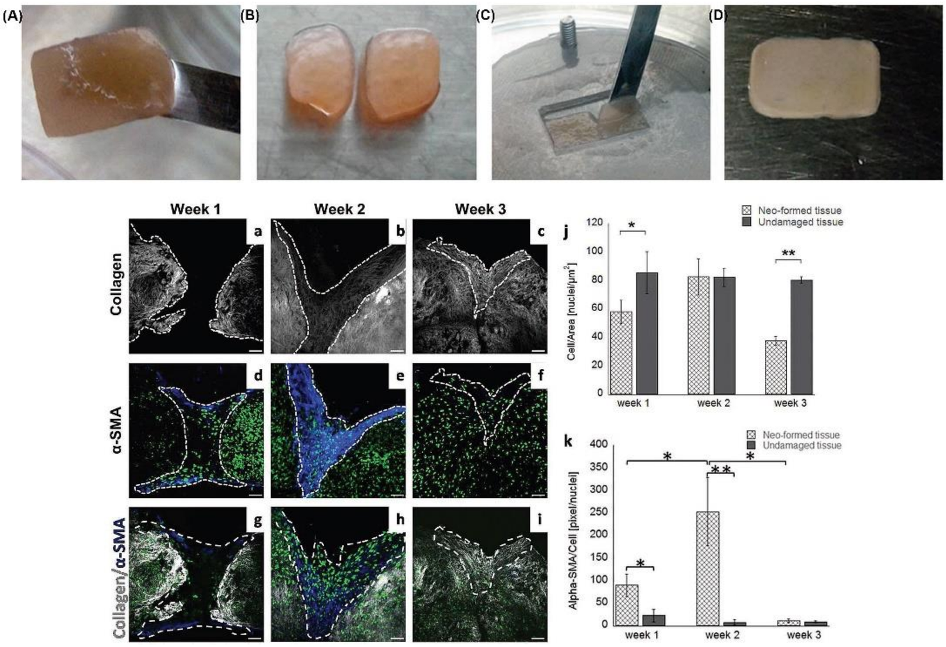

Figure 17 - Damaged 3D endogenous dermis equivalent: (A) – (D) Workflow of the 3D-HDE cutting. Specifically, after 4 weeks of maturation, a 3D-HDE is cut with a scalpel into two parts; then, these parts are reallocated close together in a maturation chamber to reproduce a first intention wound healing in a dynamic regime.
(a)-(c) SHG of the 3D-HDE after wounding over 3 weeks illustrate the neoformation of collagen fibres, (d)-(f) Qualitative evaluation of α-SMA expression, over 3 weeks from wounding, shows how this protein is abundant during the second week which approximately corresponds to the proliferation phase, as the in vivo counterpart. This expression is suppressed during the third week which is reasonable since the remodelling phase is starting, (g)-(i) Merge of the signals previously described, (j)-(k) Quantitative analyses of the number of cells per area and α-SMA production per number of cells.

2.3.3 The need of the immune response *in vitro*

The epilogue of the wound healing process is the simple reconstruction of the compromised tissue architecture. The event may end with chronic, hard-to-heal wounds or tissue fibrosis, both of which represent an enormous burden on the health system worldwide and are associated with significant patient morbidity and mortality. Consequently, it is ever more pressing the request to acquire more information about the mechanisms that regulate the wound restorative progression and that leads to the identification of new treatments which aim to improve the injuries treatment.

The use of animals for preclinical research has been the standard method for decades, contributing to important advances in the understanding of human biology[108]. However, because wounds do not always heal rapidly due to different aetiologies, no animal model can be considered universally valid while a specific configuration could mimic a desired aspect of the human condition and provide a complete understanding of this intricate mechanism. To meet the requirements regarding the species-specific and the cause of the wound, *ex vivo* skin derived from skin explants was proposed as a viable model, which made it possible to assess wound healing in human tissues, as it has all the native structures of human skin. However, due to its limited availability and life cycle and together with the lack of immune cells and blood supply, its use is restricted to very limited applications[109]. Since the adoption of the principles of the 3R and the animal testing ban[78], the development and use of alternative *in vitro* platforms have increased significantly. Preclinical screening of new substances for better healing can be evaluated with 2D tests and 3D models of more complex skin wounds, as previously described. In this digression on useful and valid models for detailed assessment of healing dynamics, 3D models of skin seem to be the most appropriate as they ensure the implementation of a more physiologically relevant environment. Full-thickness skin models, consisting of a dermal compartment with fibroblasts and a fully differentiated epidermis on top of it, better recapitulate what happens *in vivo*. Indeed, the paracrine signalling among residing cells is ensured and the fibroblasts influence on re-epithelialization is reproduced with good accuracy. However, the use of fibroblasts and keratinocytes alone is a limitation to the progress of skin models as validated preclinical platforms for wound healing investigation. This co-culture reproduces only a fraction of how the skin appears when a chronic wound or scar tissue occur.

In the context of wound healing research, significant efforts have been made to replicate *in vitro* fibrotic tissue, exploring various methodologies and approaches. Numerous studies in the literature have tackled this challenge, attempting to recreate conditions that lead to scar formation or fibrotic tissue through advanced cell culture models.

An approach commonly employed involves the use of cells derived from keloid biopsies[110], considered natural models of excessive scar tissue formation. These cells have been integrated into 3D constructs to study their response to the *in vitro* environment and evaluate the model's ability to reproduce fibrotic phenomena similar to those observed *in vivo*.

Other researchers have explored the effect of specific components known to promote the formation of fibrotic tissue. For instance, the incorporation of macromolecular crowding[111,112], a process simulating the crowded environment in which cells can interact, has been integrated into *in vitro* models. This strategy aims to replicate conditions where tissue cells are tightly packed, facilitating intercellular communication and influencing cellular behaviour towards scar formation.

Another molecule of interest is TGF-β1, known for its key role in regulating collagen production and promoting scar tissue formation. Some studies[113,114] have introduced TGF-β1 into *in vitro* models to examine how this molecule influences the dynamics of scar formation and fibrotic tissue.

At this point, it is emphasized the need to establish direct communication between skin cells and immune system cells, reflecting the complex and delicate interaction required for all four normal stages of wound healing. While classical studies have largely focused on key molecules involved in the process, creating models that facilitate dynamic interaction between dermal cells and the immune system represents a crucial step forward in approaching a more accurate reproduction of physiological events *in vivo*.

The preclinical development phase of a drug would gain greater impact and significance by the use of *in vitro* models able to physiologically recapitulate the native counterpart. To improve the *in vitro* models already available and implemented for the study of lesions on the skin, the missing dowel is the immune system responsible for triggering the inflammatory response.

There is a need to recreate an organotypic equivalent of immunocompetent skin to be damaged and in which all the steps leading to a chronic wound or fibrotic tissue can be traced. At present, several immunocompetent skin models have been developed for a detailed study of specific diseases (Figure 18).

The incorporation of melanocytes has made it possible to study the skin's response to UV radiation[115] and the progression of melanoma[116], Langerhans cells have been successfully implemented to study their recruitment to the epidermis for skin sensitization analysis[117,118], the co-culture of dendritic cells in skin equivalents has allowed the assessment of their role in cases of allergic contact dermatitis[119] and the introduction of T cells in these models has allowed an in-depth study of Candida Albicans infection[120]. When studying wound healing, of all the cellular components involved in the process, macrophages and T cells are the only cell types that persist in the wound area at all stages. Whether they reside on the skin or are recruited by precursors circulating in the blood, their contribution to healing is crucial and dysfunction of their activity results in an ineffective resolution of inflammation. Therefore, the incorporation of these cells is of utmost importance and relevance for the exploration of new healing therapies. During the healing of wounds, macrophages and T cells adopt a dual phenotype as a result of microenvironmental signals, each contributing to the process with distinct functions. The dual role and function of these innate and adaptive immune system cells is a challenge when it comes to implementing them in 3D skin models. Initial attempts to include T cells for an *in vitro* lesioned skin model were done by Lorthois et al.[121] and Shin et al.[122]. In these works, it was shown that starting from both lesional psoriatic cells[121] and skin cells derived from healthy individuals[122], the infiltration of T cells into these 3D skin equivalent constructs was validated by anti-CD3 immunofluorescence staining. Furthermore, these immuno-competent skin models can secrete more pro-inflammatory mediators than 3D skin without immune cells under the same experimental conditions. Linde et al.[123] and Bechetoille et al.[124] tried to include macrophages in *in vitro* skin cultures. In the former work, the group co-seeded macrophages with a tumour epidermis stimulating the overall model with IL-4. In the latter, the authors co-cultured macrophages with fibroblasts and then, stimulated this construct with lipopolysaccharide to trigger an inflammatory response. In both studies, cell survival have been proved for 1 week[124] and 3 weeks[123] but in one case the epidermis was absent and in the other, the presence of a diseased epidermis limited the relevance of the models. It is, therefore, necessary to incorporate macrophages or T cells into healthy engineered skin models to subsequently reproduce the effect of mechanical or chemical trauma.

In some studies[125,126], M2-differentiated macrophages were introduced into 3D constructs without replicating a wound. The aim was to assess the impact of these cells on scar formation, despite the absence of a simulated injury, considering the pivotal role of macrophages in modulating the inflammatory response and controlling scar tissue.

As we have seen, experiments conducted on endogenous 3D models have demonstrated to provide more representative and applicable results for understanding the biological events at play. The presence of a lesion in endogenous tissues, combined with interaction with M2 macrophages, offers a more comprehensive picture of the dynamics involved in wound healing and scar tissue formation.

This would significantly and remarkably increase the relevance of wound healing investigations. Working in this direction, these immune-competent endogenous models may be perfect emulators of the human trauma response. For instance, they could be used to validate on human equivalents the use of non-thermal plasma treatments, so far only tested on murine models[127,128]. These treatments have not only been shown to speed up the repair of wounds but have also had a considerable anti-fibrotic role acting on the reduction of TGF-β1 released by macrophages and of the subsequent expression of α-SMA and collagen I deposition.

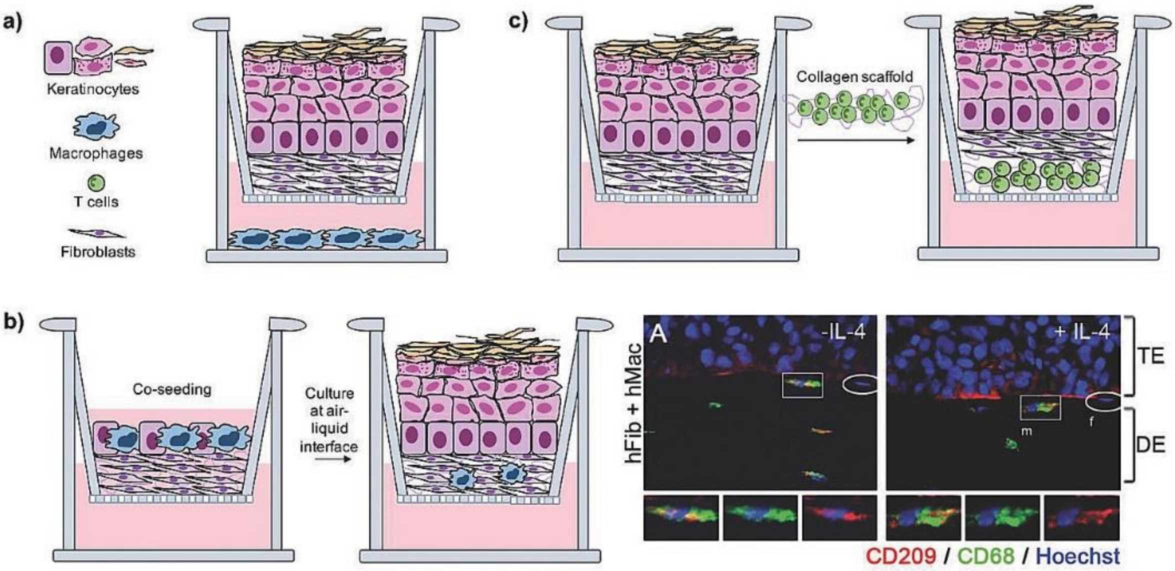

Figure 18 - Immunocompetent skin models: (a)-(c) Schematic representation of macrophages or T cells co-seeded with a full-thickness skin equivalent, (b-right panel) Experimental results of pan macrophages and M2 macrophages migration towards the epithelium.

2.3.4 Wound Healing Studies through Microfluidic Systems

In recent years, the convergence of microfluidic and Lab-on-a-Chip technologies has led to a new era for conducting complex studies across diverse scientific domains. Notably, these technologies have found valuable applications in the realm of cutaneous wound healing studies, where the ability to create controlled microenvironments and precisely manipulate fluids on a miniature scale has transformed the approach to understanding the complexities of wound healing processes. This section aims to elucidate the significance and applications of microfluidic and Lab-on-a-Chip systems in the investigation of cutaneous wound healing, highlighting their contributions to unravelling the intricacies of this physiological phenomenon.

Over the preceding two decades, numerous on-chip wound healing assays based on microfluidics have been documented, utilizing diverse microchannel designs to create cell-free areas through either cell depletion or cell exclusion[129], as illustrated in Figure 19. In the context of cell depletion, various principles such as thermal, electric, enzymatic, or mechanical methods are employed to remove portions of cells from confluent monolayers, resulting in designated cell-free wound areas. Conversely, microfluidic assays for cell exclusion employ mechanisms to prevent initial cell adhesion on specific substrate regions using an actuated structure or removable cover before the introduction of cells, thereby creating a wound defect upon subsequent removal of the structure obstructing cell attachment.

Zhang et al. employed microfluidic technology to establish an *in vitro* wound-healing assay based on the exclusion method, utilizing pillar structures to create wound areas[130]. Employing the PDMS pillar approach, the authors investigated the stimulatory effects of EGF, revealing a 50% increase in cell proliferation and a concentration-dependent rise in cell migration speed. Poujade et al. utilized micro stencil cell exclusion to assess focal adhesion quality on diverse substrates, such as cell-culture plastic and fibronectin-coated glass and examined the overall impact of bio-interface properties on wound closure speed[131]. Gao et al. presented a wound-healing assay based on multi-layered microfluidics[132], inducing a cell-free area through mechanical force between two microchannels. The subsequent pressure release facilitated cell migration into the cell-free areas, thereby enhancing the inhibition of melanoma cell migration over 18 hours, employing a minimal number of EGFR+ and BRAFV600E wild-type MV3 cells. Despite presenting a viable tool for personalized wound healing applications with minimal cell requirements, the primary focus of the study lays in the domain of cancer biology.

Hani Go's[133] group designed microfluidic devices wherein murine fibroblasts were cultured. Upon reaching confluence, external pressure damaged the cell mat, involving the removal of cells from areas in contact with micro-structured pillars and introducing pneumatic actuators into the chip.

In addition to mechanical depletion or exclusion methodologies, enzymatic detachment emerges as another frequently employed technique for creating wounds, involving the depletion of cell-free areas through the application of enzymatic detachment solutions over portions of confluent cell monolayers.

Nie et al. provided a detailed account of a migration assay for NIH-3T3 fibroblasts, employing enzymatic wound creation through hydrostatic laminar flow patterning of trypsin/EDTA on one side of microfluidic channels[134]. Similarly, Lin et al. investigated the impact of shear and wound size on the migration and closure speed of NIH-3T3 fibroblasts, utilizing a PMMA-based microdevice. Their findings indicated that an increased flow rate significantly accelerated wound healing in 6-mm-wide defects compared to 3-mm-wide defects[135]. However, fibroblasts subjected to higher shear forces before wounding in 3 mm channels exhibited slower migration speeds. Conant et al. also examined the proliferation and migration speed of rat epithelial cells under starvation conditions[136].

Wie et al. delved into the effects of microchannel height, surface coating, and chemokine stimulation on the migration rate of primary human vascular smooth muscle cells, affirming that FBS, PDGF, TNF-α, and chamber height positively influenced cell migration speed[137]. Conde et al. employed a single-channel microdevice with three inlets to enzymatically induce a central wound area with two opposing wound edges on melanoma cell monolayers[138]. Similarly, Lee et al. conducted a wound healing assay on NIH-3T3 fibroblasts[139], investigating how the orientation of surface nanopatterns could expedite wound closure.

Furthermore, van der Meer et al. utilized an enzymatic wound-healing chip for Human Umbilical Vein Endothelial cells (HUVEC) monolayers, revealing that VEGF gradients and fluid shear enhance endothelial cell migration speed. However, shear significantly impacts migration directionality along the fluid flow direction[137]. Murrel et al. analysed the influence of enzymatic cell depletion at the leading edge of tight epithelial cell layers on cell spreading and motion, concluding that reactive oxygen species generation plays a vital role in inhibiting cell migration[140].

Jeong et al. presented a migration assay for endothelial cell migration and sprouting using microfluidic chip technology[141], offering endothelial cells a 3D microenvironment in two scaffold channels to examine the impact of growth factors on cell migration behaviour. Shih et al. advanced a conventional enzymatic endothelial wounding assay with an on-chip chemical oxygen concentration generator, demonstrating that oxygen gradients have a more significant influence than homogeneous hypoxic oxygen tension on the directionality of endothelial cell migration towards low oxygen concentrations[142]. Only the gradient, not stable hypoxia, induced this migratory directionality, unaffected by migration inhibitory drugs.

Similar to the actuated pillar methods mentioned earlier, Sticker et al. developed two microdevices for automated cell migration assays, employing both cell exclusion and cell depletion methods for wound creation[143]. Both devices comprised three layers, with the middle layer being the point of distinction. The cell depletion device included a top pneumatic layer, a middle PDMS layer, and a bottom layer with multiple microchannels. This technology platform facilitated highly automated and reproducible wounds for both methods, demonstrating how TNF-α and mitomycin C decreased wound healing speed. In a follow-up study, Monfared et al.[100] adapted this approach using PDMS rapid prototyping through xerography to automatically create more wounds with a single pneumatic actuation cycle. The authors applied their microsystem to explore the impact of medium supplements, such as growth factors and proliferation inhibitory drugs, on HDF cell migration. For instance, fibroblast stimulation with bFGF increased fibroblast wound closure while enhancing migration distance, whereas Mitomycin C decreased the cell migration rate due to proliferation inhibition. The MEK inhibitor U0126 exhibited no effect on migration speed and total wound closure relative to untreated control samples, selectively inhibiting only cell proliferation by approximately 32%. With a relative standard deviation of around 3%, both mechanical studies outperformed the standard deviation of conventional scratch assays independently of cell type (e.g., endothelial or fibroblast cells) and wound diameter (e.g., 1 vs. 1.5 mm^2), highlighting how reproducibility and comparability of wound-depletion approaches can be improved.

Shaner et al.[144] proposed an innovative work in which the impact of direct current stimulation on wound healing in healthy and diabetic *in vitro* models of human keratinocytes has been evaluated.

The researchers used a compact bioelectronic platform with non-metal electrode materials and microfluidic design to study the effects of different sustained electric field configurations on wound closure dynamics. They compared the effectiveness of a unidirectional electric field (closing the wound's gap from one edge) and a pseudo-converging electric field (alternatingly polarizing both edges) in promoting wound closure.

The study suggests that controlled electrical stimulation can be a viable approach to accelerate wound repair and provides a baseline for developing optimal electrode designs for *in vivo* direct current stimulation.

The limit of all these works is that wound healing processes are investigated by simply monitoring the migration and proliferation of the cells with an optical microscope, not allowing an exploration of inflammatory processes and the formation of a new reconstituted matrix which may lead to the generation of scar tissue.

Only in this work[145] there is an attempt to simulate an inflamed 3D microenvironment. It describes a microfluidic device consisting of three interconnected channels in which fibroblasts, endothelial cells and macrophages are seeded, with the final goal of being able to model the inflammatory phase during wound healing following the introduction of a pro-inflammatory factor, TNF-α. In this case, however, the cellular layer is not damaged, so no formation of fibrotic tissue is mimicked, but the purpose is to recreate a three-dimensional culture system by immersing the cells in Matrigel, representing the limit of the exogenous matrix.

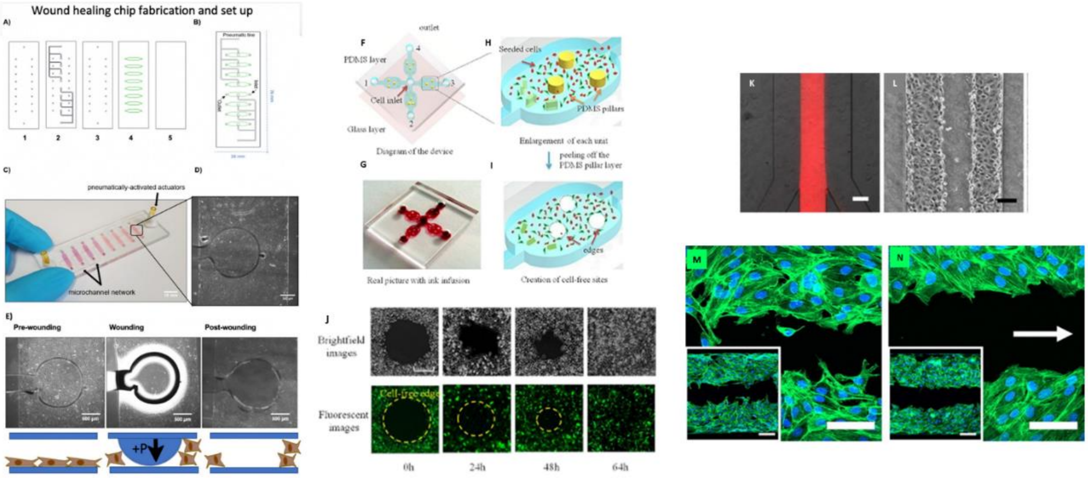

Figure 19 - Microfluidic wound healing assays: (A-E) Schematic illustration of the pneumatic wound healing-on-a-chip microdevice. (E) Illustration of the on-chip cell depletion procedure including a pre-wounding stage for monolayer growth, a wounding stage where pressure is applied on the flexible membrane and a final analytical post-wounding stage where the cell migration of fibroblasts into the wounded cell-free area created by membrane deflection is analysed over time. (Scale bar = 500 µm). (F-I) Microfluidic device for physical cell exclusion (J) Brightfield images of cell migration at 0, 24, 48, and 64 hours. Fluorescence images at the same time points. Cell-free areas at 0 hours are about 0.5 mm^2*. Cells are stained with a green live cell tracker. Scale bar = 0.4 mm. (K) Enzymatic microfluidic wound healing chip. (L): micrograph of a wound that was prepared by treating an endothelial monolayer with parallel trypsin- and serum-containing fluid flows in a microfluidic device. Scale bar, 100 µm. (M-N) Influence of flow direction and shear stress (arrow) on endothelial cells migration. Scale bars of close-ups, 50 µm. Scale bars of insets, 100 µm.*

Chapter 3: Decryption of the healing dynamics: Exploring cellular responses and ECM tissue healing in a 3D-HDE after a secondary intention wound.

3.1 Introduction

Injuries and scarring are highly complex biological processes that have been extensively studied in the scientific literature[1,146–148]. The study of these phenomena is of paramount importance, as injuries and scarring can have a significant impact on both physical and emotional well-being, particularly in cases of severe or disfiguring injuries. Understanding the underlying mechanisms of injury and scarring is essential for the development of effective treatment strategies.

One of the key organs to analyse and deepen our understanding of these phenomena is the skin and in particular the dermis. The skin is the largest organ in the body and plays a critical role in protecting us from external threats. The dermis, which is the layer of the skin that contains the majority of the cells and ECM that participate in injury and scarring, is of particular interest to researchers. The dermis is composed of various cell types, such as fibroblasts, which are responsible for the production of the ECM, and the ECM itself is composed of various proteins and polysaccharides that provide structural and functional support to the skin.

To better replicate the cellular and extracellular aspects of these phenomena, bioengineers and researchers have developed *in vitro* derma 3D models. These models are particularly useful because they allow for the study of cellular and extracellular processes in a controlled and isolated environment[101,103].

The quest to solve the enigmatic nature of wound healing has led to multifaceted investigations that explore the complexity of cellular behaviours and the molecular dynamics that govern tissue repair.

Cell migration plays an essential role in tissue repair and regeneration processes. While, during the inflammatory phase, immune system cells respond to chemotactic signals with individualized movement, tissue cells, such as epithelial and endothelial cells, coordinate their migration in the damaged space through a phenomenon known as collective cell migration[149,150]. This process involves a coordinated movement of cells, resembling a "cellular train"[150], characterized by rapid formation and dissolution of cell junctions.

On the other hand, fibroblasts, a cell type renowned for its multifunctional role in the secretion of ECM components, in tissue microenvironment modulation and help in wound closure, exhibit a tendency to interact more intensely with the surrounding matrix[101], minimizing the formation of cell junctions. Responding to chemotactic and hapoptatic signals, in addition to being influenced by the mechanical properties of the substrate, their coordinated movement is of an *en mass* type[11,12]. They move grouped, responding to the same cues, signifying the initiation of the process of new tissue formation and remodelling.

Fibroblasts, upon activation, turn into myofibroblasts, marked by the expression of α-SMA, and begin the deposition and remodelling of ECM proteins[151].

Understanding the intricate molecular environment that governs wound healing and the behaviour of fibroblasts has been a primary focus of contemporary research efforts. During this exploration, the need for robust and physiologically relevant models to emulate the repair of human dermal tissue led to the choice of 3D-HDE models.

Unlike conventional models presented in the previous chapter, these 3D endogenous models offer an unprecedented advantage by closely mimicking the structural and functional attributes of native tissues[73–75,104], providing a superior platform for dissecting the complexities of wound healing.

The importance of using 3D endogenous models lies in their ability to summarize the dynamic interaction between fibroblasts and the ECM, favouring a microenvironment conducive to studying the complexities of wound closure, fibroblast migration, and ECM remodelling. The authenticity of these models in reflecting the physiological complexities of tissue repair positions them as indispensable tools to clarify the enigmatic aspects of wound healing.

The intricate dynamics between fibroblasts, ECM components (including collagen, fibronectin, and tenascin) and temporal regulation of MMPs during the wound repair process remain focal points. Deciphering their profiles of interaction, modulation, and temporal expression serves as a cornerstone to reveal the precise molecular events that govern tissue regeneration and scar formation.

In this sense, this study undertakes an in-depth exploration of fibroblast-ECM interactions within a 3D-HDE model, intending to interpret fibroblast migration dynamics, ECM remodelling, and the role of the main molecular actors during the process of wound closure.

3.2 Materials and Methods

3.2.1 Cell source

Human dermis biopsies from the breast of 25- or 45-year-old donors have been used for the extraction of HDFs. These biopsies have been obtained after the approval of the ethical committee (Prot.N. 00019018).

The HDFs at passages 5-7 were subcultured onto 150 cm^2 cell culture flasks (VWR 734-1719) in a complete culture medium composed of E-MEM (VWR 392-0424) containing 20% FBS (Merck F7524), 100 mg mL^{-1} l-glutamine (Merck G7513-100ML), 100 U mL^{-1} penicillin/streptomycin (Sigma-Aldrich P4333-100ML), and 0.1×10^{-3} m Nonessential Amino Acids (Thermo Fisher Scientific 11140050).

3.2.2 3D-Human Equivalent Dermis fabrication

According to a well-characterized and optimized bottom-up approach protocol[76], *in vitro* 3D-HDE tissues of 13 mm diameter and 1 mm height were manufactured.

Briefly, precursors to HD-µTPs were produced by HDF coculture with porous gelatine microspheres in a spinner flask and used as basic elements for the manufacture of macroscopic 3D-HDE.

The porous gelatine microbeads were produced using a modified double O/W/O emulsion technique. Gelatine type B (Sigma-Aldrich Chemical Company, Bloom 225, Mw = 176 654 Da) was added in water preheated to 40 °C containing TWEEN 85 (6% w/v) (Sigma-Aldrich Chemical Company) to get the water phase. In parallel, the oil phase comprising toluene and SPAN 85 (3% w/v) (Sigma-Aldrich Chemical Company) was heated at 40 °C. The oil solution was dropwise added to the aqueous solution (8% w/v) to obtain an O/W/O emulsion. The resulting microspheres were filtered, and 4% glyceraldehyde was used to ensure stability in an aqueous environment at body temperature. HDFs and porous gelatine microspheres were placed in a spinner flask bioreactor and after 10 days of culture, these cells were able to produce and assemble dermal ECM components generating the HD-µTPs. The HD-µTPs were then moulded into maturing chambers for six weeks. Biological sintering among HD-µTPs led to the formation of a completely scaffold-free dermal structure, the aforementioned 3D-HDE. The maturation chambers used in this work consisted of a silicon mould with 4 circularly shaped sites with dimensions of 13 mm in diameter where HD-µTPs were seeded. They have been closed with porous stainless-steel grids, which support enhanced mass transport and nutrient exchange for tissue growth. They were placed at the bottom of a spinner flask bioreactor and completely covered by culture medium for 6 weeks. The culture media was replaced every 3 days for the first two weeks, then it was changed once a week. Ascorbic acid was added together with the medium at a concentration of 50 µg/mL, which promotes collagen production and organization, contributing to the formation of a human dermis more similar to the natural one.

3.2.3 3D Wound Experimental set-up.

As the maturation phase was completed (Figure 20a), the wounding experiment started. Due to the presence of 3D models incorporating an endogenous matrix, executing a secondary intention wound becomes straightforward, given the availability of a pre-existing matrix. Full-thickness excision wounds (Figure 20b, c) were made using a sterile 1 mm punch biopsy (Ted Pella Inc.) by laying the sample on a PDMS substrate (Figure 20). The HDEs were placed in 35 mm fluorodishes (World Precision Instruments) to ensure optical accessibility and blocked inside it through a custom-made PDMS mold (Sylgard 184, Mascherpa), (Figure 20d). This mould serves a double purpose: to prevent a strong contraction of the tissue mediated by the active fibroblasts and to keep the HDE, and especially the wound inflicted, in the same position so you can make scans over time, sure to still capture the same XY coordinates.

These moulds were obtained by demoulding PDMS from a PMMA (Goodfellow) stamp previously fabricated on the micromilling machine (Minithech CNC Mini-Mill).

The PMMA masters were designed by AutoCAD software that generated a CAD file, which was subsequently converted into a CAM format by using Deskam. The CAM file was read by the Micromilling machine, and a positive relief geometry was printed by digging on the PMMA slab.

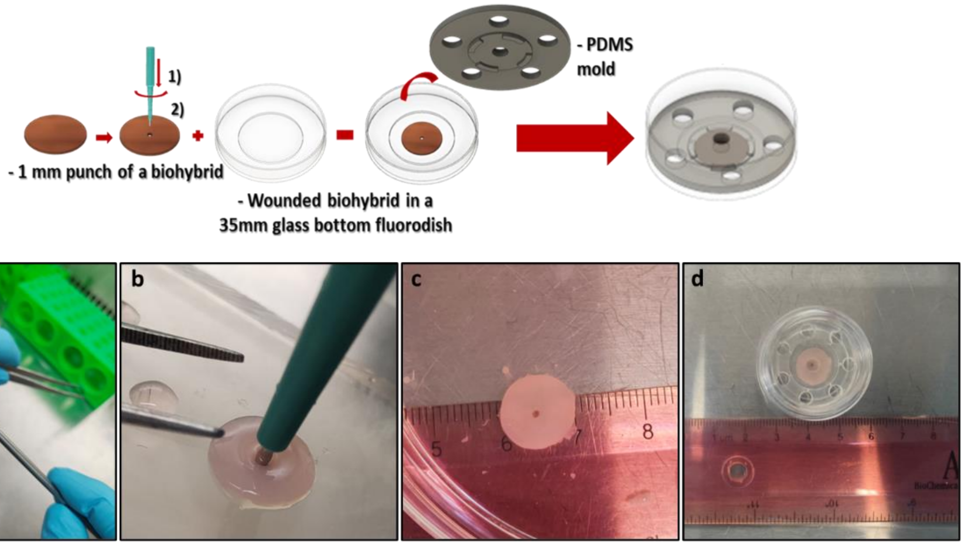

Figure 20- Schematic sequence of a punch conducted on a 3D-HDE: a) 3D-HDE freshly extracted from the maturation chamber, b) punch applied to the 3D-HDE; c) image of our model after replicating the secondary intention wound; d) 3D-HDE inside the fluorodish and blocked with a PDMS mould.

3.2.4 Image acquisitions and time-lapse microscopy

As soon as the lesions were done on the samples, the wound closure dynamics were monitored over time, capturing photos every day in brightfield. This allowed us to follow the evolution of the process, helping to determine how long the tissue takes to heal the wound and to individuate the characteristic times in which to follow the samples with time-lapse video.

For time-lapse acquisitions, wound regions were acquired every 20 min for 18 hrs, starting from day 4 after wounding up to the closure day.

HDEs were, then, stained with Hoechst 33342 (ThermoFisher) 1:10000 v/v in complete E-MEM for 30 min at 37 °C in agitation. This was a live nuclear fluorescent staining technique that helped track cells during the closure days.

Brightfield images and time-lapse videos have been acquired with an Inverted Fluorescence Motorized Microscope (Zeiss Axio Observer 1) equipped with an incubation system with either a 10X or 20X magnification lens.

3.2.5 Traction Force Microscopy

To assess matrix deformation within 3D-HDE following wound induction, HD-µTPs were assembled within maturation chambers alongside fluorescent carboxylate microspheres measuring 6 µm in diameter (Polysciences 18141-2, excitation/emission: 441 nm/486 nm). Time-lapse acquisitions of the fluorescent microspheres were conducted at 20-minute intervals for 7 days, from the initial wound creation to closure. Time-lapse images have been acquired with an Inverted Fluorescence Motorized Microscope (Zeiss Axio Observer 1) equipped with an incubation system with a 10X magnification lens.

Post-acquisition, image processing involved the extraction of fluorescent particle signals while eliminating background noise and drift. This meticulous processing step isolated the component of motion attributed specifically to matrix contraction initiated by fibroblasts, effectively mitigating any unintended sources of movement.

Then two consecutive images at a time, representing the initial, undeformed state, and the subsequent deformed state were considered.

Subsequent analysis of these refined images was conducted through the application of TFM and PIV techniques to quantitatively assess and characterize the resultant field of deformations throughout the experimental timeline. The deformation field was analysed by the PIV plugin[152] within the ImageJ software.

Each image is subdivided into small interrogation regions for analysis, and within each section, the displacement vector between the two images is computed using cross-correlation techniques. The interrogation window size underwent iterative reduction, starting from 256 x 256 pixels down to 64 x 64 pixels, conducting 3 iterations at each window size variation. The overlap between interrogation windows was set to 50% for all window sizes.

3.2.6 Mathematical models of cell migration and tissue deformation

To mathematically model cell migration, two computational approaches were pursued. These approaches were aimed at elucidating the migratory behaviour of cells, specifically within the context of *en mass* fibroblast migration and wound-directed motion in our engineered dermis prototype.

MTrackJ, a plugin for Image J, was used to track fibroblast nuclei and characterize their trajectories from each time-lapse video.

The initial step involved the processing of cell trajectories. Using a first custom-made MATLAB script, this dataset was meticulously analysed to derive cell velocity distributions.

Moreover, a secondary computational analysis was executed to discern the peculiarities of cell migration concerning the distinctive wound shape, resembling an elliptical form. Employing another tailored MATLAB script, the raw cell trajectories were transformed into curvilinear elliptical coordinates, extracting crucial metrics such as ρ, θ, the radial velocity (v_ρ) and the angular velocity (v_θ) with the following equations:

$$\rho = \sqrt{\frac{(x-x_0)^2}{a^2} + \frac{(y-y_0)^2}{b^2}} \tag{3.1}$$

$$\theta = \begin{cases} arctag\left(\frac{a(y-y_0)}{b(x-x_0)}\right) + \pi, & x < 0 \\ arctag\left(\frac{a(y-y_0)}{b(x-x_0)}\right), & x \geq 0 \end{cases} \tag{3.2}$$

where a and b are, respectively, the major and minor semiaxis of the ellipse describing the wound perimeter and x_0 and y_0 are the centre of the ellipse.

$$v_\rho = \frac{\Delta\rho}{\Delta t} \tag{3.3}$$

$$v_\theta = \rho\frac{\Delta\theta}{\Delta t} \tag{3.4}$$

From this, one can derive the expression for total velocity:

$$v = \sqrt{v_\rho^2 + v_\theta^2} \tag{3.4}$$

This transformation was crucial to align the cell movements with the wound's elliptical configuration.

Furthermore, this elliptical transformation facilitated a nuanced exploration of cell migration tendencies—whether tangential or radial concerning the wound. By assessing the angle formed between the tangent at a specific point on the ellipse, dictated by the cell's position (ρ, θ) and the velocity vector, the inclination of cells to migrate either tangentially along the wound's periphery or radially towards the centre was comprehensively evaluated. Additionally, discerning the directional migration pattern, whether clockwise or counterclockwise, was a crucial aspect of understanding the orchestrated motion of cells around the wound site.

To assess the direction of cell movement, an approach based on the angle θ was employed. The derivative of θ with respect to time was computed to identify the angle's variation along cellular trajectories. It was hypothesized that an increase in the θ over time corresponded to a positive derivative, indicating cell movement in an anti-clockwise manner concerning the ellipse. Conversely, a decrease in θ over time was associated with a negative derivative, suggesting cell movement in a clockwise direction relative to the elliptical trajectories.

Finally, to strengthen the analysis of the collective motion of fibroblasts, the distribution of the intercellular distances (d) and the directional correlation were evaluated.

The intercellular distance between two cells in curvilinear elliptical coordinates was computed with the following equation:

$$d = \sqrt{\rho_i^2 + \rho_j^2 - 2\,\rho_i \rho_j \cos(\theta_i - \theta_j)} \qquad (3.5)$$

Where i and j are referred to the two cells.

The alignment of cell movements was estimated by calculating the directional correlation between two trajectories at overlapping time points[153]. Directional correlation measures how closely cells move together: a value of 1 indicates they move perfectly in parallel and in the same direction, while -1 suggests they move in parallel but in opposite directions. This directional correlation, defined as $\cos(\theta_{i,t} - \theta_{j,t})$, was computed for each overlapping time frame. By averaging these correlations across all overlapping time points, we assessed the overall similarity in migration direction between different cell trajectories. This comparison was then related to the distance between the cells at the start of their paths d.

To evaluate the dynamic interplay between migrating cells and substrate deformation, our objective was to isolate the elastic contribution within the total deformation tensor previously discussed. This involved a process aimed at extracting solely the elastic component by removing the growth-related contribution.

In biological tissue deformations, it is crucial to recognize the presence of two primary contributors[154,155]: the elastic deformation developing from mechanical responses and the deformations induced by growth processes. These deformations occur concurrently and are combined within the overall tissue deformation, creating a comprehensive tensor representation,

$$F = F_e \cdot F_g \qquad (3.6)$$

where F is the total deformation tensor, F_e represents the elastic deformation tensor, and F_g signifies the growth-induced deformation tensor.

Conceptually (Figure 21), the idea of growth originating from the reference configuration B_0 illustrates a pure growth F_g, transitioning an elastic body from B_0 to a stress-free configuration B_g. Post-loading, the body undergoes deformation into the current configuration B_t via an elastic deformation gradient F_e.

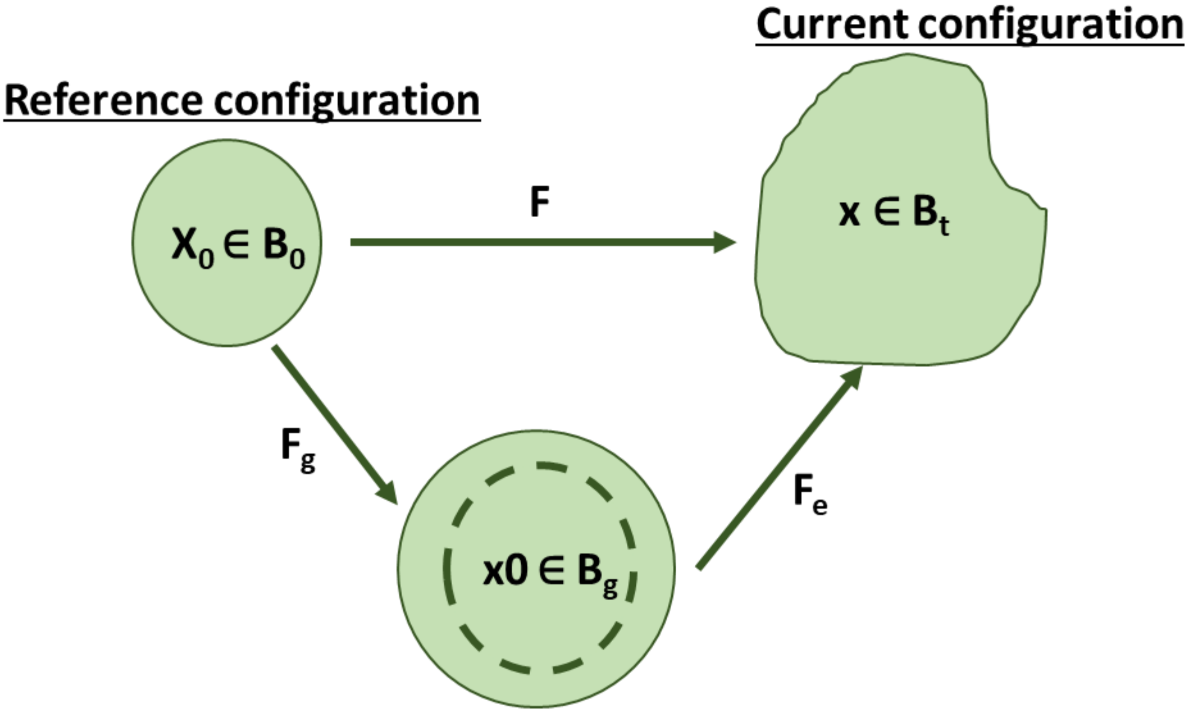

Figure 21 - Kinematics of growth shows the intermediate configuration and decomposition of the deformation gradient into the growth and elastic components.

In the context of our analysis, the overall deformation gradient F encompasses both the effects of the pure growth and the elastic deformation gradient F_e. This understanding contributes significantly to delineating the distinct influences within tissue deformations, aiding in the isolation and evaluation of the elastic contribution F_e, during complex cellular and substrate interactions.

To compute F_e, one must first determine the growth-induced deformation tensor, F_g. Given that the tensor F is the one evaluated with the TFM technique, it encapsulates the spatial coordinates of fluorescent particles P along with the deformation incurred; the construction of F_g necessitates compatibility with F to facilitate inversion.

Identifying the growth contribution entails examining time-lapse brightfield videos capturing wound closure over seven consecutive days. The growth contribution becomes discernible where new material, comprising new cells and ECM, visibly fills the wound area.

To discern this specific growth contribution, filtration is performed on points P within the F tensor, residing within the region of active growth. This region is demarcated by two ellipses delineating the wound's perimeter at the beginning and the end of each day. Points P falling within these ellipses denote areas experiencing ongoing material growth (Figure 22). They must obey this mathematical notation:

$$P(x_p, y_p): F_1(x, y) < 1 \cup F_2(x, y) > 1 \tag{3.7}$$

Where F_1 and F_2 are the equations describing, respectively, the outermost and innermost ellipses. Their formulation is the following:

$$F(x, y) = \frac{(x - x_0)^{\,2}}{a^2} + \frac{(y - y_0)^{\,2}}{b^2} \tag{3.8}$$

in which

$$\begin{gathered} x = x' \cos\alpha + y' \sin\alpha \\ y = -x' \sin\alpha + y' \cos\alpha \end{gathered} \tag{3.9}$$

Also considering the inclination of the ellipse by an angle α.

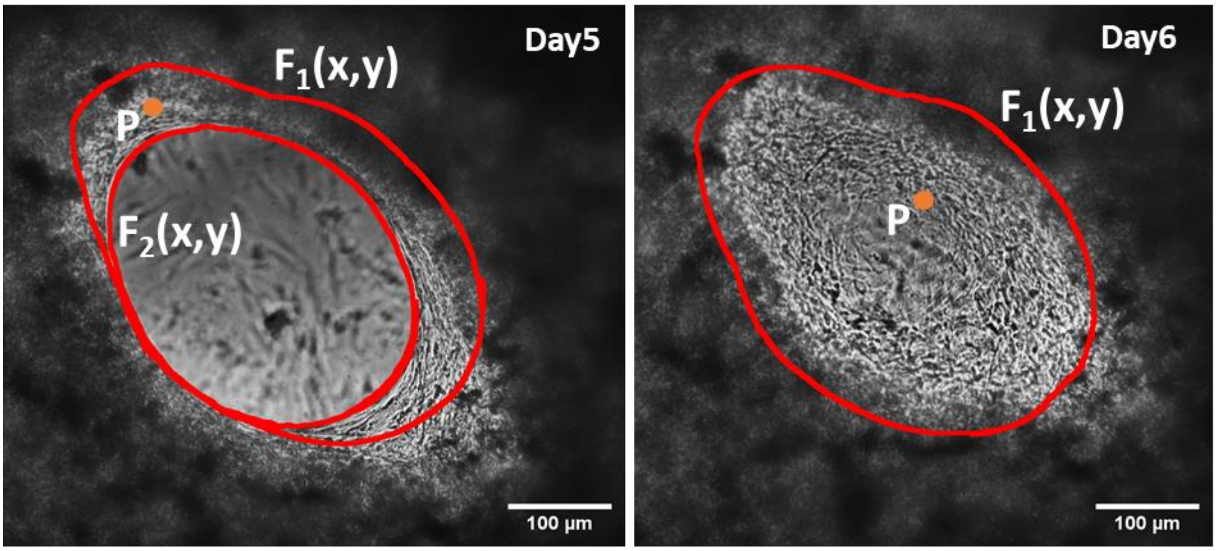

Figure 22 - Determinations of the points belonging to the growing area, identified by the two ellipses F_1 *and* F_2*. Original magnification 10x, scale bar 100 µm.*

Subsequently, local growth-induced deformations at these identified points are computed using the canonical definition:

$$\varepsilon_g = \frac{A_f - A_i}{A_i} \qquad (3.10)$$

Where A_i and A_f refer to the area of the wound at the beginning and the end of the day.

Here, A_f is derived by the integral definition of the ellipse's area based on its major and minor axes alongside the x_1 and x_2 which are the abscissae obtained when the line passing through point P intersects the ellipse.

$$A_f = 4\int_{x_1}^{x_2} b \cdot \sqrt{1 - \frac{x}{a^2}} dx \qquad (3.11)$$

Once these localized growth contributions ($\boldsymbol{\varepsilon}_g$) are established, the growth-induced deformation tensor (F_g) is constructed. Utilizing relationship 3.6, the elastic deformation part (F_e) within the tissue deformation tensor can be calculated.

3.2.7 Morphological characterization of 3D-HDE wound healing process.

Brightfield acquisitions quantifications

Measurements of the wound area from time-lapse photos and videos were made using Fiji. In particular, once the files were uploaded into the software, they were converted to 8-bit. Thus, to discriminate the "full" region of tissue from the "open" region of the lesion, enhancement of the contrast was applied to improve tissue perception in images by improving the difference in brightness between the tissue and its background. To further distinct the gap from the tissue edges a Sobel filter was applied.

Since the open wound area might contain single cells or cell islets, to avoid these regions as part of the wound, images were thresholded and binarized to perform morphological operations: erosion, which smoothes objects and fills in small holes, and Fill Holes, this command fills cavities in objects by filling the background. Erosion will make the binary image objects smaller, as a pixel will be adjusted to the background value if other pixels in the neighbourhood are in the background. It may divide single objects into several.

The hole-filling operator detects all connected components enclosed in the wound area and incorporates them into the wound.

In the end, the wound area was selected with Fiji's magic wand tool and placed in the ROI manager to be measured later.

Once collected the wound area measurements of each day, they were normalized with respect to the area of the wound measured immediately after punching:

$$A(t)|_i = \frac{A_i}{A_0} \cdot 100 \tag{3.12}$$

where A_i is the area measured the ith day after the wound is performed and A_0 is the area measured soon after injury.

Confocal and multiphoton imaging

Characteristic time points were chosen to fix the tissues and to make the morphological analysis of some of the components which are fundamental in the wound healing process. In particular, to try to reproduce the entire wound healing process, days 0, 2, 4 and 9 were chosen to study the process from the day of injury (day 0) to the day of closure. Even though closure occurs after 7 days, we chose to fix the tissue on the 9th day to let the healed wound stabilize. After this, days 14 and 21 were also selected to evaluate the phenomena of maturation and remodelling.

Fluorescence staining

Samples were fixed in Formalin solution (HT501320-9.5 L Merck) overnight at 4°C and washed three times in PBS1X. They were permeabilized using 0,1% Triton (Triton X-100T9284-100ML Sigma) in PBS1X for 5 min at RT, washed in PBS 1X and blocked in 1% BSA (A9418-100G Sigma) for 1 h at RT. For the detection of specific molecular structures, HDEs were incubated with primary antibodies. For the recognition of cellular markers, α-SMA and vimentin expression was identified respectively with anti-α-SMA (ab5694, Abcam, Rabbit Polyclonal) and anti-vimentin (ab8978, Abcam, Mouse Monoclonal) antibodies both diluted 1:100 in blocking solution. To identify ECM proteins, anti-fibronectin (F0791-100UL, Merck, Mouse Monoclonal) and anti-tenascin C (ab86182, Abcam, Mouse Monoclonal) antibodies were used both diluted 1:100 in bocking solution. Furthermore, MMP-1 secreted by cells after the wound was quantified by using anti-MMP-1 (ab3899, Abcam, Rabbit polyclonal) diluted 1:100 in blocking solution. Samples were left in the solution with the antibodies overnight (ON) at 4°C in the dark and in continuous agitation to homogeneously add antibodies everywhere. The morning after, a Goat Anti-Rabbit IgG (H + L) Secondary Antibody Alexa Fluor 546 (A11035 diluted 1:500 in PBS1X) and a Goat Anti-Mouse IgG (H + L) Secondary Antibody Alexa Fluor 488 (A11029 diluted 1:500 in PBS 1X) were used for 1 h at RT. The nuclei of all the cells were stained with DAPI (Sigma-Aldrich D9542) diluted 1:10.000 in PBS 1X for 20 min at RT.

Samples were investigated by Confocal Leica TCS SP5 II by using a 40-water immersion objective. Z-stacks were done in the wounded region and in the unwounded region to make comparisons.

Morphological analysis of the wound closure process

Images and z stack were analysed using Image J. For each image, 10 ROIs were chosen both in the region of the expressed marker and in the background region. To calculate the CTF the following formula was used:

$$\begin{aligned}&\text{CTF}\\&= \text{Integrated Density}\\&- (\text{selected Area X Mean Fluorescence of background regions})\end{aligned} \tag{3.13}$$

Moreover, in the same regions of interest, the number of nuclei was evaluated through the “Analyse particle” plugin in Image J. This was done to normalize the fluorescence data with the number of cells.

SHG

SHG imaging was performed after tissue fixation in Formalin overnight at 4°C and washing in PBS 1X. Whole samples were investigated by Two-photon excited fluorescence (Leica TCS SP5 II coupled with a Multiphoton Microscope stage Chameleon Compact OPO-Vis, Coherent) to induce SHG and obtain high-resolution images of unstained collagen structures. Samples were observed by using λex = 840 nm (two photons) and λem = 415–425 nm. Z-stacks were performed in the wounded region and in the unwounded region to make comparisons. The SHG stacks were acquired with a resolution of 8 bit, 1024·1024 pixels, by using a 25-water immersion objective (HCX IRAPO L 25.0 0.95 Water, n.a. 0.95).

Collagen amount quantification

Neo-synthetized collagen fibres were further quantified from SHG images thorough ImageJ software. Since the collagen in the SHG images is related to the brighter pixels, Collagen Fraction (%) was defined as the percentage of the ratio between bright pixels to total pixels in the image:

$$\text{Collagen Fraction }(\%) = \frac{N_C}{N_{TOT}} * 1000 \tag{3.14}$$

Where N_c and N_{TOT} represent, respectively, the number of pixels of the collagen region and the total image.

3.2.8 FFT analysis

Cell nuclei and collagen fibres orientation was determined by making use of the FFT plugin of Image J. Exploiting the FFT function, the information contained in an image is converted from a “real” domain to the frequency domain. The results obtained from this mathematical tool represent grayscale pixels disposed in a pattern representative of the nuclei and/or the collagen fibres alignment.

The transformed images were rotated by 90 degrees to correct the mathematical transformation driven by the FFT, to easily identify the main axis of orientation from the position of the peak in the resulting intensity graph.

To graphically visualize how FFT frequencies are distributed, the Oval profile plugin of Image J (author Bill O'Connell) was used. An oval ROI is then drawn on the image transformed into the frequency domain and, launching the aforementioned plugin, a radial sum of pixel intensities for each degree between 0 and 360 was done.

In our analysis, pixel intensities were summed along each degree and then, for some data, plotted between 0 and 180, because the FFT is symmetrical to the horizontal axis; this means that a sum of pixels at 360 degrees is redundant.

Statistical Analysis

Experiments were performed in triplicate and n=100 cells were chosen for the cell migration analysis. Data are expressed as mean ± SEM. Differences between groups were determined using the statistic test ANOVA Tukey HSD test. Significance between groups was established for p-value < 0.05.

3.3 Results and Discussion

3.3.1 The role of fibroblasts-ECM interaction in driving wound repair process.

To examine the response of 3D-HDE to damage, an injury was made in the centre of the tissue with a punch biopsy and then it was observed how it evolved (Figure 23a). Within 2 days after the full-thickness excision, the gap widened further. As the gap area stabilizes over the next 2 days, the rough edge of the wound smoothened to form an ellipse, a process that, as we will see later, may be related to the alignment and elongation of myofibroblasts along the edges of the wound. In the following days, the gap gradually closed, while maintaining its elliptical shape and keeping the central position of the wound steady, thanks to the use of the mould in PDMS.

Healing of HDEs was observed to occur within approximately one week (Figure 23b) progressing from the bottom to the top.

The initiation of the wound closure process appears to have started on day 4, as depicted in Figure 23b, where a noticeable decrease in the initial area is evident. This reduction is clearly observed in the wound area versus time graph through the downward slope of the line, indicating a progressive decrease in size over time. Here, the fibroblasts began to turn along the edge of the wound to repair the torn flaps. In this way, they released collagen fibres oriented in the direction of their motion to thicken the domain, fortify the structure, and create additional tracks that allow the cells to migrate (Figure 23c). This trend is kept even after the gap is closed. The alignment between cells (depicted in blue) and collagen (depicted in grey) is clearly discernible in the SHG images presented in Figure 23c-left, both on day 4 and day 9. These entities exhibit orientation along the same direction, a characteristic highlighted by the angles depicted in the FFT graph in Figure 23c-right. This demonstrates that activated fibroblasts play a pivotal role as the primary stromal cells responsible for synthesizing ECM components, predominantly collagen. Moreover, it emphasizes that the success of the tissue repair process relies heavily on the intricate interconnection between cells and ECM - a noteworthy advantage of our proposed model. Furthermore, our endogenous model simplifies the tracking of cell-ECM alignment, as the matrix is dynamically synthesized and remodelled by the same cells, rather than being a mere inert material.

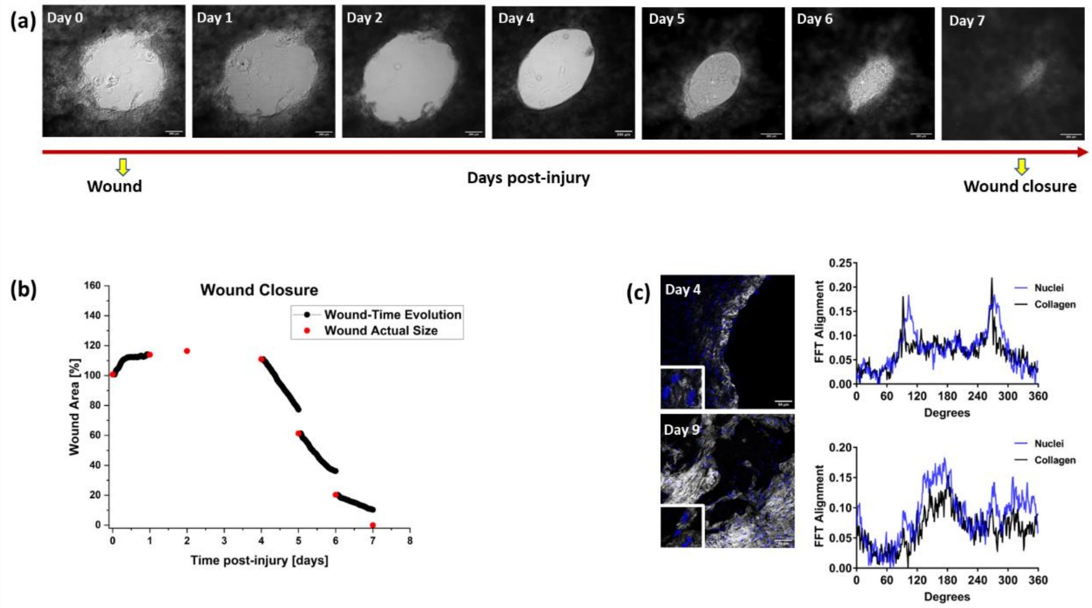

Figure 23 - 3D-HDE wound healing process: (a) Micrographs of 3D-HDE before, during and after damage. The light grey zone delimits the gap area (original magnification x10, scale bar 200 µm). (b) Plot showing the wound area as a function of time. (c) Analysis of cell directionality and orientation of collagen fibres: (c-left) Confocal images of collagen fibres and nuclei on day 4 and day 9 (original magnification 40x, scale bar 50 µm), (c-right) graphical plots after radial summation of pixel intensities depicting FFT alignment along orientation angles.

3.3.2 Effect of dynamic ECM deformation on *en mass* fibroblast migration

Fibroblast migration was tracked from day 4 until closure. This time frame was chosen strategically, as it became evident from time-lapse videos that, from day 4 onward, the wound initiated the closure process. In the preceding days, as we have already discussed, there was primarily an expansion of the wound due to the release of residual stresses, followed by stabilization. The decision to start cell tracking from day 4 aligns with the critical period when the hole began closing. On day 4 it was seen that when the wound began to heal, cells at the edges of the wound started to migrate in a tangential direction along the perimeter of the ellipse formed by the hole as highlighted by the coloured cell trajectories in Figure 24a.

This is evident from the small angles formed by the velocity vectors with the tangent to the ellipse, ranging between 0 and a maximum of 30 degrees. The predominant motion is tangential to the corresponding ellipse of the wound, as depicted in the rose plot in Figure 24b.

This interesting phenomenon can be further evidence of the dynamic and reciprocal relationship between fibroblasts and ECM. Fibroblasts, on one hand, are responsible for the deposition and spatial configuration of ECM components, and on the other hand, ECM molecules can influence intracellular events by also determining cell alignment with the matrix.

However, approaching the closing day, cells begin to deviate from a purely tangential motion. Cellular trajectories now exhibit a tendency towards the centre (Figure 24d), with angles ranging from 0 to 90 degrees, as depicted in Figure 24e. This shift in motion suggests a change in cellular behaviour as the closing day approaches, introducing a radial component to their migration patterns. The velocity distribution of fibroblast migration exhibited significant differences between the fourth and sixth days (Figure 24f, g). On day 4 (Figure 24f), velocities ranged from 0 to 30 µm/hour indicating an active migratory phase. However, by the sixth day, velocities decreased to a range of 0 to 15 µm/hour (Figure 24g), suggesting a potential slowdown in cellular activity due to the near-complete closure of the wound. This deceleration aligns with the natural progression of wound healing, where reduced cell activity follows the initial phase of tissue repair and granulation tissue formation. The variance in migration speed might also stem from increased ECM production, which fills gaps but simultaneously impedes cell movement. Interestingly, these observed speeds fall within the range of *in vivo* fibroblast migration during wound healing[156], ranging between 3.11 and 15 µm/hour, suggesting consistency between observed migration rates and those in biological contexts.

An intriguing aspect involves the directional behaviour of migrating cells. The recorded distribution of 65.5% clockwise and 34.5% counterclockwise movement suggests a predominant unidirectional migration (Figure 24c). Importantly, this trend persisted across three independent samples on both day 4 and day 6. This consistent pattern highlights the robust nature of the observed unidirectional migration among the sampled cells.

This uniform directional bias implies a coordinated response to a common stimulus, likely orchestrating migration around the healing site. Such behaviour might stem from growth factor secretion or structural cues, indicating a preference for coordinated cell movement during wound healing.

The coordinated and *en mass* nature of cellular migration is further supported by the close clustering of cells and the directional correlation analysis. This analytical tool underscores the consistency in coordinated cell movements and highlights the maintenance of synchronized migration, whether directed or random.

Intercellular distance analysis (Figure 24h) showed a decrease in distances between cells from day 4, ranging from 0 to 3 µm, to day 6, ranging from 0 to 2 µm (Figure 24i). This reduced intercellular distance might facilitate enhanced cellular cooperation, encouraging more *en mass* organized migration and tissue reorganization.

Finally, the analysis of directional correlation showed interesting behaviour. On the fourth day (Figure 24j), a positive directional correlation was observed when they were grouped (between 0 and 1 µm), followed by a decrease at greater distances to -1 indicating a directed motion but opposite, and then rearranged from 3 um upwards to directional correlations again positive. This suggests a possible relationship with the elliptical configuration of the wound and that even distant cells may feel the same stimulus and move together accordingly. Similarly (Figure 24k), day 6 exhibited analogous behaviour, further supporting a correlation between migration direction and the elliptical healing site morphology. It is important to note that while this specific migration pattern appears to be influenced by the elliptical shape of the wound, our HDE model can effectively represent wound dynamics across various geometries.

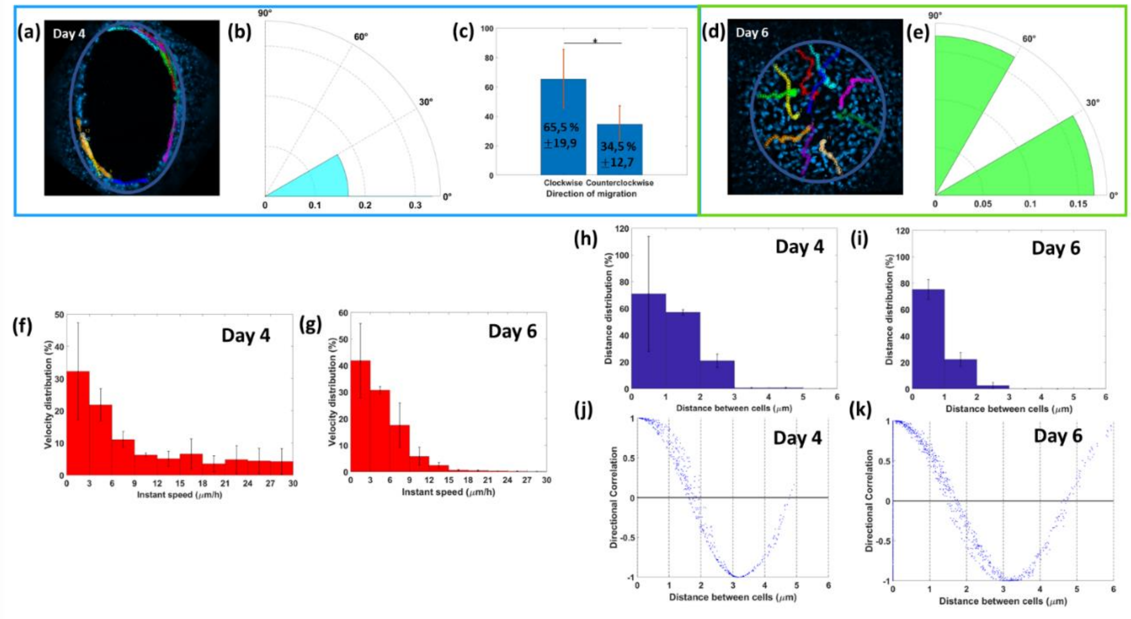

Figure 24 - Fibroblasts migration dynamics: (a, d) Representation of cellular trajectories on day 4 and day 6 depicting a tangential trend of motion at the beginning and a radial one at the end; (b, e) Rose plot showing the distribution of the angles between the tangent in a point (corresponding to the coordinates of a cell) and the velocity vector on day 4 and day 6 as a mathematical proof of the tangential or radial motion; (c) Tendency of the cells to migrate together in the clockwise or counterclockwise direction; (f, g) Cellular velocity distribution, expressed in µm/h, on day 4 and day 6 after wounding show values close to the physiological ones; (h-i) Intercellular distance distribution, expressed in µm, on day 4 and day 6 enhancing a grouped fibroblasts motion; (j-k) directional correlation of fibroblasts motion, on day 4 and day 6, with respect to the initial distance between the cells. *$p<0.05$

From this point onward, we evaluated whether this collective cell movement was in any way dependent on the ECM and the manner in which it deforms in response to the wound and cell movement.

We observed that, due to the interaction between cells and ECM, the dynamic remodelling of the matrix by the cells provides a deep influence, imprinting both the direction and speed of the *en mass* fibroblasts migration within the matrix, crucial to accelerate the healing process.

The migration of fibroblasts is closely related to the ECM environment, which undergoes significant transformations during the movement *en mass* of fibroblasts. This process is not only modulated by the mechanical signals of the ECM but also leads to a dynamic reshaping of the latter.

The deformation gradient generated in the matrix guides the movement of fibroblasts which preferentially migrate from low stiffness to high stiffness regions through a process known as durotaxis[157].

From the deformation analysis conducted on our endogenous matrices (Figure 25), we can appreciate an initial opening of the wound, which expands gradually, due to the release of residual stress, showing deformation gradients that extend outwards. After that, the cells exert tension along wound margins, helping to profile the initial shape in an elliptical configuration. The deformation gradients developed along the edges of the lesion could also justify the tangential movement observed around its edges. With the continuation of the migration process, in the last stage of closure, a gradient is observed that moves from the outside to the inside of the hole, which explains the radial movement of the cells towards its centre. This complex dynamic highlights the direct involvement of cells in modelling the matrix, with deformations reflecting the cooperation and coordination of fibroblasts during migration.

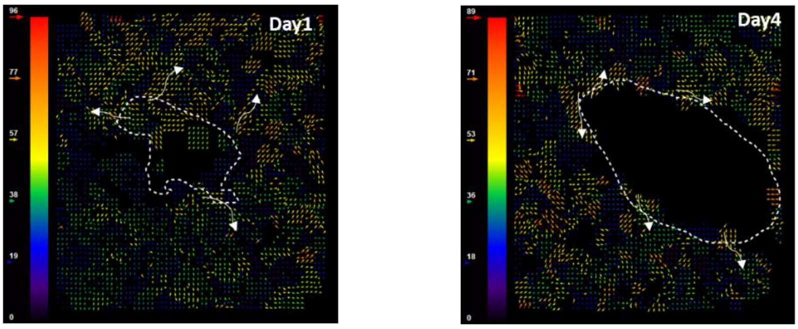

Wound opening **Wound smoothing and ellipse formation**

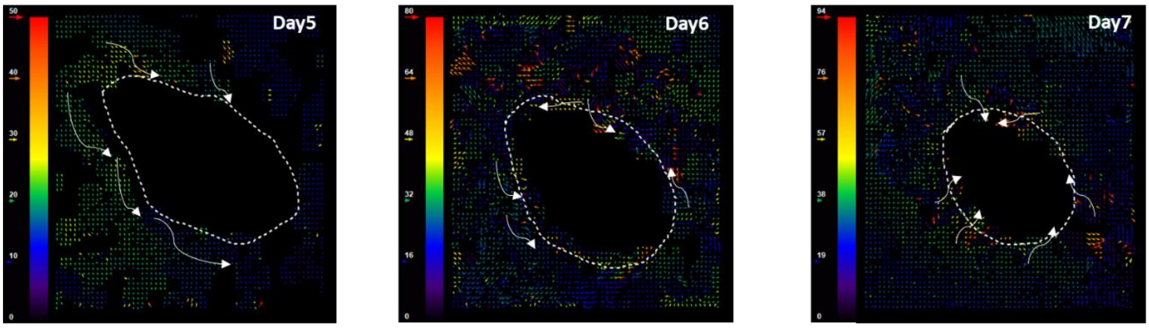

Direction of movement dictated by deformation gradient

Figure 25 - Deformation field maps spanning from the wound initiation to the closure day illustrate how deformation gradients, primarily driven by cell remodelling, play a pivotal role in orchestrating the collective behaviour of fibroblasts. The colour bar corresponds to the adimensional deformation values, while the dotted geometric shapes

delineate the wound perimeter for each day. Additionally, white arrows indicate the trajectories of individual cells at each corresponding day. All the images have the same magnification (original magnification 10x).

3.3.3 Fibroblasts activation and ECM rebuilding during dermal wound healing

Next to these considerations, it was evaluated if these equivalent models of the human dermis can summarize the wound healing pathophysiology. The expression and localization of α-SMA and vimentin were monitored over time (Figure 26a-down). As we expected, from the day of the injury the fibroblasts differentiate into myofibroblasts, recognizable by the expression of α-SMA. Figure 26 indicates that α-SMA reaches reasonably a peak at day 9 because myofibroblasts have both to close the wound by contraction and start to release ECM components. Its expression, then, begins to decrease until reaching values comparable to those of undamaged tissue, because they are no longer needed once new tissue is formed (Figure 26c).

In addition, the results obtained confirm the role of vimentin in the cellular-mediated repair process[158], as it guides fibroblasts toward the phenotypic transition in myofibroblasts. Its expression increases over time until the day of closure, and this leads to a parallel increase in the expression of α-SMA (Figure 26b).

Since fibroblasts begin to differentiate into myofibroblasts, these start with the release of new matrix components. In this context, at the beginning of the wound healing process, fibronectin plays a special role in supplying temporary support for fibroblast migration and proliferation (Figure 26a-up). In fact, we see an increase in time of this protein, which by binding to collagen provides adhesion signals to cells. The expression of this fibrous protein was found to increase up to the 21st day (Figure 26d).

It is known that in damaged tissues the fibrosis process is characterized by excessive accumulation of fibrous connective tissue (composed mainly of collagen and fibronectin), which can lead to permanent scarring, organ malfunction, and, eventually, death.

Activated fibroblasts, along with collagen and fibronectin, also began to secrete and organize tenascin to support the structural and functional integrity of interstitial ECM. Generally, the tenascin-C expression in intact tissues is minimal. In turn, it is overexpressed in the regions of tissue lesions and found on the edges of wounds. During the stages of repair and tissue fibrosis, tenascin plays a unique and fundamental role. It promotes the migration of fibroblasts along the fibrin-fibronectin matrices.

Tenascin C was extensively upregulated during the HDE repair process (Figure 26e). In particular, with damage to the tissue, there is a noticeable increase from day 4, the day we remember to be the real starting point of wound closure, up to the third week (Figure 26f), as in the *in vivo* context.

Finally, it is also worth analysing the expression of one of the enzymes that reshape the matrix from the beginning to the end of the wound healing process (Figure 26e).

As indicated in Figure 26g, MMP-1 increases up to day 4, reasonably since, as *in vivo*, this enzyme manages the degradation of the broken matrix components. After day 4, MMP-1 levels dropped since at the same time both the tenascin peak and the considerable increase of α-SMA were responsible for the downregulation of MMP-1, thereby creating space for the synthesis of a new matrix. It is also interesting to note that MMP-1 starts to increase again on day 14. This is comparable to what happens *in vivo* because these enzymes at the beginning of the remodelling phase start to digest excess collagen fibres.

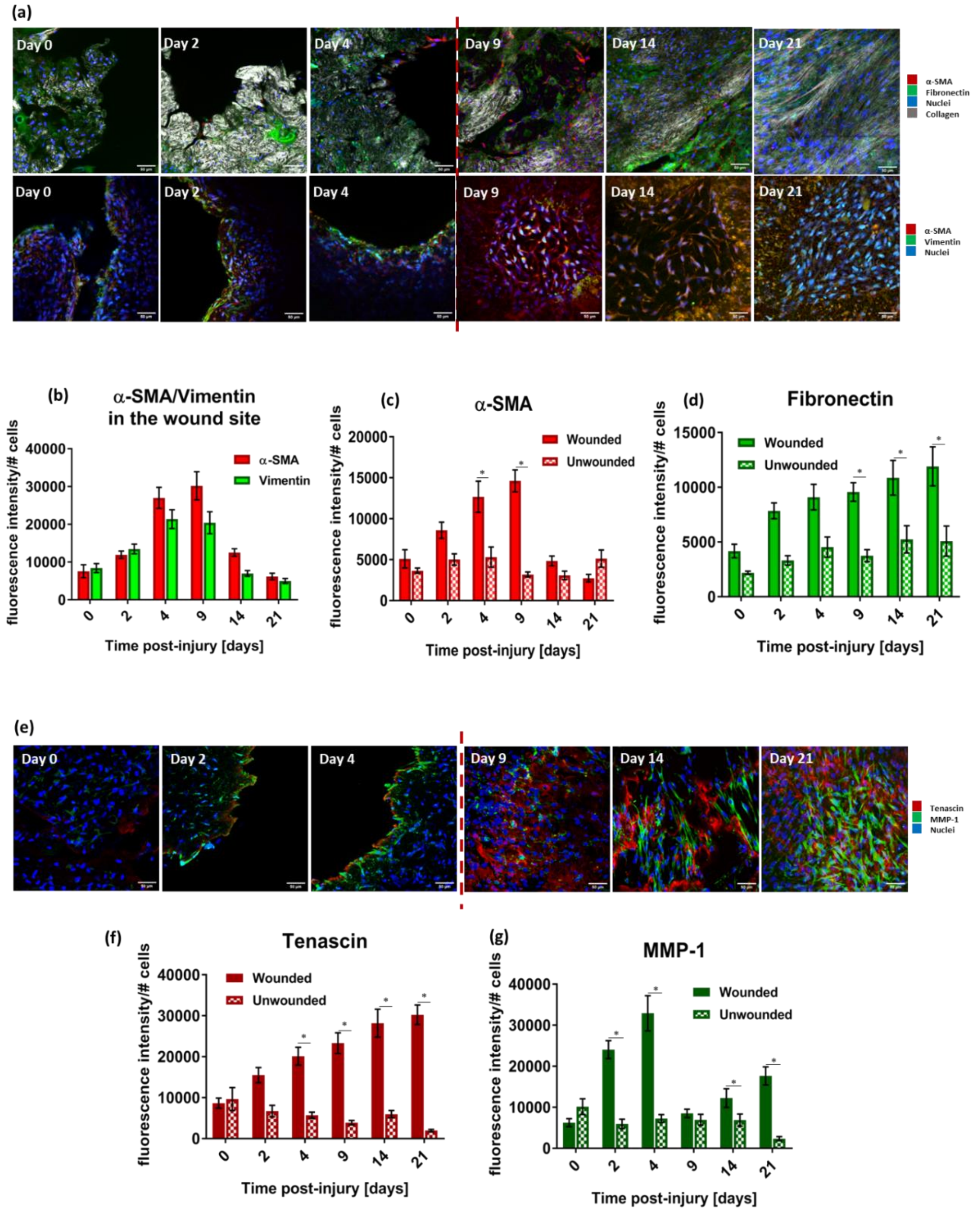

Figure 26 - (a) Representative images of immunofluorescence-stained 3D-HDEs showing α-SMA (red), fibronectin (green), nuclei (blue), collagen (grey), vimentin (green), (original magnification 40x, scale bar 50 µm). Quantitative analysis of (b) α-SMA and vimentin production expressed as fluorescence intensity/nuclei in wounded and unwounded regions on days 0, 2, 4, 9, 14 and 21. (c) α-SMA production expressed as fluorescence intensity/nuclei in wounded and unwounded regions on days 0, 2, 4, 9, 14 and 21. (d) Fibronectin production was expressed as fluorescence intensity/nuclei in wounded and unwounded regions on days 0, 2, 4, 9, 14 and 21. (e) Representative images of immunofluorescence stained 3D-HDE showing tenascin (red), MMP-1 (green) and nuclei (blue) (original magnification 40x, scale bar 50 µm). Quantitative analysis of (f) Tenascin production expressed as fluorescence intensity/nuclei in wounded and unwounded regions on days 0, 2, 4, 9, 14 and 21. (g) MMP-1 production was expressed

*as fluorescence intensity/nuclei in wounded and unwounded regions on days 0, 2, 4, 9, 14 and 21. *p<0.05.*

3.3.4 Collagen remodelling after wound closure.

It is now interesting to investigate how collagen, the main component of dermal connective tissue and constituent of scar tissue, evolves during the repair process. Collagen levels increased over time, especially weeks after wound closure until they settled to the levels of collagen present in the equivalent undamaged tissue (Figure 27a-c).

In Figure 27a, images of collagen fibres at days 9, 14, and 21 in the wounded region reveal the release and assembly of new collagen fibres by activated fibroblasts. Meanwhile, Figure 27b displays images at the same time points for the collagen in the unwounded region. Figure 27c includes a histogram illustrating the collagen fraction in both the wounded and unwounded regions at these time points. Notably, a progressive increase in collagen is observed in the wounded region from day 9 to day 21, eventually levelling off to match the levels observed in the unwounded region by day 21. This temporal evolution of collagen content provides visual insights into the dynamic changes occurring in the wounded and unwounded areas during the repair process, shedding light on the maturation and normalization of collagen levels over time.

To figure out the morphometric orientation of collagen fibres, the FFT method was used to assign an organization degree to an image. FFT analysis is especially useful for characterizing fibrillar collagen images by their degree of symmetry. In fact, for an image having a set of aligned fibres, we expect a corresponding FFT image with higher values along the direction of the fibres, and its intensity plot is expected to have an elliptic behaviour (Figure 27d). On the other hand, for an image with randomly oriented fibres, the intensity graph of the corresponding FFT image shows a circular shape (Figure 27d). In the core of the wounded region, collagen fibres showed an almost parallel texture with a preferential angle of disposition; in the unwounded areas, an equiprobable random distribution was detected (Figure 27e).

The FFT analysis for the wounded region revealed that collagen fibres tended to align along a common direction, as indicated by the dominant peak in the frequency spectrum. It is crucial to emphasize that the absolute value of the angle is not as significant, as it may vary depending on the direction in which these fibres are deposited and the z-axis of acquisition. What holds significance is the consistent alignment of all fibres along the same direction, indicating a robust preferential orientation in the wounded region.

This intriguing result can be readily correlated with the natural phenomenon of scar tissue formation. In normal skin tissue, fibres exhibit a random orientation to each other, whereas in scar tissue, the very same collagen fibres align in a preferential direction, running parallel to each other[159].

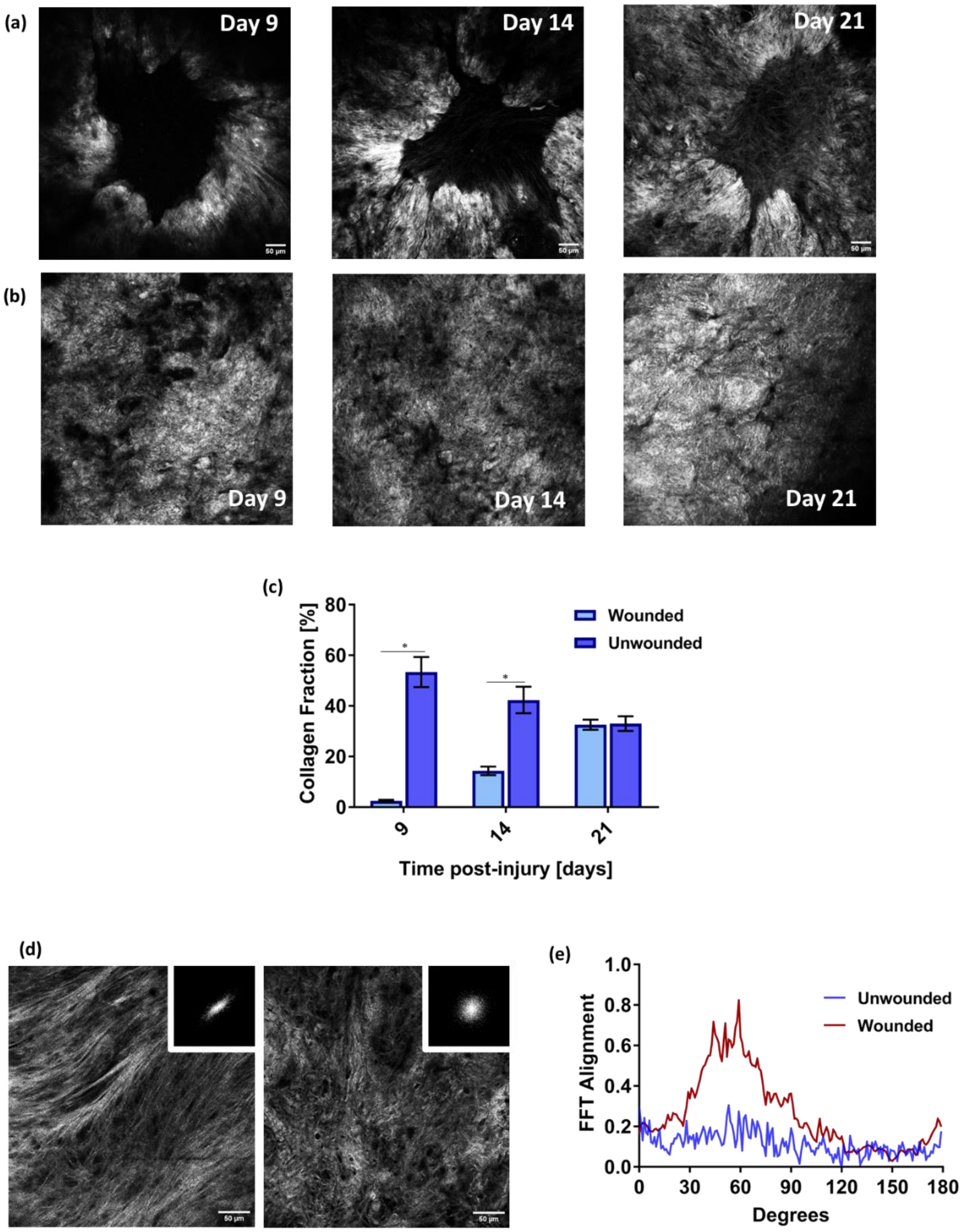

*Figure 27 – SHG representative images of the 3D-HDE (a) after wounding and (b) in unwounded regions (original magnification 25x, scale bar 100 µm). Quantitative analysis of (c) collagen fraction in wounded and unwounded regions on days 9, 14 and 21. (d) FFT analysis of SHG images of wounded and unwounded regions on day 21. SHG images (original magnification 40x, scale bar 50 µm). (e) Angle orientation distribution of collagen fibres obtained by FFT analysis showing a preferential orientation in the wounded region and a random distribution in the unwounded region. *p<.05*

3.4 Conclusion

This study has replicated the intricate interactions observed in the native dermis, offering a precise portrayal of *in vivo* processes. Notably, our approach stands out from existing literature as it does not involve exogenous mediation in the repair process, such as the use of fibrin gel within the gap or the incorporation of molecules designed to mimic repair. We aimed to faithfully replicate the biological processes (Figure 28a) from the initial wound formation through a three-week period, allowing for an in-depth investigation into the cells-ECM interaction and the neoformation and remodelling of the stroma going beyond a simple study of re-epithelialization. A fundamental aspect that emerged from our study concerns the complex dynamics of *en mass* fibroblast movement in close association with the structural modification of the ECM, emerging as a crucial point for the correct repair of tissues and the formation of functional scars.

This detailed analysis of the coordinated movement of fibroblasts and the deformation of the ECM has been made possible thanks to the use of our endogenous 3D models. These models have been essential tools in accurately reproducing cellular dynamics and ECM interactions in a controlled environment. The ability to recreate conditions similar to those of the original tissue has allowed a thorough exploration of the complex interactions between the cells and the surrounding environment during the wound-healing process.

From the results obtained, we believe that these models are useful for analysing the migration and proliferation processes of fibroblasts, which are important for wound repair, and the synthesis and assembly of the ECM, which is essential for the recovery of skin function (Figure 28b).

Our results show that the overall cellular and extracellular phenomena occurring during *in vitro* wound closure were similar to those observed *in vivo* and that the closure was associated with the migration and proliferation of fibroblasts, as well as the formation of new ECM.

Bypassing the early haemostatic and inflammatory phases, we wanted to focus first on the proliferative phase of our engineering model of injury and compare it to what happens naturally. Fibroblasts appear to be activated from day four, which corresponds *in vivo* to the beginning of granulation tissue formation[146]. In secondary intention wounds, these cells undergo a transformation and begin to express a protein called α-SMA, which gives them the name of myofibroblasts. Myofibroblasts acquire the ability to contract, similar to smooth muscle cells, and work to reduce the wound by moving tangentially towards its edges[160]. By monitoring our samples from the beginning of the injury to the closure, we also noticed changes in cell velocity from day 4 to the closing day. Studies[161] showed that the composition of the ECM can influence the speed of fibroblasts. Fibroblasts tend to move more efficiently on fibronectin than on collagen, due to the effect of the matrix on the motility of fibroblasts[161].

In this stage, we noticed that fibronectin levels started to increase with respect to the unwounded regions and that myofibroblast nuclei and collagen fibres were aligned. This is because the transformation of fibroblasts into myofibroblasts is triggered by the interaction of fibroblasts with EDA fibronectin in the wound[162], then the myofibroblasts' actin proteins eventually connect to fibronectin in the ECM, anchoring to collagen fibres[163]. The contraction of the actin pulls these fibres inwards, which leads to the contraction and eventual closure of the wound. Furthermore, during the early stages, fibroblasts align collagen fibres in the direction of their movement, and this pattern is strengthened as more fibroblasts follow the established path of the fibres[164].

In the meanwhile, MMP-1 levels started to increase as well not only to degrade cellular and extracellular debris but also because it has been demonstrated that MMPs play a role in the development of myofibroblasts, as the inhibition of MMPs prevents the formation of myofibroblasts in living organisms[165]. Next to the ninth day, alpha-SMA levels started to decrease by equating with levels in the unwounded regions. This is owing to the fact that, after the wound has healed, myofibroblasts are eliminated from the site through a process called apoptosis, which is a type of programmed cell death[166]. This occurs once the tissue is strong enough to maintain its integrity.

Proliferative and remodelling phases are critical for the repair of dermal connective tissue. During the proliferative phase, we witnessed the appearance of ECM-producing cells. The remodelling phase then takes over, during which the ECM is rebuilt, and the tissue is reorganized to regain its original strength and structure. This process also includes the removal of damaged or excess tissue with a further increase of MMP-1 expression. Without these two phases, the repair process would be incomplete, and the tissue would remain weak and susceptible to further injury. For this reason, we observed and analysed the behaviour of our samples also during the second and third week after injury; these weeks are considered the onset of the remodelling phase[146].

Among all the molecules in the ECM, we focused on fibronectin and tenascin-c. These molecules are responsible for rebuilding stromal tissue. Particular attention should be paid to the last 2 weeks under examination: there were statistically significant increases in the amount of fibronectin per cell and of tenascin per cell when compared to cell lines from normal adjacent dermis. Our data suggest that there is a progression of scar-like tissue formation. Tenascin, which is normally expressed at almost negligible levels, is found accumulated in the granulation tissue during the advancement of wound healing. Elevated levels of this protein are often considered a biomarker for excessive fibrosis in patients with fibrotic conditions[167]. Additionally, it has been observed that fibrotic conditions are characterized by a build-up of fibrous tissue primarily made up of fibronectin and collagen.

Regarding collagen, we found that during the initial phase, this molecule needs to be synthesized and assembled correctly. In fact, cells use fibronectin as the initial substrate to invade and proliferate in the wound, just as it does *in vivo*. After 1 week the fibroblasts have invaded the damaged area, and the collagen fibres type I and III are deposited[168]. Then, a peak in collagen deposition is observed during the third week as in the typical wound healing process[147]. In the end, what we obtained is very well-organized and parallel distributed collagen fibres, as in scar tissue, with respect to the undamaged counterpart in which the collagen network is composed of fibres randomly laid down.

Ultimately, 3D-HDEs stand at the forefront of wound and scarring research. Comprising primary cells within their self-generated matrix, our models surpass traditional counterparts in reliability and efficiency, faithfully replicating the physiological intricacies of the original tissue. Notably, they prove exceptionally valuable for investigating key processes like the migration and proliferation of fibroblasts, as well as the synthesis and assembly of the ECM-critical components in understanding both wound healing and scar formation. In a nutshell, we think that our models can empower researchers to gain deeper insights into the intricacies governing wound healing mechanisms, thereby facilitating the development of innovative treatments to enhance therapeutic outcomes.

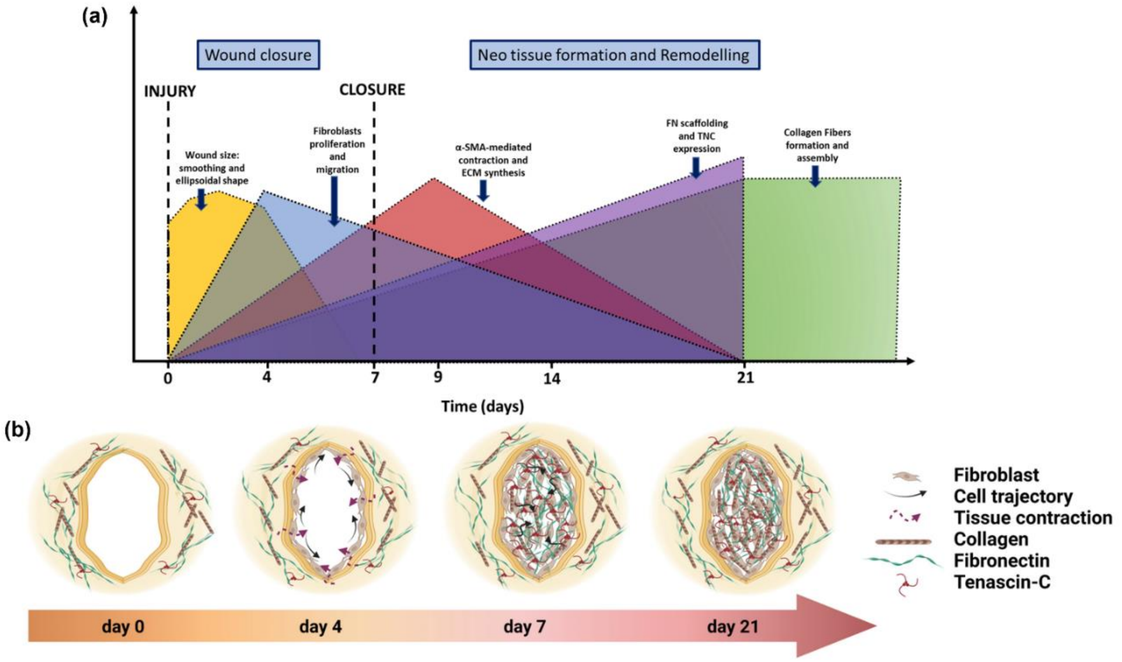

Figure 28 - (a) A visual representation of the various phases of 3D-HDE wound healing. (b) An illustration showing how cells move tangentially around the wound border and deposit a temporary ECM to fill and seal a gap. On closure, an increased fibronectin, tenascin-C and collagen expression and collagen fibres parallel disposition can be related to scar tissue formation. Created with BioRender.com

Chapter 4: Replication of a scar tissue: Immune system orchestrates microenvironmental changes and matrix remodelling in 3D-HDE upon injury.

4.1 Introduction

Scars represent a physiological and fundamental aspect of the tissue healing process, resulting from the body's response to skin lesions or various forms of trauma. However, scar formation can often present problems, ranging from cosmetic complications to potentially serious medical conditions, since a well-defined scar can have negative impacts on the aesthetics, functionality, and overall health of the tissue[169].

One of the main complications related to scars is represented by hypertrophic scars and keloids. These scars, characterized by excessive tissue production, can protrude beyond the boundaries of the original wound area, they can be painful and itchy, causing significant discomfort[2]. In addition, scar formation and extension can compromise the flexibility and functionality of surrounding tissues, limiting movement, and causing functional problems[169].

Some scars can become life-threatening when they turn into more severe conditions such as contracture scars: these occur when the skin and underlying tissues shrink, creating tension and limiting movement[170]. For example, scarring contractures around the neck can restrict breathing or those around the joints can cause movement restrictions that lead to a functional disability[171].

Furthermore, scars can lead to medical complications such as adherence of tissues, in which the inner layers of the body attach to each other, creating problems with the surrounding organs or blood vessels[172]. This adhesion can also occur in the internal organs after internal surgery, causing serious medical complications or even risking life[55].

Scars may also be associated with fibrosis, a pathological process characterized by excessive production of fibrous connective tissue. Although it is a natural process in the body's attempt to heal, fibrosis can lead to serious complications, especially when it occurs in vital organs such as the liver, lungs or heart[173]. For example, pulmonary fibrosis can impair respiratory capacity[174], while hepatic fibrosis can lead to cirrhosis and liver failure[175].

Additionally, although the direct relationship between scarring and cancer is unclear, a correlation has been observed between scar fibrosis and some forms of cancer; for example, chronic hepatic fibrosis is a known risk factor for the development of hepatocellular carcinoma[176]. The presence of increased scar tissue as a result of chronic injury or inflammation may predispose to the occurrence of certain types of tumors[177].

Aware of the issues related to scars and fibrosis, the need arises to replicate laboratory models.

In wound healing research, the use of *in vitro*[15,178–182], *in vivo*[183–188] and *ex vivo*[189–192] models is crucial to understand the mechanisms involved in scar formation and to develop effective treatment strategies. While *in vitro* models allow more controlled manipulation of experimental conditions, *in vivo* models offer a more realistic context that considers the interaction between cells, growth factors and ECM. In contrast, *ex vivo* models, using tissues taken from live organisms, provide an interface between *in vitro* and *in vivo* models, allowing the analysis of specific processes in a more controlled context.

Despite the benefits, *in vivo* models for studying skin scars have some limitations such as the differences in wound healing processes between humans and animals, the ethical concerns regarding animal use, the high animal maintenance costs, the limitations in reproducibility, and the limited ability to fully study the role of specific genes in scar formation[9,15]. When exploring *ex vivo* models, their ability to faithfully replicate scar environments is hindered by the variability in donor tissues, introducing heterogeneity in experimental outcomes and the absence of standardized protocols, which should incorporate comparable biological replicates from diverse donors, exacerbating challenges related to reproducibility and result relevance[15]. Additionally, ethical considerations about the use of human tissues in *ex vivo* models underscore the pressing need for alternative model systems[15,193]. Limitations inherent in *in vitro* models encompass their potential inability to faithfully replicate the native scar formation environment, variability in accurately representing human scars, and constrained ability to investigate the intricate molecular, cellular, and structural mechanisms associated with healing. The current organotypic models reported in the wound healing literature are deficient in essential components, such as inflammatory and vascular elements, critical in the context of the scar formation process. These limitations underscore the necessity for enhanced models that better represent human cutaneous scar characteristics and provide clinically relevant insights into scar formation.

Our endogenous scar model, based on the use of a 3D-HDE, emerges as an innovative experimental platform. Unlike conventional models present in the scientific context, our endogenous HDE model uses a more accurate representation of microarchitecture and ECM composition, better emulating the real tissue environment. Moreover, by combining an endogenous matrix more faithful to the structure of the human dermis and the immune system, responsible for the formation of scars, our model is presented as an essential tool to deepen the intricate mechanisms underlying healing and to identify innovative and more effective therapies.

In fact, when lesions or inflammation occur in the tissues, circulating monocytes and resident macrophages present in the tissues are recruited in the affected area. These monocytes can mature into M2 macrophages under the influence of several microenvironmental and molecular signals, including specific cytokines and transcription factors[194].

One of the key signals that induce the differentiation of monocytes into M2 macrophages is the presence of cytokines such as IL-4 and IL-13, released by helper T cells, epithelial cells and other immune cells present in the surrounding environment. IL-4 and IL-13 bind to specific receptors present on monocytes and macrophages, triggering a series of intracellular events that activate specific transcription factors, such as the STAT6[195].

Activation of STAT6 is crucial in determining the fate of monocytes and macrophages towards the M2 phenotype. This transcription factor regulates the gene expression involved in the formation of M2 macrophages, inducing the expression of genes characteristic of this phenotype, such as CD206[196].

Macrophages, playing a central role in the healing process of tissues, release a crucial signal, the TGF-β1, which acts as a fundamental determinant in the transformation of fibroblasts and the production of proteins essential for the formation of scars[197]. TGF-β1 is involved in the activation of fibroblasts, leading them to transition to the form of myofibroblasts, fundamental cells involved in wound contraction and ECM proteins production[197]. This growth factor, released by activated macrophages, has a significant influence in determining the direction of tissue healing and modulating the formation of the ECM. The intricate relationship between macrophages, TGF-β1 and the transformation of fibroblasts into myofibroblasts is one of the keys to understanding the process of scar formation and the importance of the cellular environment in tissue healing[1].

For these reasons, the involvement of M2 macrophages in the evolution of scars is a central aspect of our investigation. The ability of M2 macrophages to modulate inflammation, promote the deposition of ECM proteins and orchestrate tissue healing emphasizes the importance of their regulation for proper scar formation and recovery of damaged tissues[9].

Our study aims to examine in detail the processes that influence the formation of scars, focusing on the interaction between macrophages, myofibroblasts and the key molecules of the ECM. Understanding these interactions could open up new therapeutic perspectives to improve the healing process and limit the complications associated with scarring and fibrosis.

4.2 Materials and Methods

4.2.1 Cell source

THP-1 cells (TIB-202 ATCC) serve as a valuable model for human monocytes and macrophages[198–201].

THP-1 cells at passages 2-5 were subcultured both in Ultra-Low attachment 6 well plates (Corning 3471) and in 25 cm^2 cell culture flasks (VWR 734-1712) in RPMI-1640 medium modified to contain 2 mM L-glutamine, 10 mM HEPES, 1 mM sodium pyruvate, 4500 mg/L glucose, and 1500 mg/L sodium bicarbonate (ATCC-30-2001) supplemented with 10% heat-inactivated FBS (Merck F7524), 100 U mL^{-1} penicillin/streptomycin (Sigma-Aldrich P4333-100ML) and 0.1×10^{-3} m Nonessential Amino Acids (Thermo Fisher Scientific 11140050).

Figure 29 shows how THP-1 cells were differentiated into M2 macrophages. In detail, using 8.5 nM PMA (Abcam ab120297-1mg) in RPMI-1640 complete culture medium led to the monocytes to M0 macrophage differentiation. After 24 h, the differentiation medium was removed and replaced with fresh culture medium excluding PMA. Cells were allowed to rest for 72 hours. Following the resting period, cells were activated into M2 macrophage phenotype over 48 hours by treatment with 20 ng/ml IL-4 (Peprotech 200-04) and 20 ng/ml IL-13 (Peprotech EC-LTD 200-13). Activated macrophages were, subsequently, detached from culture plates using a 5mM EDTA (Themo Fisher Scientific 15575020) solution for 15 min at 37ºC.

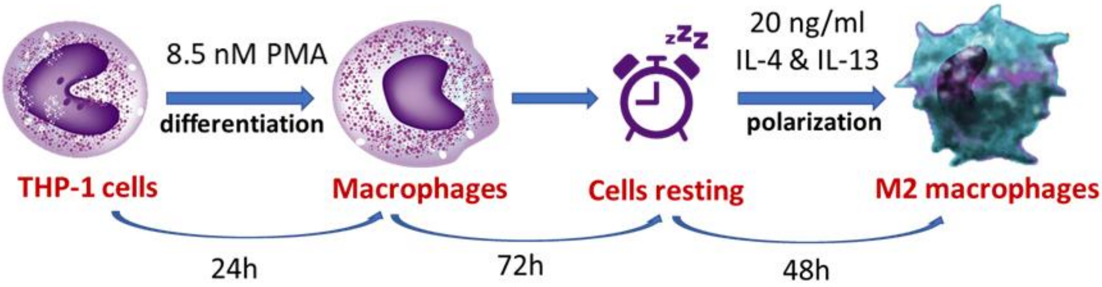

Figure 29 - Detailed experimental protocol for inducing monocyte polarization into M2 macrophages, emphasizing key stages, treatments utilized, and timeframes.

4.2.2 Immuno-3D Wound Experimental set-up.

Once the 3D-HDE tissues were prepared following the procedures outlined in Chapter 3, they were carefully punched out, placed in fluorodishes, and blocked with PDMS moulds, as already discussed, without adding the culture medium to keep them dried until the exposure to the macrophages. To establish an immunocompetent model (Figure 30), a 150 µl-drop containing $4 \cdot 10^5$ M2 macrophages/ml was strategically injected into the full-thickness hole created by the punch biopsy within the 3D-HDE structure. For the effective infiltration of macrophages into the 3D-HDE, the samples were kept dry for 15 minutes following the addition of the cell drop. Subsequently, complete E-MEM supplemented with ascorbic acid was gently introduced. The medium, enriched with ascorbic acid, was refreshed every two days throughout the duration of the experiment.

Concurrently, wounded 3D-HDE models without M2 macrophages (wounded -M2) were also developed to facilitate comparative analysis with the immunocompetent models (wounded +M2).

The experiment concludes two weeks after the wound CT. The CT has been defined as the day when there is no longer any empty space within the wounded region that for wounded -M2 models corresponds to 1 week after injury and for wounded +M2 models corresponds to 10-14 days after injury.

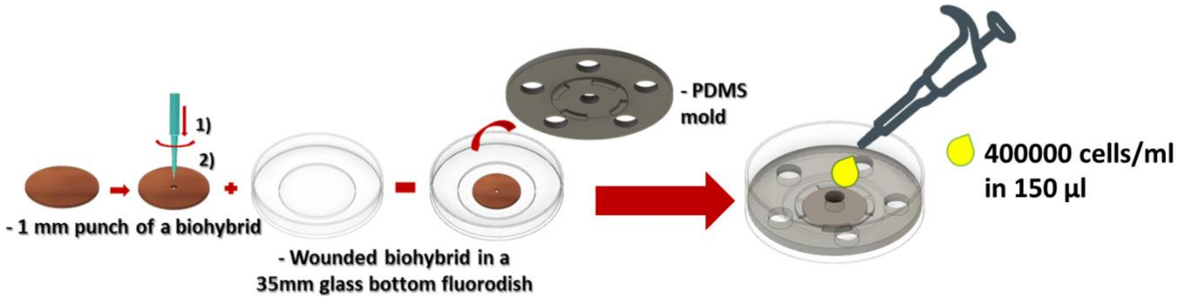

Figure 30 - Diagram illustrating the methodology for establishing an immunocompetent model using 3D-HDE tissues and M2 macrophages.

4.2.3 Morphological characterization of the immunocompetent 3D-HDE model

Brightfield acquisition

Brightfield images have been acquired with an Inverted Fluorescence Motorized Microscope (Zeiss Axio Observer 1) equipped with an incubation system with either a 10X or 20X magnification lens.

Confocal and multiphoton imaging

Specific time points were selected to fix the tissues and conduct morphological analyses on key components critical to the wound healing process. To capture the dynamic nature of tissue repair, we focused on three key intervals: the CT, one-week post-closure (CT+1w), and two weeks post-closure (CT+2w). Additionally, the CT+2w time point was specifically chosen to assess the progression of scar formation.

Fluorescence staining

Tissue samples underwent fixation in Formalin solution (HT501320-9.5 L Merck) at 4°C overnight, followed by triple washes in PBS 1X. Permeabilization was achieved using 0.1% Triton 100 X (T9284-100ML Sigma) in PBS 1X for 5 minutes at RT. After PBS 1X rinsing, samples were blocked with 1% BSA (A9418-100G Sigma) for 1 hour at RT.

Primary antibodies were utilized for specific molecular detection. Anti-α-SMA (ab5694, Abcam, Rabbit Polyclonal), anti-vimentin (ab8978, Abcam, Mouse Monoclonal) and anti-CD206 (Biorbyt, orb4941-200ug, Rabbit Polyclonal) antibodies, diluted to 1:100, 1:100 and 1:400, respectively, in blocking solution, were employed for cellular marker identification. For macrophages-collagen interaction studies, anti-α2β1 integrin (ab30483, Abcam, Mouse Monoclonal) at a 1:100 dilution was used. ECM proteins were targeted using anti-fibronectin (F0791-100UL, Merck, Mouse Monoclonal), anti-tenascin C (ab86182, Abcam, Mouse Monoclonal) and anti-hyaluronic acid (GTX17370, GeneTex, Rabbit

Polyclonal) antibodies, each at a 1:100 dilution in the blocking solution. Additionally, anti-MMP-1 (ab3899, Abcam, Rabbit polyclonal) at a 1:100 dilution in blocking solution was used to quantify MMP-1 secreted post-wounding.

Samples were incubated overnight at 4°C in agitation for even antibody distribution. The subsequent day, secondary antibodies—Goat Anti-Rabbit IgG (H + L) Alexa Fluor 546 (A11035 diluted 1:500 in PBS 1X) and Goat Anti-Mouse IgG (H + L) Alexa Fluor 488 (A11029 diluted 1:500 in PBS 1X)—were applied for 1 hour at RT. Nuclei staining was accomplished by exposing samples to DAPI (Sigma-Aldrich D9542) diluted 1:10,000 in PBS 1X for 20 minutes at RT.

Confocal microscopy was performed using a 40-water immersion objective (Confocal Leica TCS SP5 II) to facilitate the investigation. Z-stack imaging was conducted in wounded-M2, wounded+M2 and unwounded regions for comparative analysis.

Morphological analysis of the wound closure process

Images and z-stacks were subjected to analysis using Image J software. For each image, 10 specific ROIs were selected, encompassing both areas expressing the marker of interest and background regions.

To determine CTF, the following formula was applied:

$$\text{CTF} = \text{Integrated Density} - (\text{selected Area X Mean Fluorescence of background regions}) \tag{4.1}$$

Additionally, within these chosen ROIs, the number of nuclei was assessed using the "Analyze Particle" plugin in Image J. This step aimed to normalize fluorescence data based on the actual cell count within the regions of interest.

Histological and immunofluorescence staining of tissue slices.

The specimens were fixed using a 10% neutral buffered formalin solution overnight. After fixation, gradual dehydration was accomplished through successive immersions in ascending concentrations of alcohol (75%, 85%, 95%, and two cycles of absolute alcohol), each immersion lasting 30 minutes at RT. Post-dehydration, the specimens underwent xylene treatment for 30 minutes and were then embedded in paraffin. Longitudinal sections measuring 7 µm in thickness were obtained from both the wounded-M2 and wounded+M2 specimens using a microtome (Thermo Scientific HM 355S).

The paraffin embedding process creates an anhydrous environment, whereas histological dyes used for tissue staining are water-based. To facilitate the compatibility of aqueous dyes with the tissue sections, the deparaffinization step in xylene was conducted to remove the paraffin. Subsequently, rehydration was executed using a series of ethanol solutions in descending concentrations (100%, 95%, 85%, 75%) concluding with immersion in water.

Histological staining involved the application of H&E (Bio Optica), Alcian Blue (Sigma Aldrich), and Picrosirius Red (Sigma Aldrich Chemical Company). Upon completion of the staining process, sections were mounted onto coverslips using Histomount Mounting Solution (Invitrogen).

Morphological examinations were conducted utilizing a precision light microscope (Olympus, BX53). For detailed inspection of the Picrosirius Red-stained sections, a thorough examination was performed via linear polarized light microscopy. This technique involved the positioning of a linear polarizer between the specimen and the light source, complemented by an analyser in the optical pathway toward the camera. This setup facilitated the discernment and distinction between collagen type III fibres (distinguished in green hues) and collagen type I fibres (exhibited in yellow and red hues).

Quantification involved the assessment of pixel counts within distinct hue ranges, expressed in relation to the overall collagen pixel count.

For the immunofluorescence staining of the tissue slices, sections were deparaffinized, hydrated and washed in water, Triton 0.2%, and PBS 1X.

Antigens unmasking was achieved through a heat retrieval protocol employing citrate buffer and sections were, then, blocked using a solution comprising 6% BSA, 5% FBS, 20 mM $MgCl_2$, and 0.2% Triton 100X in PBS 1X for 2 hours at

RT. Subsequently, sections were incubated overnight at 4°C in a moist environment with anti-CD206 and anti-vimentin.

Samples were stained with secondary antibodies, accompanied by nuclei labelling using DAPI. Post-staining, the samples were ready for investigation utilizing the Confocal Leica TCS SP5 II.

SEM examination

To evaluate the collagen network architecture in wounded-M2, wounded+M2 and unwounded samples at CT+2w, collagen fibres were characterized with SEM (Thermo Scientific, HELIOS 5 CX).

Samples were fixed in 4% Paraformaldehyde/2.5% Glutaraldehyde in 0.1 M sodium cacodylate overnight at 4ºC and, subsequently, washed in a solution of 0.1 M sodium cacodylate/0.1 M sucrose buffer at RT.

A 1% aqueous OsO_4 solution in 0.1 M sodium cacodylate/0.1 M sucrose buffer at 4ºC is added after the fixation. OsO4 can bind to components such as lipids and proteins, rendering them visible under the electron microscope. The solution of OsO4 is employed post-fixation to help maintain structure and preserve cellular features during the preparation process for electron microscopic analysis.

The 1% OsO4 solution in sodium cacodylate/sucrose buffer is utilized at low temperatures (4ºC) to reduce artefact formation and better preserve cellular structures. Sodium cacodylate acts as a buffering agent to maintain the pH of the solution, while sucrose helps protect cells from ice crystal formation during freezing.

Then, samples are dehydrated in ascending percentage of ethanol (30%, 50%, 70%, 95% and 100%, each for 60 min at 4ºC) and placed in a critical point chamber (Leica EM CPD300) overnight.

Fibres diameters were evaluated through the ImageJ’s plugin DiameterJ.

SHG

Tissues were fixed overnight in Formalin at 4°C, followed by washing in PBS 1X. Whole-sample analysis was performed using Two-Photon Excited Fluorescence with the Leica TCS SP5 II coupled with a Multiphoton Microscope stage Chameleon Compact OPO-Vis, Coherent. This method allowed the generation of high-resolution images illustrating unstained collagen structures through SHG.

Samples were examined using $\lambda ex = 840$ nm (two photons) and $\lambda em = 415–425$ nm. Z-stacks were captured in wounded-M2, wounded+M2 and unwounded regions for comparative analysis. SHG stacks were acquired with an 8-bit resolution at 1024·1024 pixels, utilizing a 25-water immersion objective (HCX IRAPO L 25.0 0.95 Water, n.a. 0.95).

Collagen bundle diameter was estimated thanks to the CT-FIRE algorithm[202,203].

Collagen amount quantification

Newly synthesized collagen fibres were quantified from SHG images using ImageJ software. In SHG images, collagen is associated with brighter pixels. The Collagen Fraction (%) was calculated as the ratio of bright pixels to total pixels in the image:

$$\text{Collagen Fraction (\%)} = \frac{\mathrm{N_C}}{\mathrm{N_{TOT}}} * 1000 \qquad (4.2)$$

Where N_C represents the number of pixels in the collagen region, and N_{TOT} represents the total number of pixels in the image.

4.2.4 FFT analysis

The FFT plugin in Image J was used to determine the orientation of collagen fibres. This mathematical transformation translates image data from the space domain to the frequency domain, displaying grayscale pixels that represent the alignment patterns.

After applying FFT, the transformed images were rotated by 90 degrees to correct the transformation effects. This adjustment facilitated identifying the primary orientation axis by locating the intensity peak in the resulting graph.

In the process, a threshold was applied to identify the long and short axes of the ellipsoid observed in the FFT amplitude images. Employing the FFT method, the COI[204–206] was determined by the formula:

$$\mathrm{COI} = 1 - \frac{W}{H} \tag{4.3}$$

Here, W and H denote the width and height of the ellipse or circle within the power plots extracted from the SHG images.

A COI value of 0 signifies a state of perfect isotropy in collagen fibre behaviour, indicating a completely random distribution of fibres with no prevailing orientation. Conversely, a COI value of 1 indicates a state of perfect parallelism, signifying that all fibres are uniformly aligned in the same direction.

4.2.5 Lacunarity analysis

In this study, lacunarity analysis was performed on images of collagen fibres obtained through SHG. The Frac_Lac plugin, an ImageJ add-on (available at: http://rsbweb.nih.gov/ij/plugins/fraclac/fraclac.html), was utilized for assessing lacunarity. A slow scan autothreshold method was employed, using a sliding window ranging from a minimum size of a single pixel to a maximum of 45% of the ROI.

Lacunarity, denoted as L, served as a measure of non-uniformity or heterogeneity within the structure or the structural variance within our analyses. Low L values indicate homogeneous objects, while higher values suggest heterogeneity. Lacunarity ranges from 0 to 1, with 0 representing complete homogeneity, while higher values indicate greater heterogeneity in the orientation of collagen fibres. Additionally, lacunarity values provided insights into the porosity of examined structures: more porous structures exhibited higher lacunarity values compared to smoother ones[207]. Therefore, lacunarity can be considered an indicator of tissue density, as it quantifies the number of empty spaces within the tissue[208].

4.2.6 TGF-β1 1 ELISA assay

An ELISA assay was conducted to determine the levels of TGF-β1 present in the daily culture medium samples. A specific kit designed for TGF-β1 analysis via ELISA (Merck - RAB0460-1KT) was used, and the manufacturer's instructions were followed for the assay procedure. The culture medium samples underwent centrifugation to remove cellular debris, yielding the supernatants used for subsequent analysis.

ELISA microplates were prepared according to the kit instructions and uniquely labelled for sample and standard identification. Known standards of TGF-β1 were prepared to construct a calibration curve. Culture medium samples were appropriately diluted and added to the microplate wells alongside the prepared standards.

Subsequently, the microplates were incubated and washed repeatedly to eliminate unbound substances. A specific conjugate provided by the ELISA kit was added, followed by a chromatic substrate. Absorbance readings were taken using a spectrofluorometer (Perkin Elmer 2300 Enspire Plate Reader) at 450 nm.

4.2.7 Mechanical test

Nano-indentation tests were performed using Nano-Indenter Piuma (Optics11). In simpler words, the tip of the nano-indenter penetrates the sample surface until it reaches a predefined value.

The calculation of the effective Young module was obtained by adjusting the part of the F-h curve below 20% Pmax (maximum load) with the Hertz contact model[209], represented by the following equations:

$$\mathrm{F} = \frac{4}{3} E_{eff} \cdot \sqrt{R} \cdot h^{\frac{3}{2}} \tag{4.4}$$

$$\mathrm{E} = E_{eff} \cdot (1 - \nu^2) \tag{4.5}$$

where F is the load, R is the radius of the tip, h is the depth of indentation, ν is the Poisson's ratio, E_{eff} is the effective Young module, and E is the Young module, which can be estimated when the Poisson ratio is known.

The cantilever is strategically positioned at the end of a fibre optic, wrapping the end itself. A spherical tip with a radius of 56.5 µm is attached to the end of the cantilever and used to induce sample indentation by applying a known displacement to the entire probe.

Using a cantilever with a rigidity of 4.2 N/m, an indentation depth of about 10 µm was obtained in each test on several areas of the samples.

Tests were conducted on both wounded +M2 and wounded -M2 samples in three different positions of the wounded and unwounded areas, with at least a grid of 3x3 indentations on each surface of each sample.

Statistical Analysis

Experiments were performed in triplicate. Data are expressed as mean ± SEM. Differences between groups were determined using the statistic test ANOVA Tukey HSD test. Significance between groups was established for p-value <0.05.

4.3 Results and Discussion

4.3.1 Macrophages-ECM interaction in a 3D immunocompetent HDE model before and after wound closure

Our results highlight the crucial role played by macrophages in their interaction with the ECM during the wound-healing process. The early adhesion of macrophages (in bright blue) to the wound edges within an hour post-injury (Figure 31) underscores their immediate response to the traumatic event. This rapid mobilization may indicate an instant action by macrophages in maintaining tissue homeostasis and initiating the healing process. The active movement of macrophages within the wound area indicates their continuous surveillance to identify areas requiring further repair, ensuring adequate support for the ongoing healing process.

Moreover, the observation of macrophages adhering to and moving around the wound periphery may imply their interaction with fibroblasts and the ECM. This interaction serves to release chemical signals, including cytokines and growth factors, crucial in activating fibroblasts and orchestrating the assembly of the ECM, fundamental for effective tissue repair.

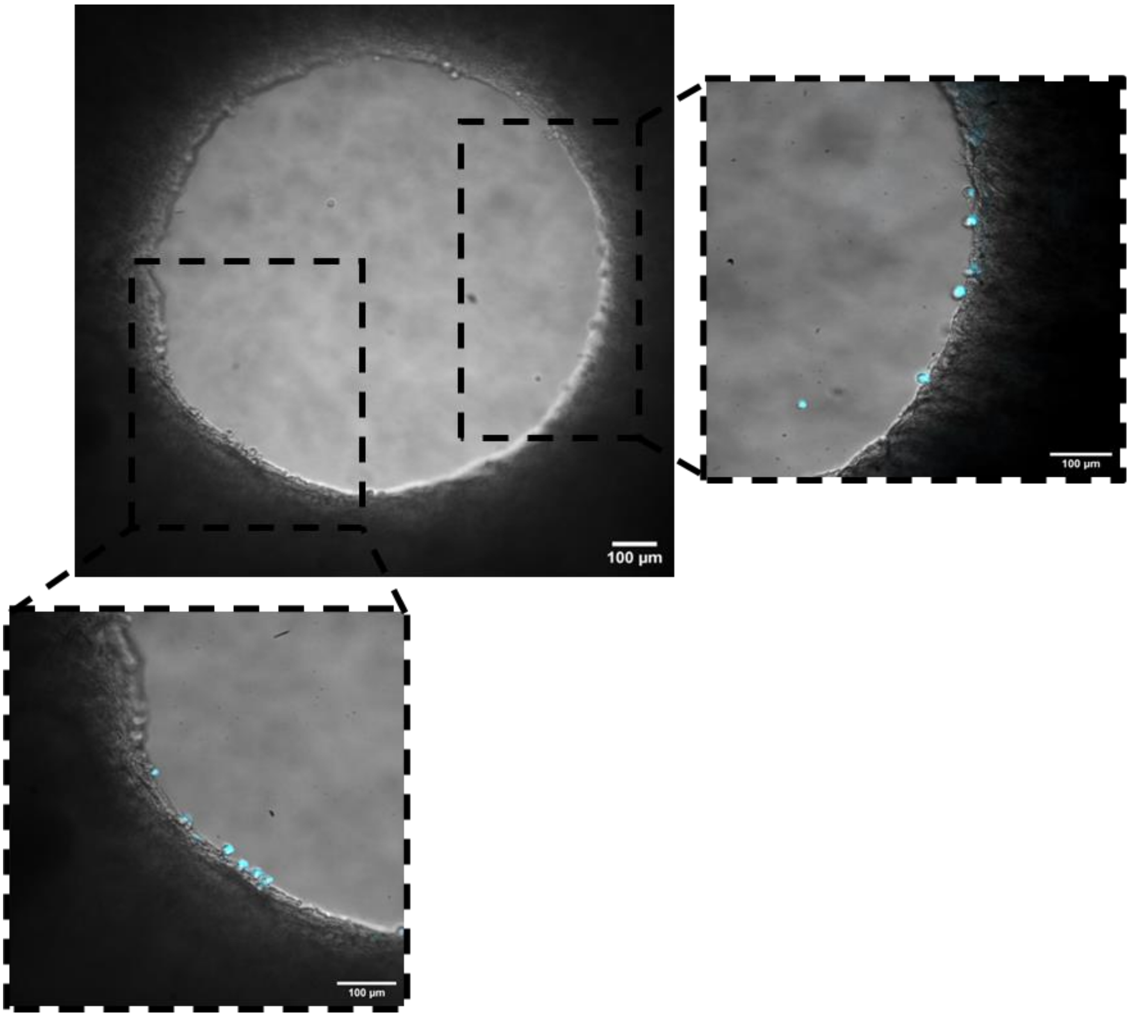

Figure 31 - Image displaying the wound generated within the 3D-HDE model, captured one-hour post-injury. Macrophages (identified in blue through Hoechst staining) are observed adhering to the wound edges. (original magnification 5x, scale bar 100 µm) The bottom and right squares show a zoom of the wound boundaries. (original magnification 10x, scale bar 100 µm)

From the immediate adhesion and mobilization of macrophages within the first hour post-injury, our exploration extends to what happened at the wound CT, at approximately 10-14 days post-injury.

The subsequent phase, as depicted by the images obtained at CT (Figure 32a), illustrates a more advanced integration of macrophages within the newly formed matrix at CT. This suggests a critical role of macrophages in both the formation and maturation of the ECM; this confirms their contribution to providing essential structural support crucial for the tissue regeneration process.

The immunofluorescence image (Figure 32b), showcasing the colocalization of CD206 and integrin $\alpha_2\beta_1$ signals, proves the integration of macrophages into the newly formed matrix. This outcome stands as a cornerstone, indicating an effective interplay between M2 macrophages and collagen fibres via the integrin $\alpha_2\beta_1$[210], further fortifying the notion of their active involvement in tissue reconstruction. The CD206 and integrin $\alpha_2\beta_1$ signals exhibit robust colocalization, affirmed by a Manders coefficient of approximately 0.85.

In the sphere of immunofluorescence image analysis, the Manders coefficient is employed to evaluate the co-localization of two specific markers within studied cells or tissues. For instance, when delineating the overlap between two species within a cell, as observed with macrophages and integrin $\alpha_2\beta_1$, the Manders coefficient quantifies the extent to which these molecules colocalize within the same cellular space.

Evidence from H&E staining in Figure 32c shows a notable accumulation of nuclei (in violet) in proximity to the wound. Traditionally, such nuclear aggregations are observed in models encompassing complete skin structures, inclusive of the overlying epithelium. Yet, given the exclusive dermal composition of our models, it is highly plausible that the amassed nuclei predominantly correspond to the macrophages that have focalized within the region of injury.

To prove this observation, immunofluorescence staining for CD206 (indicative of M2 macrophages), and vimentin (relative to fibroblasts) was performed on the same tissue sections. This analysis aimed to confirm whether the observed accumulation indeed corresponds to macrophages. A distinct accumulation of CD206 (in red) within the wound area and an evident presence of vimentin (in green) in the surrounding tissue (Figure 32d) in observed. The concurrent localization patterns observed sustain and validate the histological findings obtained through H&E staining. The convergence of immunofluorescence data, highlighting the co-localization of CD206 and integrin $\alpha_2\beta_1$, along with these supporting histological observations, establishes a robust foundation, emphasizing the intricate involvement of M2 macrophages in orchestrating the remodelling of the tissue microenvironment.

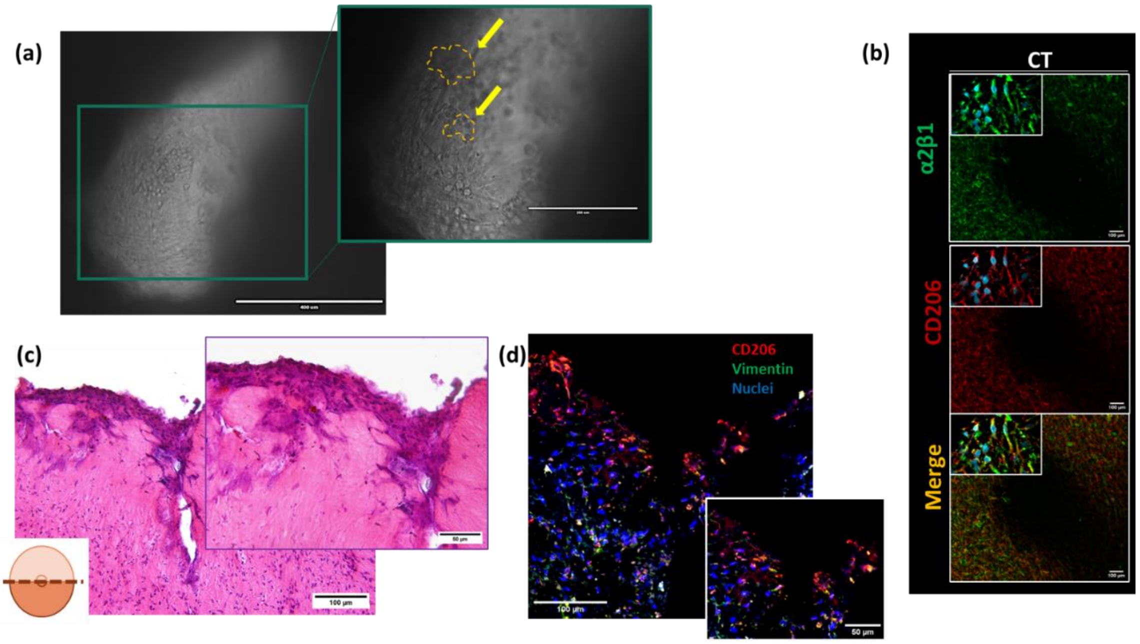

Figure 32 - Sequential images depicting macrophage integration and co-localization within the matrix during tissue regeneration at CT: (a) Macrophages integration in the neoformed ECM. Dashed lines and yellow arrows highlight macrophages within the newly formed matrix. (original magnification 5x and 10x, scale bar 400 µm and 200 µm) (b) Representative images of immunofluorescence-stained 3D-HDEs showing CD206 (red), integrin $\alpha_2\beta_1$ *(green), nuclei (blue), (original magnification 40x, scale bar 50 µm). (c) H&E Staining reveals nuclei accumulation, potentially associated with macrophages, within the wound region. (original magnification 10x and 20x, scale bar 100µm and 50 µm) (d) Representative images of immunofluorescence-stained 3D-HDEs showing CD206 (red), vimentin (green), nuclei (blue), (original magnification 40x, scale bar 50 µm).*

4.3.2 Fibroblasts-macrophages interplay shapes the repair mechanism.

Subsequently, our focus shifted towards investigating the temporal dynamics of cellular and molecular activities. This provided additional insights into the dynamic interplay between macrophages and fibroblasts during the healing process. From CT to CT+2w, the concentration of the M2 macrophage signal at the injury centre indicates their specific presence in the region requiring intensified repair, while fibroblasts uniformly distribute around the lesion site (Figure 33a). This observation implies fibroblasts contribution to a supportive architecture for new cell growth, as M2 macrophages actively remove damaged tissues and activate tissue repair processes. This hints at potential spatial coordination in cellular activities, suggesting a guiding role of macrophages in tissue regeneration. To validate our *in vitro* replication of observed *in vivo* processes, we pursued additional analysis. Previous studies[74] by our group demonstrated that implanting HDE in mice led to the formation of a fibrotic capsule around the inserted material after nine days, mimicking acute wound scenarios. Examining stained sections of these fibrotic capsules, both with H&E staining (Figure 33b left) and with immunofluorescence (Figure 33b right), revealed a notable accumulation of M2 macrophages in the lesion area, confirming their crucial role in scar formation and extracellular microenvironment organization during the healing process.

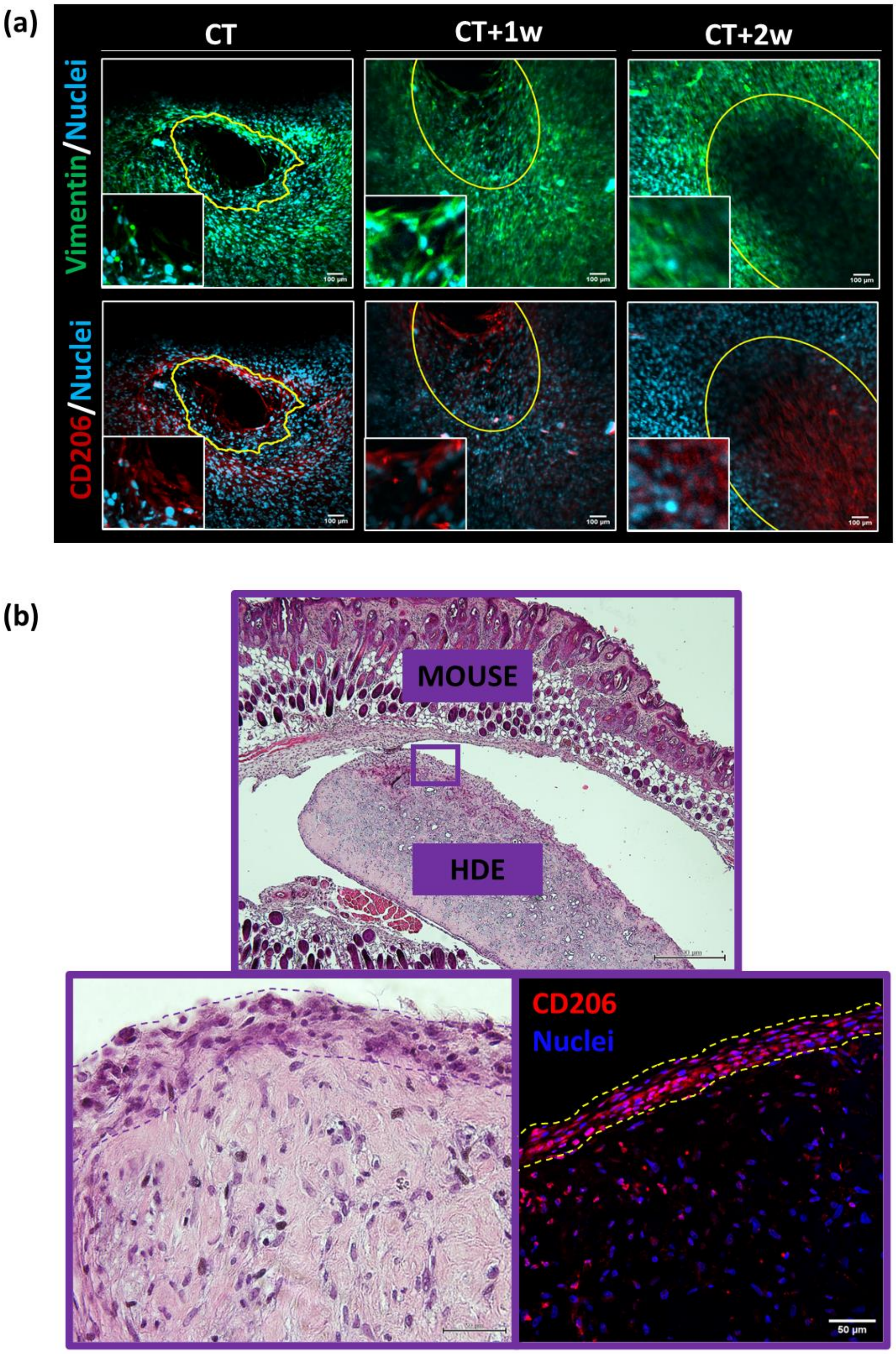

Figure 33 - Temporal dynamics of macrophages and fibroblasts in tissue healing processes. (a) CT to CT+2w Comparison: The M2 macrophage signal remains concentrated at the injury epicentre, signifying specific involvement in intensified repair, while fibroblasts exhibit uniform distribution around the lesion site. This suggests the supportive role of fibroblasts in facilitating new cell growth while M2 macrophages actively engage in tissue repair. (Original magnification 40x, scale bar 100 µm) (b) In

vitro Replication Validation: Bottom Left - H&E staining displays a fibrotic capsule formation around implanted material with cell nuclei accumulation. (Original magnification 4x and 40x, scale bar 500 µm and 50 µm); Bottom Right - Immunofluorescence exhibits notable accumulation of M2 macrophages (CD206 in red) within the fibrotic capsule, confirming their pivotal role in scar formation and orchestrating the extracellular microenvironment during healing processes. (Original magnification 40x, scale bar 50 µm)

Additionally, in our immunocompetent models, a continuous and progressive upregulation in α-SMA expression is detected (Figure 34a) in wounded +M2 models. This sustained increase implies the ongoing activation of fibroblasts by M2 macrophages, fostering wound contraction and facilitating the generation of new ECM components.

The α-SMA staining, indicative of myofibroblast activation, shows a substantial disparity between models with and without macrophages (Figure 34b). In models featuring macrophages, the progressive augmentation of α-SMA expression after wound closure suggests an active involvement of macrophages in regulating myofibroblasts to facilitate wound contraction and scar tissue formation.

Conversely, in models without macrophages, α-SMA decreases over time, showing that their continued presence might not be necessary after the initial healing phase.

Upon exposure to TGF-β1 released by M2 macrophages, fibroblasts tend to be excessively activated, transitioning into myofibroblasts that generate surplus ECM, thereby disrupting the regular tissue architecture and function and leading to the formation of scars and fibrosis.

A contributing factor to this activation of fibroblasts and the accumulation of ECM lies in the imbalance between matrix degradation and synthesis. Matrix degradation, a process facilitated by enzymes known as MMPs responsible for ECM component breakdown, typically maintains a delicate equilibrium with their inhibitors[1], TIMPs, regulating ECM turnover. However, in pathological scenarios like chronic wounds or inflammation, a decrease in MMP levels is observed, consequently resulting in diminished matrix breakdown and an augmented synthesis of matrix components (Figure 34c). This imbalance fosters a positive feedback loop that sustains both fibroblast activation and ECM accumulation.

The differential expression of MMP-1 in models with and without macrophages (Figure 34d) might indicate the critical role of TGF-β1 in the healing process. Lower MMP-1 levels in models with macrophages suggest an inhibitory action of TGF-β1 on the secretion of this enzyme[211], thereby promoting scar tissue formation and preventing excessive collagen degradation.

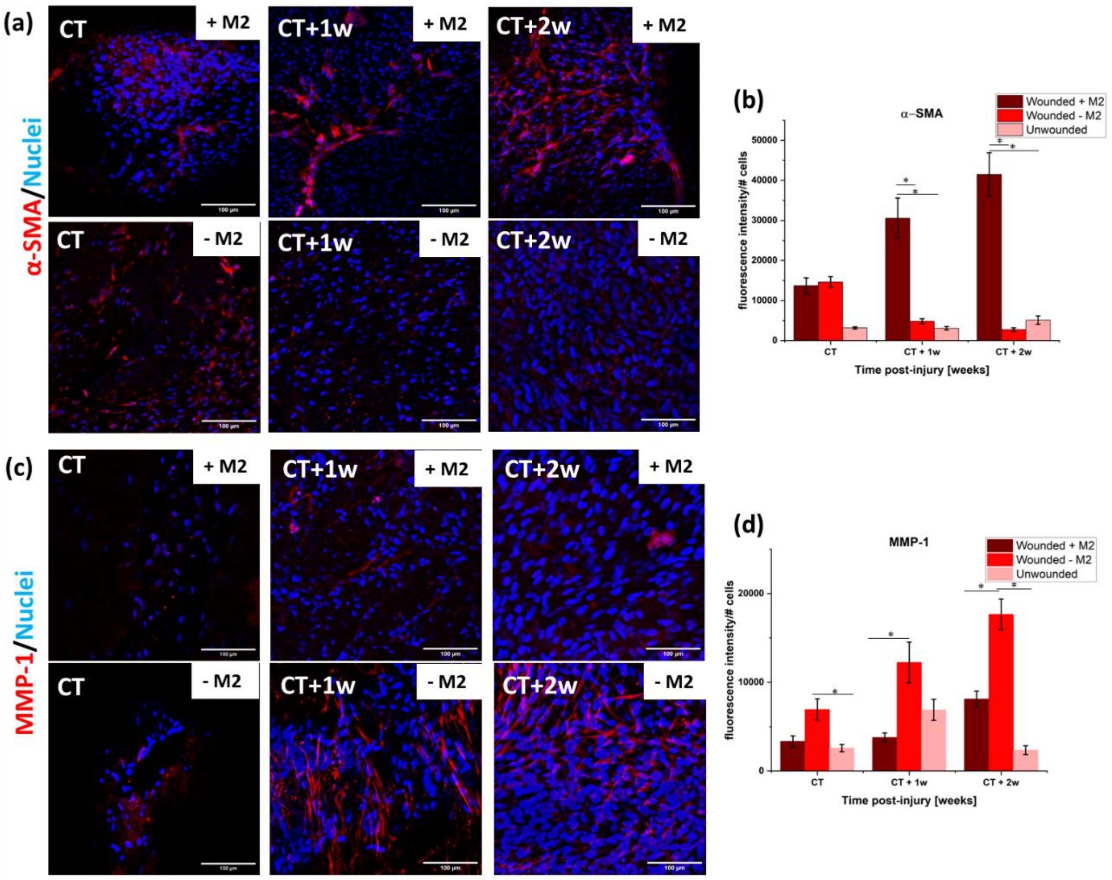

*Figure 34 - (a) Representative images of immunofluorescence-stained 3D-HDEs showing α-SMA (red), nuclei (blue), (original magnification 40x, scale bar 100 µm). Quantitative analysis of (b) α-SMA production expressed as fluorescence intensity/nuclei in wounded+M2, wounded-M2 and unwounded regions at CT, CT+1w and CT+2w. (c) Representative images of immunofluorescence-stained 3D-HDEs showing MMP-1 (red), nuclei (blue), (original magnification 40x, scale bar 100 µm). Quantitative analysis of (d) MMP-1 production expressed as fluorescence intensity/nuclei in wounded+M2, wounded-M2 and unwounded regions at CT, CT+1w and CT+2w. *p<0.05.*

4.3.3 ECM neoformation and remodelling after wound closure.

The analysis of immunofluorescence images depicting tenascin, fibronectin, and collagen at CT, CT+1w, and CT+2w intervals revealed intriguing insights into the role of these proteins in wound healing dynamics (Figure 35). The observed elevation in levels of tenascin, fibronectin, and collagen in both macrophage-present (wounded +M2) and macrophage-absent (wounded -M2) models compared to unwounded samples signify their involvement in the wound response process. Notably, their expression is significantly heightened in the presence of macrophages, indicating these immune cells' profound impact on their regulation. The heightened expression of these proteins in wound models, particularly in the presence of macrophages, suggests an enhanced and organized wound healing process, marked by robust tissue remodelling and scar formation. Their increased levels signify a critical phase in the wound healing cascade where the provisional matrix formed by tenascin and fibronectin facilitates cell migration, and collagen deposition provides structural integrity to the healing tissue.

The increased expression of tenascin, as depicted in green in Figure 35c, and fibronectin, shown in green in Figure 35a, particularly in the presence of macrophages, underscores their crucial involvement in scar formation and tissue remodelling. Tenascin-C is a matricellular protein that plays a significant role in wound healing and fibrosis. It is involved in chronic inflammation, differentiation, and recruitment of myofibroblasts[212]—key processes in fibrosis development. It has been discovered that tenascin-C influences the activation and signalling of TGF-β1 and plays a fundamental role in tissue remodelling and scar formation[212]. For this reason, its heightened expression, as observed in our results (Figure 35d), is commonly employed as a fibrotic biomarker, given that under normal conditions it is minimally expressed[26], as evidenced in our unwounded results. Similarly, increased fibronectin presence (Figure 35b), a mediator of cell adhesion and migration, implies active participation in wound contraction and wound bed organization crucial for tissue regeneration.

Moreover, the significant increase in collagen, as evidenced by SHG signals (Figure 35e), notably in models with macrophages, underscores the critical role of these immune cells in collagen synthesis and deposition during wound healing. Collagen, as the principal structural protein in the ECM, forms the framework for tissue repair, and the substantial increase (Figure 35f) observed in wounded +M2 models signifies their profound contribution to tissue matrix remodelling and scar formation.

Collagen deposition in the wound area provides tensile strength and stability to the healing tissue. However, an excessive accumulation or disorganized arrangement of collagen can lead to fibrosis and scar formation. This emphasizes the importance of a balanced collagen synthesis and proper alignment to prevent excessive scarring.

Moreover, the ELISA assay results for TGF-β1 between days 1 and 21 revealed compelling patterns in macrophage-present (+M2) and macrophage-absent (-M2) models (Figure 35g). Notably, the statistically significant elevation of TGF-β1 levels between days 10 and 14, corresponding to the closure phase in models with macrophages, suggests a potential correlation between macrophage presence and TGF-β1 release. This elevation underscores the influence of macrophages on TGF-β1 secretion, enhancing its availability in the wound microenvironment. It is noteworthy that fibroblasts also release TGF-β1, possibly explaining the presence of this molecule in higher amounts in macrophage-absent models, even if with varying levels due to the absence of macrophages.

Additionally, the TGF-β1 assay, conducted in the supernatant, likely retains a considerable amount trapped within the matrix, implying its utilization by fibroblasts. This trapped TGF-β1 within the matrix possibly facilitates prolonged exposure of fibroblasts to this growth factor, influencing their activation and contributing to ECM regulation.

The role of TGF-β1 in the context of scars is extremely significant. TGF-β1 is a multifunctional cytokine involved in various biological processes, including tissue healing. Its overexpression or excessive activation during the healing process can lead to the excessive formation of scar tissue. Under normal conditions, TGF-β plays an essential role in regulating the healing process by promoting collagen synthesis. However, an excess of TGF-β1 can surpass physiological regulation and lead to excessive scar tissue formation.

The high presence of TGF-β1 in models with macrophages, especially during the wound closure phase, suggests its dynamic regulation during healing. The increase in this cytokine might be related to macrophage activation, releasing more significant amounts of TGF-β1, flooding the wound area, and stimulating the transformation of fibroblasts into myofibroblasts, thereby accelerating scar formation.

As already observed for MMP-1 expression, an excessive concentration of TGF-β1 can also disrupt the balance between ECM synthesis and degradation, leading to excessive collagen production and compromising the proper tissue remodelling. This process of excessive ECM production and accumulation may contribute to hypertrophic or keloid scar formation.

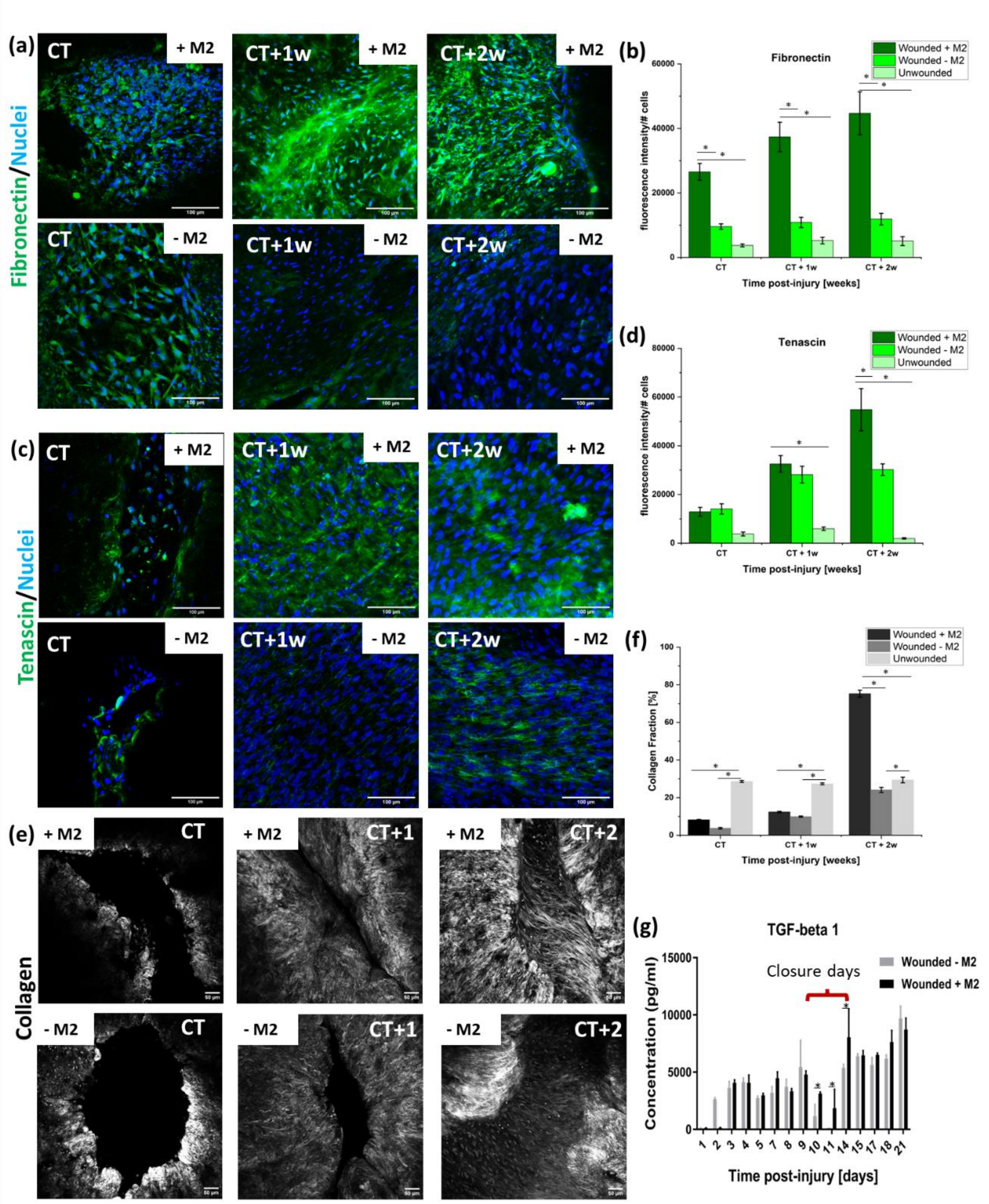

Figure 35 - (a) Representative images of immunofluorescence-stained 3D-HDEs showing Fibronectin (green), nuclei (blue), (original magnification 40x, scale bar 100 µm). Quantitative analysis of (b) Fibronectin production expressed as fluorescence intensity/nuclei in wounded+M2, wounded-M2 and unwounded regions at CT, CT+1w and CT+2w. (c) Representative images of immunofluorescence-stained 3D-HDEs showing tenascin (green), nuclei (blue), (original magnification 40x, scale bar 100 µm). Quantitative analysis of (d) MMP-1 production expressed as fluorescence intensity/nuclei in wounded+M2, wounded-M2 and unwounded regions at CT, CT+1w and CT+2w. (e) SHG representative images of the 3D-HDE in the wounded region with and without macrophages (original magnification 25x, scale bar 100 µm). Quantitative analysis of (f) collagen fraction in wounded and unwounded regions at CT, CT+1w and CT+2w. (g)

*ELISA assay results for TGF-β1 between days 1 and 21 after wound, in macrophage-present and macrophage-absent models *p<0.05*

Among the remarkable results obtained, there is one referred to the expression of HA. In the wounded -M2 models, a transient pattern of the HA signal has been observed (Figure 36a-up), with an increase from CT to CT+1w followed by a decrease from CT+1w to CT+2w (Figure 36b). This finding is significant as it aligns with a previous study[103] from our group that revealed a similar profile in a first intention wound model in the HDE model.

Moreover, this observation is consistent with literature[28,29] where it is reported that in adult wound healing, HA is initially expressed but disappears after 7 days, as in our case, unlike foetal wounds where HA persists for 3 weeks to stimulate regeneration. This result suggests that the transient HA profile in both wounded -M2 models and first intention wounded-HDE model[103] reflect normal healing processes.

On the other hand, in wounded +M2 models, the HA signal not only persists at the three-time points but increases over time from CT to CT+2w (Figure 36b). This result aligns with literature[30,31] indicating an accumulation of HA in fibrotic conditions, which can lead to permanent scarring. The persistence and increase in the HA signal in wounded +M2 models (Figure 36a-down) suggest a potential contribution of macrophages to the fibrotic process during wound healing.

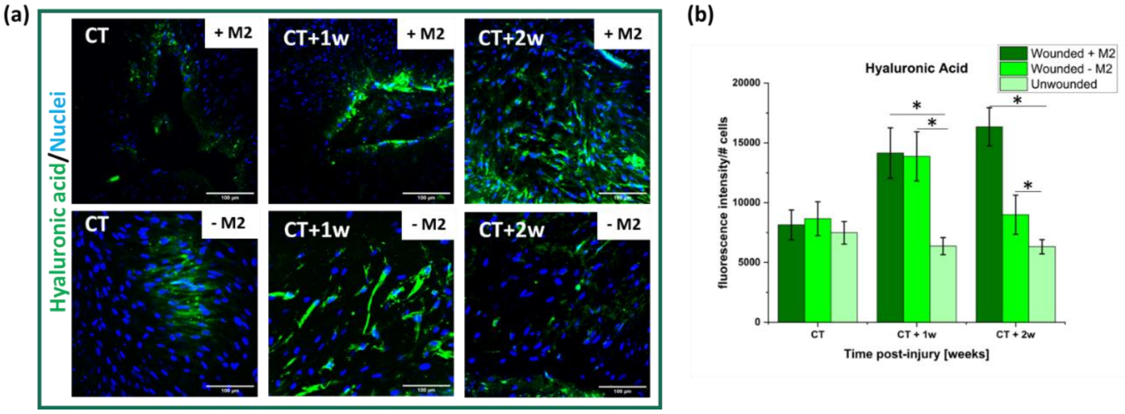

*Figure 36 - (a) Representative images of immunofluorescence-stained 3D-HDEs showing Hyaluronic acid (green), nuclei (blue), (original magnification 40x, scale bar 100 µm). Quantitative analysis of (b) Hyaluronic acid production expressed as fluorescence intensity/nuclei in wounded+M2, wounded-M2 and unwounded regions at CT, CT+1w and CT+2w. *p<0.05.*

4.3.4 Structural evaluation of Scar tissue: collagen and GAGs detection

Our investigation delved into the histological and imaging analysis of SHG and SEM micrographs from wounded+M2, wounded-M2, and unwounded models, focusing on the CT+2w time point. The SHG examinations unveiled a heightened expression of collagen in the models featuring M2 macrophages revealing a striking resemblance between the collagen organization observed in our immunocompetent models and the typical collagen arrangement found in human scars (Figure 37a). In particular, the obtained lacunarity values offer insight into the distribution and homogeneity of collagen fibres across the different models (Figure 37c). Specifically, the lower lacunarity value in the wounded+M2 models (around 0.35) suggests a more homogeneous distribution and less presence of empty spaces within the collagen structures compared to the wounded-M2 models (approximately 0.83) and the unwounded model (0.92). These values indicate a higher accumulation of densely aligned collagen fibres in the models featuring M2 macrophages, a characteristic typical of human scars.

The lower lacunarity in the M2 macrophage models implies greater uniformity and density of collagen fibres, consistent with the formation of mature scars. This denser organization of collagen fibres is further supported by the higher values of the COI in the wounded+M2 models compared to the wounded-M2 and unwounded models (Figure 37d). The higher COI indicates more alignment of collagen fibres in the M2 macrophage-present models, implying greater consistency in fibre direction compared to the other models. Moreover, SEM images corroborated these findings, highlighting more compact and aligned collagen fibres in the +M2 models analogous to the organized collagen bundles seen in human scar tissue (Figure 37e).

In the analysis conducted through SHG and SEM imaging, the measurement of collagen fibre diameter did not reveal significant differences among the +M2, -M2, and unwounded models (Figure 37b). These findings align with literature values that have measured collagen fibre diameter in scar biopsies and healthy tissue, showing no substantial differences[213].

This aspect suggests that collagen fibre diameter might not be the primary discriminator in scar organization and appearance. Instead, it appears that density, alignment, and organization of fibres are the predominant elements in scar formation, as indicated by lacunarity data, COI, and microscopic images.

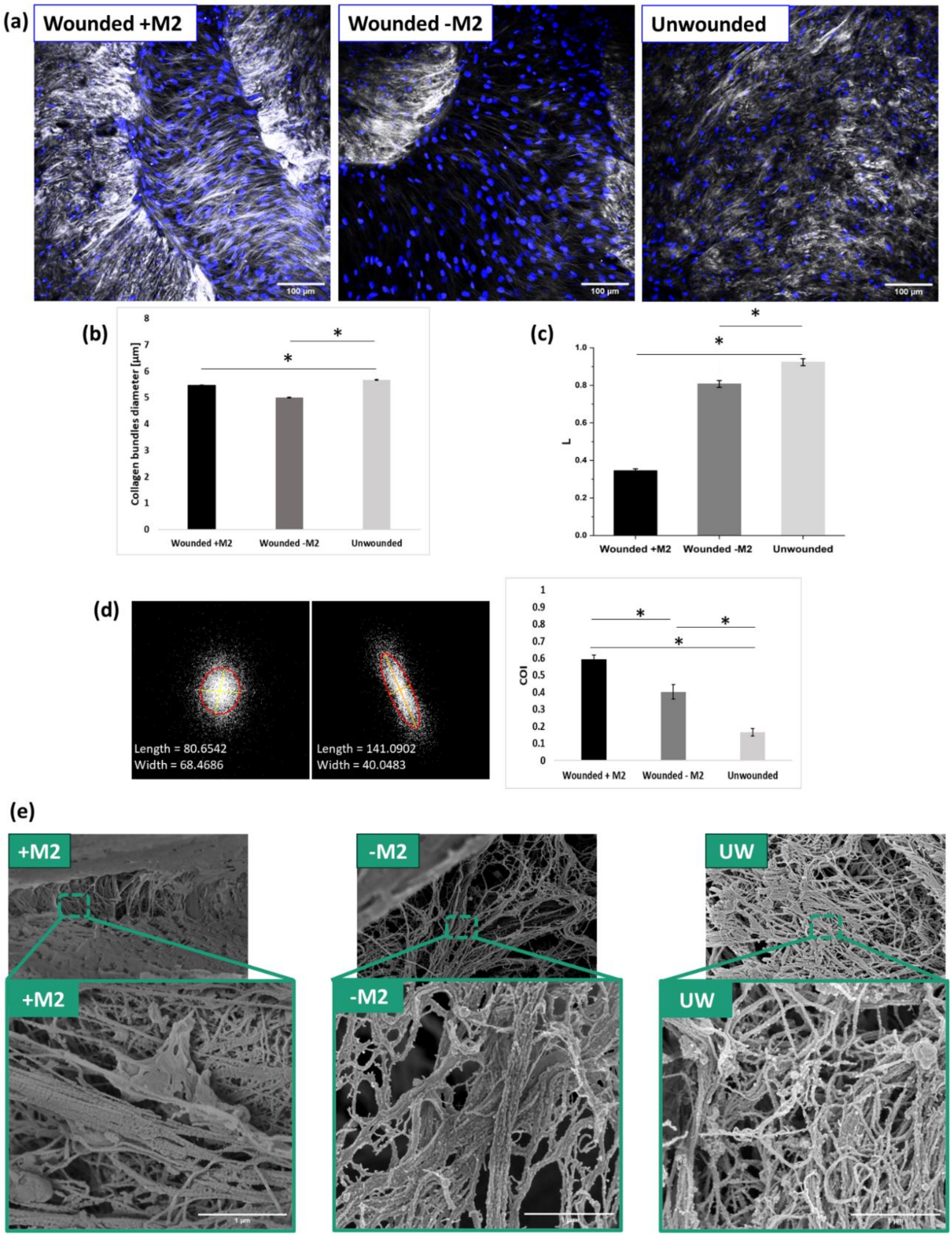

Figure 37 - Comparative analysis of collagen organization and structure in immunocompetent models. (a) SHG microscopy images of wounded +m2, wounded -m2

and unwounded regions at CT+2, (original magnification 25x, scale bar 100 µm). (b) Measurement of collagen fibre diameter. (c) Lacunarity values indicate varying distribution and homogeneity of collagen fibres in wounded+M2, wounded-M2 and unwounded at CT+2w. (d) COI displaying the alignment consistency of collagen fibres in wounded+M2, wounded-M2 and unwounded regions at CT+2w with FFT spectra. (e) SEM micrographs highlighting compact and aligned collagen fibres in the wounded+M2 models, akin to organized collagen bundles observed in human scar tissue.

Moreover, in the analysis conducted using the Piuma nano-indenter, notable findings emerged.

The results shown in Figure 38 indicate that, in wounded +M2 models, despite the matrix is still in a phase of neoformation and assembly, the values of the effective Young's modulus are already comparable to those observed in unwounded regions. Conversely, in wounded -M2 models, the values of the elastic modulus are lower and statistically differ from both unwounded and wounded +M2 models.

This discrepancy underscores the substantial influence of the presence of M2 macrophages in facilitating the efficient and rapid formation of new matrix.

An intriguing hypothesis arises from these data, suggesting that in wounded +M2 models, the values of the elastic modulus may further increase during the complete maturation and remodelling of the matrix. This phenomenon draws parallels with *in vivo* scars, known for their reduced elasticity and increased rigidity compared to surrounding tissues.

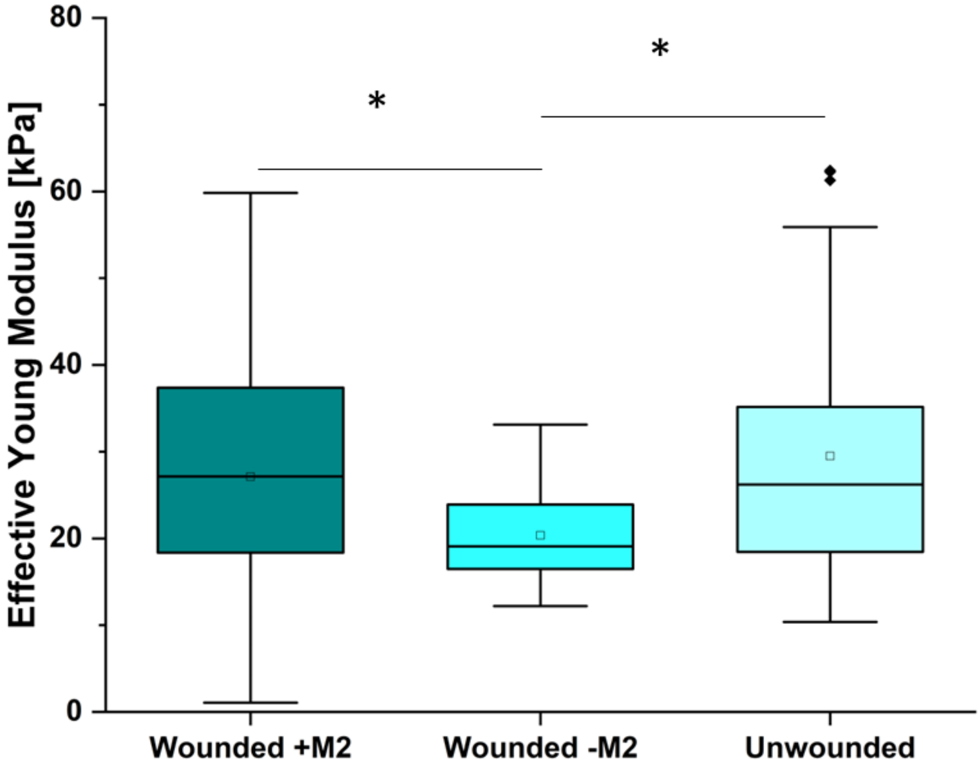

*Figure 38 - Diagram of the effective elastic modulus of the wounded +M2, wounded -M2 and unwounded regions. *p<0.05*

The histological stains, specifically Picrosirius and Alcian Blue, offered additional insights (Figure 39). The Picrosirius stain at CT+1w and CT+2w revealed an augmented presence of aligned collagen fibres in red hues, resembling the formation of a fibrotic capsule in the +M2 models.

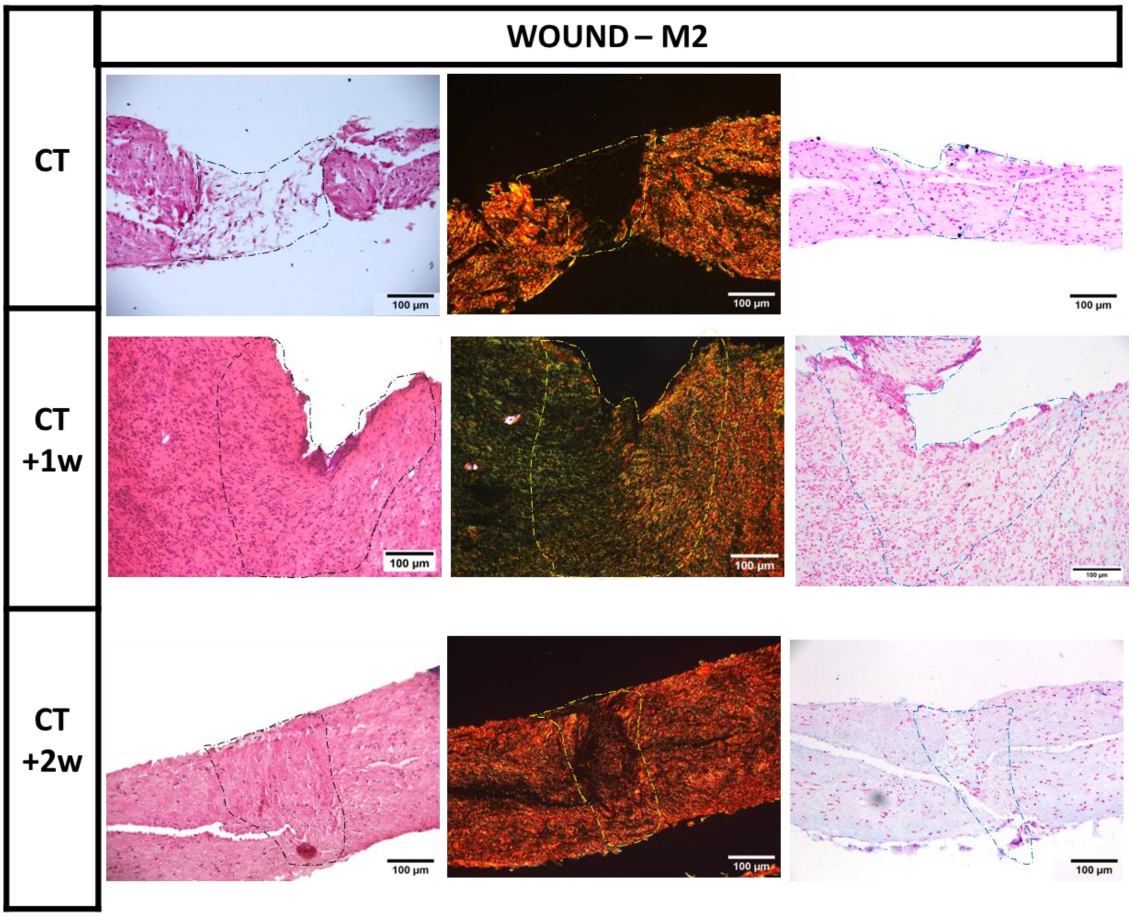
WOUND – M2
CT
CT +1w
CT +2w
100 µm

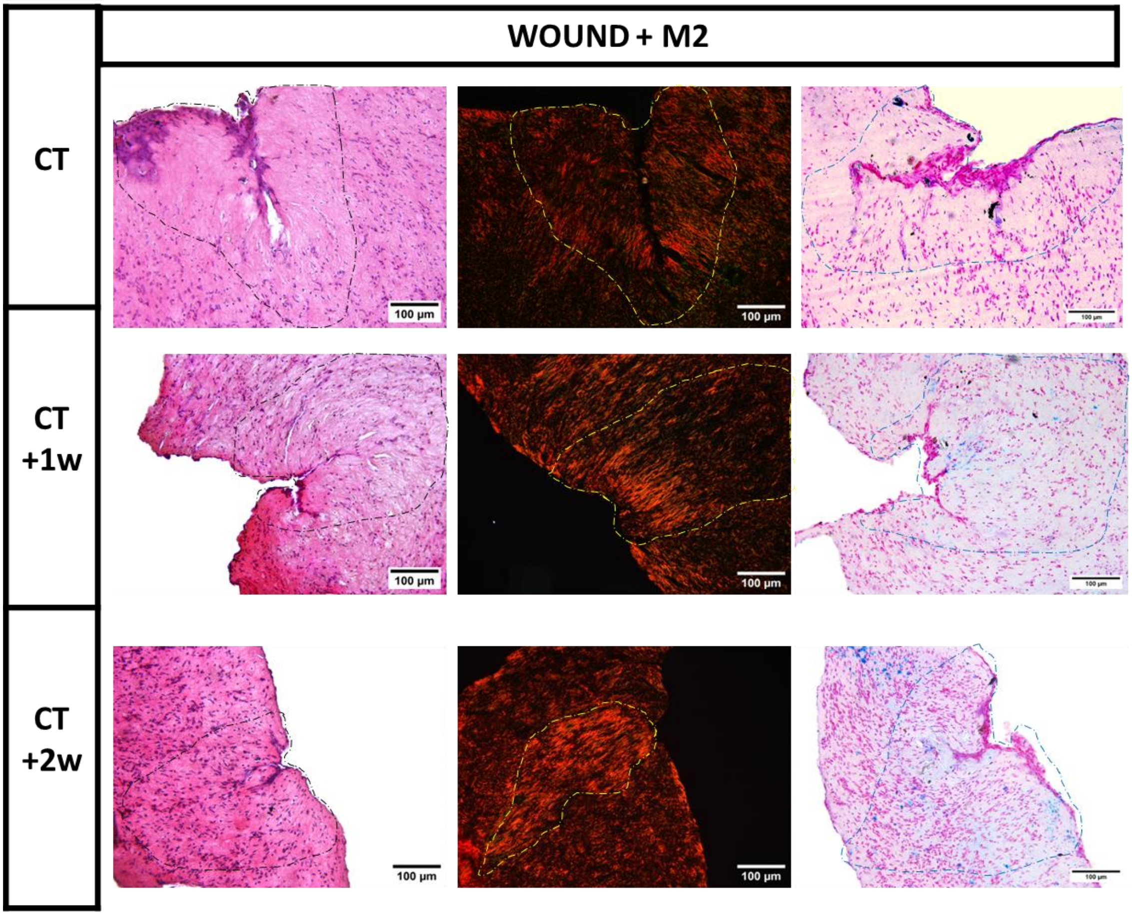
WOUND + M2
CT
CT +1w
CT +2w
100 µm

Figure 39 - Histological tissue slices staining of wounded+M2 and wounded-M2 models at CT, CT+1w, and CT+2w. The images display tissue sections stained with H&E, Picrosirius Red, and Alcian Blue, illustrating the dynamic changes in tissue morphology and composition over time. (original magnification 20x, scale bar 100 µm)

Further elaboration on the collagen fibre analysis indicated the prevalence of type I collagen, reflected by a higher red-to-green ratio in Picrosirius-stained samples from the +M2 models (Figure 40a). The abundance of red hues signifies the dominance of type I collagen, a hallmark of mature scar tissue, while green hues typically represent type III collagen. This data implies the conversion of type III collagen into type I collagen, reinforcing the formation of a stable scar in the presence of M2 macrophages.

Additionally, Alcian Blue staining demonstrated an increase in GAGs in the +M2 models (Figure 40b), suggesting a heightened presence of HA. This aligns with the human scar composition, where scar tissues also exhibit an accumulation of GAGs[31].

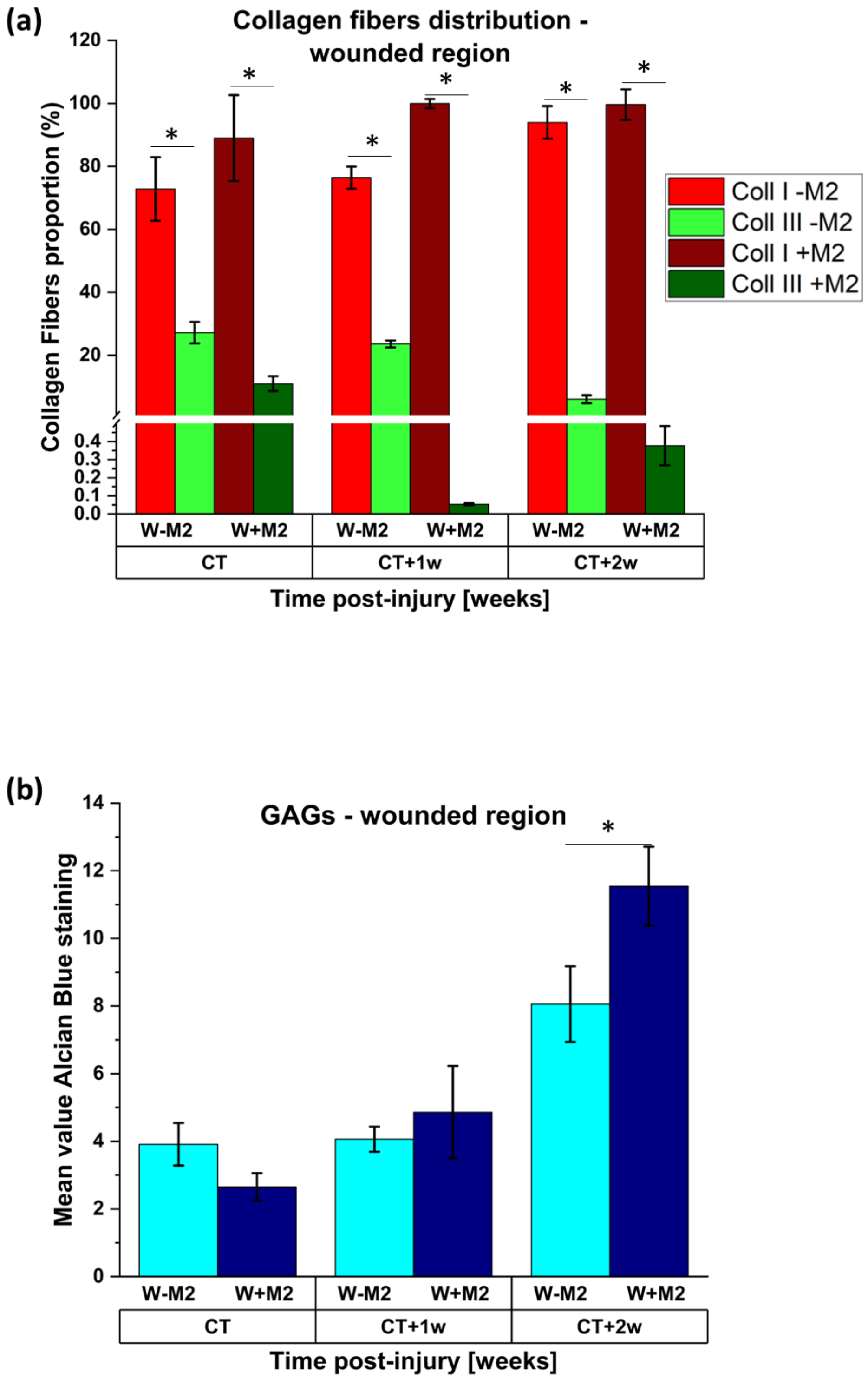

Figure 40 - Quantitative analysis of collagen fibre composition and GAGs in +M2 and -M2 wound models. (a) Histogram illustrating the red (Collagen I) and green (Collagen III) intensity ratios derived from Picrosirius staining in wounded +M2 and wounded -M2 models at CT, CT+1w, and CT+2w time points. The higher red-to-green ratio in +M2 models indicates an increased prevalence of type I collagen, characteristic of mature scar tissue formation, suggesting a shift from type III to type I collagen. (b) Histogram

*representing Alcian Blue staining intensity, highlighting elevated GAGs, potentially indicating heightened levels of hyaluronic acid (HA), in wounded +M2 compared to wounded -M2 models across CT, CT+1w, and CT+2w time points. *$p<0.05$*

This striking similarity between our +M2 models and human scar tissue emphasizes the critical role of M2 macrophages in coordinating a collagen-rich environment conducive to scar formation. The highly aligned collagen fibres and increased GAGs, akin to human scar characteristics, underscore the potential of M2 macrophages in regulating scar tissue formation and ECM remodelling, reflecting their relevance in human wound healing.

Comparison with the implanted HDE in mouse models, manifesting SHG and Picrosirius red-stained images of aligned collagen fibres, demonstrated the collagen fibres' disposition in a fibrotic state (Figure 41a). In Figure 41b, the multiphoton image illustrates both murine and fibrotic capsule collagen surrounding the HDE implant. Notably, the fibrotic capsule surrounding the HDE exhibits a more organized and aligned collagen arrangement compared to the surrounding murine collagen. The COI analysis, represented in Figure 41d, quantitatively supports these observations. The COI values demonstrate a higher index for the collagen within the fibrotic capsule compared to the surrounding murine collagen, signifying a greater degree of fibre alignment and orientation within the capsule. This aligns with the SHG images, indicating that the collagen fibres within the fibrotic capsule exhibit a more aligned disposition, contributing to a more ordered and structured collagen network as in the human scar tissue. The implanted HDE sections showed yellow and green hues instead of the prevalent red observed in our models and this discrepancy could be attributed to the immature collagen status after nine days of implantation. Nevertheless, in the analysis of Picrosirius staining of the HDE implanted in mice (Figure 41c), the fibrotic capsule formed exhibited approximately 75% red and 25% green hues, whereas the surrounding murine collagen showed roughly 25% red and 75% green (Figure 41e). Despite the immature collagen status within the fibrotic capsule, the higher presence of red hues indicates a prevalence of type I collagen. This observation suggests an intriguing aspect of the collagen composition within the fibrotic capsule, where even in its immature state, the prevalent type I collagen is indicative of early scar formation.

This divergence underscores the nuanced variations in collagen organization and composition at various stages of wound healing. It signifies that while our models exhibit mature collagen patterns resembling stable scar tissue, the HDE implanted in mice manifests an immature collagen arrangement due to the shorter healing duration.

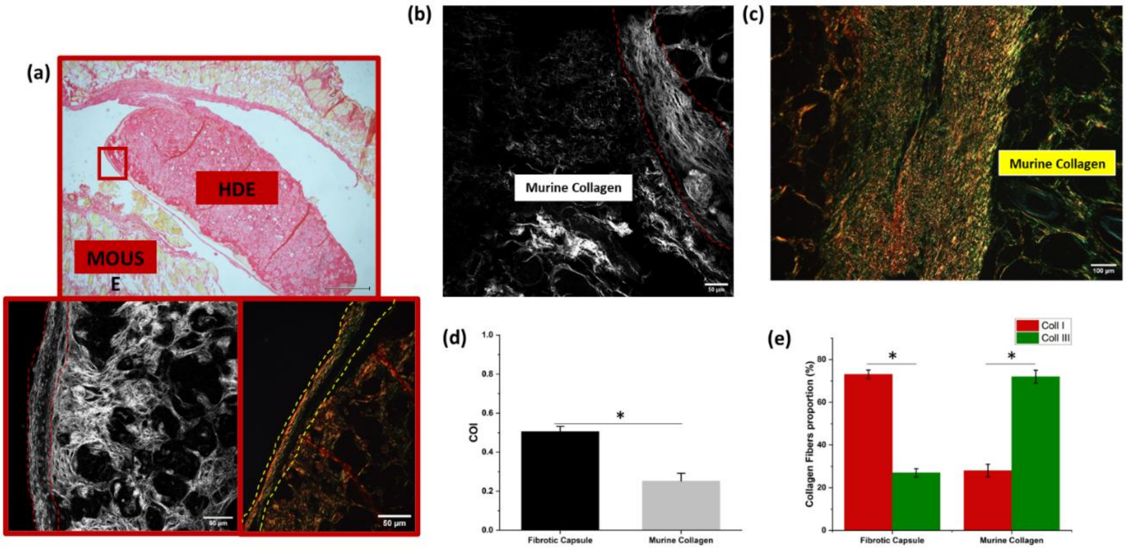

*Figure 41 - Comparative analysis of collagen organization between the fibrotic capsule around the HDE implant and the surrounding murine collagen. (a) SHG and Picrosirius red-stained images depicting aligned collagen fibres within the encapsulated HDE implant in mice after nine days. (b) Multiphoton image displaying collagen distribution, highlighting the fibrotic capsule's more organized and aligned arrangement compared to surrounding murine collagen. (c) Picrosirius staining analysis indicates red-to-green hue proportions in the fibrotic capsule and surrounding murine collagen. (d) Histogram presenting the COI comparison between the fibrotic capsule and murine collagen, showcasing increased fibre alignment within the capsule. (e) Histogram illustrating the collagen fibbers' type I to type III proportion in the fibrotic capsule and murine collagen, emphasizing a higher presence of type I collagen within the immature fibrotic capsule despite its early healing stage. *p<0.5*

4.4 Conclusions

Through a detailed analysis of our results, it is clearly outlined the crucial importance of the endogenous matrices integrated with macrophages in accurately simulating the processes of scar formation. This approach, compared to conventional models, has allowed us to replicate the real tissue environment more precisely, providing a significant and accurate experimental platform.

The integration of endogenous matrices with the immune system has marked a crucial step in understanding the complex mechanisms underlying scar formation. In particular, macrophages, with their versatility and functional plasticity, have a leading role in modulating the ECM during tissue repair. These immune cells, especially the M2 subpopulation, play a significant role in orchestrating a microenvironment favourable to tissue repair[21,194,214].

The rapid and dynamic presence of macrophages along the wound edges, observed within an hour of injury, highlights an immediate response to support tissue homeostasis and initiate the healing process.

The further integration of macrophages into the newly formed matrix after wound closure confirms their crucial role in ECM maturation. Immunofluorescence showing the co-localization of CD206 and integrin $\alpha_2\beta_1$ signals is a clear example of how macrophages actively interact with collagen fibres, reinforcing the idea of their fundamental involvement in tissue reconstruction.

This bidirectional dialogue between macrophages and the ECM significantly influences fibroblast behaviour. Results analysis revealed that the presence of macrophages positively regulates fibroblast activation, promoting an increase in the expression of markers such as α-SMA, indicating myofibroblast activation. This process was less evident in models without macrophages, highlighting the significant role of these immune cells in fibroblast activation and induction of the myofibroblast phenotype.

The reciprocal interaction between macrophages and fibroblasts not only contributes to wound contraction but also regulates the production of crucial components of the ECM, leading to the formation of stable scar tissue.

In our wound models with macrophages, a high expression of tenascin, fibronectin, collagen, and hyaluronic acid was observed.

The results of this study showed a continuous accumulation of tenascin-C and hyaluronic acid, which is supported by literature stating that excessive levels of tenascin-C[215] are found in chronic conditions such as cancer, rheumatoid arthritis, and fibrosis, and increased concentration of hyaluronic acid[30] is found in permanent fibrotic scars.

The high expression of fibronectin in HDE models with M2 macrophages is, also, a relevant aspect. This finding is consistent with the literature[216], where fibronectin emerges as a crucial component in altering the biochemical composition of stroma in pathological fibrosis conditions. The authors mention fibronectin as a regulator of collagen organization, highlighting its increased deposition in various forms of fibrosis, including pulmonary, hepatic, cardiac, and renal fibrosis.

Therefore, the high expression of fibronectin in HDE models with M2 macrophages could reflect a parallel with the observed increase in fibrotic conditions. While fibroblasts are the main source of fibronectin, article[216] highlights how monocytes, when exposed to a context rich in pro-inflammatory cytokines, can sequester this protein. This occurs in parallel with the high expression of fibronectin in alternatively activated macrophages, such as M2 types.

Moreover, the significant increase in collagen, highlighted by SHG signals, especially in models with macrophages, underlines the critical role of these macrophages in collagen synthesis and deposition during wound healing. Collagen, the main structural protein of the ECM, represents the framework for tissue repair, and its increase in models with macrophages testifies to their contribution to tissue regeneration and scar formation[217]. Concurrently, the analysis of MMP-1, an enzyme involved in the degradation of the ECM, showed different expressions in models with and without macrophages. Lower expression of MMP-1 in models with macrophages suggests an inhibitory action of TGF-β1 on the secretion of this enzyme[211,218], thus promoting scar tissue formation and preventing excessive collagen degradation. The resulting scars are characterized by a high density of collagen without an effective degradation mechanism. In the absence of precise regulation of collagen synthesis and degradation processes, excessive formation and accumulation of this structural element can destabilize the delicate tissue environment, limiting the functionality and flexibility of the affected area.

Comparison with murine *in vivo* models has highlighted significant similarities in the structure, arrangement, and type of collagen fibres. Collagen fibres, observed as oriented and aligned similarly to fibrotic murine models, suggest a high structural similarity between the scar obtained through our *in vitro* models and *in vivo* scar formation. A heightened alignment of collagen fibres has been identified in the presence of the immune system, constituting a hallmark feature of fibrotic tissues, including those associated with scarring[219].

The mutual involvement between macrophages and the ECM has proven to play a decisive role in modulating the structure and properties of the scar. Our endogenous models have contributed to understanding this interaction, highlighting how they are capable of replicating processes similar to human scar formation. This opens up new perspectives for the development of targeted and innovative therapies in scar management and tissue healing.

References

1. Nguyen, D. T., Orgill, D. P. & Murphy, G. F. The pathophysiologic basis for wound healing and cutaneous regeneration. *Biomater. Treat. Ski. Loss A Vol. Woodhead Publ. Ser. Biomater.* 25–57 (2009) doi:10.1533/9781845695545.1.25.
2. Gauglitz, G. G., Korting, H. C., Pavicic, T., Ruzicka, T. & Jeschke, M. G. Hypertrophic scarring and keloids: Pathomechanisms and current and emerging treatment strategies. *Mol. Med.* **17**, 113–125 (2011).
3. El Khouly, S. S. A. E. A., Atwa, E. M. E. S. & Samir, M. A. Atrophic Acne Scars; Insight about Future Management Lines: Review Article. *Egypt. J. Hosp. Med.* **90**, 3143–3146 (2023).
4. Connolly, D., Vu, H. L., Mariwalla, K. & Saedi, N. Acne scarring-pathogenesis, evaluation, and treatment options. *J. Clin. Aesthet. Dermatol.* **10**, 12–23 (2017).
5. Goel, A. & Shrivastava, P. Post-burn scars and scar contractures. *Indian J. Plast. Surg.* **43**, (2010).
6. Bordoni, B. & Zanier, E. Skin, fascias, and scars: Symptoms and systemic connections. *J. Multidiscip. Healthc.* **7**, 11–24 (2013).
7. Larouche, J., Sheoran, S., Maruyama, K. & Martino, M. M. Immune regulation of skin wound healing: Mechanisms and novel therapeutic targets. *Adv. Wound Care* **7**, 209–231 (2018).
8. Zhu, Z., Ding, J., Ma, Z., Iwashina, T. & Tredget, E. E. Systemic depletion of macrophages in the subacute phase of wound healing reduces hypertrophic scar formation. *Wound Repair Regen.* **24**, 644–656 (2016).
9. Urciuolo, F., Passariello, R., Imparato, G., Casale, C. & Netti, P. A. Bioengineered Wound Healing Skin Models: The Role of Immune Response and Endogenous ECM to Fully Replicate the Dynamic of Scar Tissue Formation In Vitro. *Bioengineering* vol. 9 at https://doi.org/10.3390/bioengineering9060233 (2022).
10. Tracy, L. E., Minasian, R. A. & Caterson, E. J. Extracellular Matrix and

Dermal Fibroblast Function in the Healing Wound. *Adv. Wound Care* **5**, 119–136 (2016).

11. Ozcelikkale, A., Dutton, J. C., Grinnell, F. & Han, B. Effects of dynamic matrix remodelling on en masse migration of fibroblasts on collagen matrices. *J. R. Soc. Interface* **14**, (2017).
12. Pan, Z. *et al.* Deformation gradients imprint the direction and speed of en masse fibroblast migration for fast healing. *J. Invest. Dermatol.* **133**, 2471–2479 (2013).
13. Yu, Y. *et al.* Macrophages play a key role in tissue repair and regeneration. *PeerJ* **10**, (2022).
14. Brown, B. C., McKenna, S. P., Siddhi, K., McGrouther, D. A. & Bayat, A. The hidden cost of skin scars: quality of life after skin scarring. *J. Plast. Reconstr. Aesthetic Surg.* **61**, 1049–1058 (2008).
15. Neves, L. M. G., Wilgus, T. A. & Bayat, A. In Vitro, Ex Vivo, and in Vivo Approaches for Investigation of Skin Scarring: Human and Animal Models. *Adv. Wound Care* **12**, 97–116 (2023).
16. Witte, M. B. & Barbul, A. General principles of wound healing. *Surg. Clin. North Am.* **77**, 509–528 (1997).
17. Gurtner, G. C., Werner, S., Barrandon, Y. & Longaker, M. T. Wound repair and regeneration. *Nature* **453**, 314–321 (2008).
18. Behm, B., Babilas, P., Landthaler, M. & Schreml, S. Cytokines, chemokines and growth factors in wound healing. *J. Eur. Acad. Dermatology Venereol.* **26**, 812–820 (2012).
19. Diegelmann, R. F. & Evans, M. C. Departments of Biochemistry, Anatomy, Emergency Medicine and Virginia Commonwealth University, Richmond Virginia. *Front. Biosci.* 283–289 (2004).
20. Sorg, J. M. R. H. Wound Repair and Regeneration. 35–43 (2012) doi:10.1159/000339613.
21. Delavary, B. M., van der Veer, W. M., van Egmond, M., Niessen, F. B. & Beelen, R. H. J. Macrophages in skin injury and repair. *Immunobiology* **216**, 753–762 (2011).

22. Martin, C. W. The role of lymphocytes. 655–662 (1990).
23. Ian C. Boothby, Jarish N. Cohen, M. D. R. Regulatory T cells in Skin Injury: At the Crossroads of Tolerance and Tissue Repair. *Sci Immunol.* **5**, (2020).
24. Short, W. D., Wang, X. & Keswani, S. G. The Role of T Lymphocytes in Cutaneous Scarring. *Adv. Wound Care* **00**, 1–11 (2021).
25. Grieb, G., Steffens, G., Pallua, N., Bernhagen, J. & Bucala, R. Circulating Fibrocytes-Biology and Mechanisms in Wound Healing and Scar Formation. *Int. Rev. Cell Mol. Biol.* **291**, 1–19 (2011).
26. Potekaev, N. N. *et al.* The role of extracellular matrix in skin wound healing. *J. Clin. Med.* **10**, (2021).
27. Choi, Y. E. *et al.* Effects of tenascin c on the integrity of extracellular matrix and skin aging. *Int. J. Mol. Sci.* **21**, 1–17 (2020).
28. Kavasi, R. M. *et al.* HA metabolism in skin homeostasis and inflammatory disease. *Food Chem. Toxicol.* **101**, 128–138 (2017).
29. Monavarian, M., Kader, S., Moeinzadeh, S. & Jabbari, E. Regenerative Scar-Free Skin Wound Healing. *Tissue Eng. - Part B Rev.* **25**, 294–311 (2019).
30. Wynn, T. A. Common and unique mechanisms regulate fibrosis in various fibroproliferative diseases. *J. Clin. Invest.* **117**, 524–529 (2007).
31. Ghatak, S. *et al.* Roles of Proteoglycans and Glycosaminoglycans in Wound Healing and Fibrosis. *Int. J. Cell Biol.* **2015**, (2015).
32. Senger, D. R. & Davis, G. E. Angiogenesis. 1–20 (2011).
33. Rousselle, P., Braye, F. & Dayan, G. Re-epithelialization of adult skin wounds: Cellular mechanisms and therapeutic strategies. *Adv. Drug Deliv. Rev.* **146**, 344–365 (2019).
34. Larson, B. J., Nauta, A., Kawai, K., Longaker, M. T. & Lorenz, H. P. Scarring and scarless wound healing. *Adv. Wound Repair Ther.* 77–111 (2011) doi:10.1533/9780857093301.1.77.
35. DiPietro, L. A. & Schrementi, M. Oral Mucosal Healing. *Wound Heal. Stem Cells Repair Restorations, Basic Clin. Asp.* 125–132 (2018) doi:10.1002/9781119282518.ch10.

36. Han, S.-K. *Basics of Wound Healing*. *Innovations and Advances in Wound Healing* (2023). doi:10.1007/978-981-19-9805-8_1.

37. Percival, N. J. Classification of Wounds and their Management. *Surg.* **20**, 114–117 (2002).

38. Strodtbeck, F. Physiology of wound healing. *Newborn Infant Nurs. Rev.* **1**, 43–52 (2001).

39. Foad, A. F. A. Acute and Chronic Wound Healing Physiology. *Diabet. foot ulcer An Updat.* 63–76 (2020) doi:10.1007/978-981-15-7639-3_4.

40. Simmons, J. Wound Healing and Assessment. *J. Dermatol. Nurses. Assoc.* **14**, 197–202 (2022).

41. Chhabra, S., Chhabra, N., Kaur, A. & Gupta, N. Wound Healing Concepts in Clinical Practice of OMFS. *J. Maxillofac. Oral Surg.* **16**, 403–423 (2017).

42. Repair, S. Intention Healing :

43. Donaldson, M. & Coldiron, B. Scars after second intention healing. *Facial Plast. Surg.* **28**, 497–503 (2012).

44. Harper, D., Young, A. & McNaught, C. E. The physiology of wound healing. *Surg. (United Kingdom)* **32**, 445–450 (2014).

45. B. Prucz Roni. Article. *Basic Surg. Perioper. Considerations* (2012) doi:10.2310/7800.2022.

46. Regeneration in humans - Wikipedia. (2016).

47. Ud-Din, S. & Bayat, A. Classification of Distinct Endotypes in Human Skin Scarring: S.C.A.R.-A Novel Perspective on Dermal Fibrosis. *Adv. Wound Care* **11**, 109–120 (2022).

48. Sharma, M. & Wakure, A. Scar revision. *Indian J. Plast. Surg.* **46**, 408–418 (2013).

49. Chike-Obi, C., Cole, P. & Brissett, A. Keloids: Pathogenesis, Clinical Features, and Management. *Semin. Plast. Surg.* **23**, 178–184 (2009).

50. Zhu, Z., Ding, J. & Tredget, E. E. The molecular basis of hypertrophic scars. *Burn. Trauma* **4**, 1–12 (2016).

51. Kwan, P., Hori, K., Ding, J. & Tredget, E. E. Scar and Contracture: Biological Principles. *Hand Clin.* **25**, 511–528 (2009).

52. Akita, S. *et al.* The neck burn scar contracture: A concept of effective treatment. *Burn. Trauma* **5**, 1–8 (2017).
53. Chen, J. *et al.* Techniques for navigating postsurgical adhesions: Insights into mechanisms and future directions. *Bioeng. Transl. Med.* **8**, 1–22 (2023).
54. Poole, J. H. Adhesions following cesarean delivery: A review of their occurrence, consequences and preventative management using adhesion barriers. *Women's Heal.* **9**, 467–477 (2013).
55. Herrick, S. E. & Wilm, B. Post-surgical peritoneal scarring and key molecular mechanisms. *Biomolecules* **11**, 1–17 (2021).
56. Furth, M. E. & Atala, A. *Tissue Engineering: Future Perspectives. Principles of Tissue Engineering: Fourth Edition* (Elsevier, 2013). doi:10.1016/B978-0-12-398358-9.00006-9.
57. Kaul, H. & Ventikos, Y. On the genealogy of tissue engineering and regenerative medicine. *Tissue Eng. - Part B Rev.* **21**, 203–217 (2015).
58. Chan, B. P. & Leong, K. W. Scaffolding in tissue engineering: General approaches and tissue-specific considerations. *Eur. Spine J.* **17**, (2008).
59. Loh, Q. L. & Choong, C. Three-dimensional scaffolds for tissue engineering applications: Role of porosity and pore size. *Tissue Eng. - Part B Rev.* **19**, 485–502 (2013).
60. Nitti, P. *et al.* Cell-Tissue Interaction: The Biomimetic Approach to Design Tissue Engineered Biomaterials. *Bioengineering* **10**, (2023).
61. Esdaille, C. J., Washington, K. S. & Laurencin, C. T. Regenerative engineering: A review of recent advances and future directions. *Regen. Med.* **16**, 495–512 (2021).
62. Dermenoudis, S. & Missirlis, Y. F. Bioreactors in tissue engineering. *Adv. Eng. Mater.* **12**, 592–608 (2010).
63. Salehi-Nik, N. *et al.* Engineering parameters in bioreactor's design: A critical aspect in tissue engineering. *Biomed Res. Int.* **2013**, (2013).
64. Fu, L. *et al.* The Application of Bioreactors for Cartilage Tissue Engineering: Advances, Limitations, and Future Perspectives. *Stem Cells Int.* **2021**, (2021).

65. Xie, Z., Gao, M., Lobo, A. O. & Webster, T. J. 3D bioprinting in tissue engineering for medical applications: The classic and the hybrid. *Polymers (Basel).* **12**, (2020).

66. Liu, N., Zhang, X., Guo, Q., Wu, T. & Wang, Y. 3D Bioprinted Scaffolds for Tissue Repair and Regeneration. *Front. Mater.* **9**, 1–17 (2022).

67. Persaud, A., Maus, A., Strait, L. & Zhu, D. 3D Bioprinting with Live Cells. *Eng. Regen.* **3**, 292–309 (2022).

68. Zieliński, P. S., Gudeti, P. K. R., Rikmanspoel, T. & Włodarczyk-Biegun, M. K. 3D printing of bio-instructive materials: Toward directing the cell. *Bioact. Mater.* **19**, 292–327 (2023).

69. Toprakhisar, B., Verfaillie, C. M. & Kumar, M. Advances in Recellularization of Decellularized Liver Grafts with Different Liver (Stem) Cells: Towards Clinical Applications. *Cells* **12**, (2023).

70. Schmidt, T., Xiang, Y., Bao, X. & Sun, T. A paradigm shift in tissue engineering: From a top–down to a bottom–up strategy. *Processes* **9**, 1–17 (2021).

71. Yamada, K. M., Doyle, A. D. & Lu, J. Cell–3D matrix interactions: recent advances and opportunities. *Trends Cell Biol.* **32**, 883–895 (2022).

72. Echeverria Molina, M. I., Malollari, K. G. & Komvopoulos, K. Design Challenges in Polymeric Scaffolds for Tissue Engineering. *Front. Bioeng. Biotechnol.* **9**, 1–29 (2021).

73. Casale, C., Imparato, G., Urciuolo, F. & Netti, P. A. Endogenous human skin equivalent promotes in vitro morphogenesis of follicle-like structures. *Biomaterials* **101**, 86–95 (2016).

74. Mazio, C. *et al.* Pre-vascularized dermis model for fast and functional anastomosis with host vasculature. *Biomaterials* **192**, 159–170 (2019).

75. Imparato, G. *et al.* A novel engineered dermis for in vitro photodamage research. *J. Tissue Eng. Regen. Med.* **11**, 2276–2285 (2017).

76. Palmiero, C., Imparato, G., Urciuolo, F. & Netti, P. Engineered dermal equivalent tissue in vitro by assembly of microtissue precursors. *Acta Biomater.* **6**, 2548–2553 (2010).

77. De Gregorio, V. *et al.* Immunoresponsive microbiota-gut-on-chip reproduces barrier dysfunction, stromal reshaping and probiotics translocation under inflammation. *Biomaterials* **286**, 121573 (2022).
78. Maestri, E. The 3Rs Principle in Animal Experimentation: A Legal Review of the State of the Art in Europe and the Case in Italy. *BioTech 2021, Vol. 10, Page 9* **10**, 9 (2021).
79. Sami, D. G., Heiba, H. H. & Abdellatif, A. Wound healing models: A systematic review of animal and non-animal models. *Wound Med.* **24**, 8–17 (2019).
80. Chim, S. M. *et al.* EGFL6 promotes endothelial cell migration and angiogenesis through the activation of extracellular signal-regulated kinase. *J. Biol. Chem.* **286**, 22035–22046 (2011).
81. Matsubayashi, Y., Razzell, W. & Martin, P. ‘ White wave ’ analysis of epithelial scratch wound healing reveals how cells mobilise back from the leading edge in a myosin-II-dependent fashion. 1017–1021 (2011) doi:10.1242/jcs.080853.
82. Gottrup, F., Ågren, M. S. & Karlsmark, T. Models for use in wound healing research: A survey focusing on in vitro and in vivo adult soft tissue. *Wound Repair Regen.* **8**, 83–96 (2000).
83. Bacakova, M. *et al.* Erratum to a Two-layer skin construct consisting of a collagen hydrogel reinforced by a fibrin-coated polylactide nanofibrous membrane (Int J Nanomedicine, (2019), 14, (5033–5050)). *Int. J. Nanomedicine* **14**, 7215–7216 (2019).
84. Bellas, E., Seiberg, M., Garlick, J. & Kaplan, D. L. In vitro 3D Full-Thickness Skin-Equivalent Tissue Model Using Silk and Collagen Biomaterials. *Macromol. Biosci.* **12**, 1627–1636 (2012).
85. Das, D. & Noh, I. *Biomimetic Medical Materials: From Nanotechnology to 3D Bioprinting*. *Advances in Experimental Medicine and Biology* (2018).
86. Chaudhari, A. A. *et al.* Future prospects for scaffolding methods and biomaterials in skin tissue engineering: A review. *Int. J. Mol. Sci.* **17**, (2016).
87. Vig, K. *et al.* Advances in skin regeneration using tissue engineering. *Int. J.*

Mol. Sci. **18**, (2017).

88. Larouche, D. *et al.* Improved Methods to Produce Tissue-Engineered Skin Substitutes Suitable for the Permanent Closure of Full-Thickness Skin Injuries. *Biores. Open Access* **5**, 320–329 (2016).
89. Imparato, G., Urciuolo, F., Casale, C. & Netti, P. A. The role of microscaffold properties in controlling the collagen assembly in 3D dermis equivalent using modular tissue engineering. *Biomaterials* **34**, 7851–7861 (2013).
90. Urciuolo, F., Garziano, A., Imparato, G., Panzetta, V., Fusco, S., Casale, C., Netti, P. A. Biophysical properties of dermal building-blocks affect extra cellular matrix assembly in 3D endogenous macrotissue. *Biofabrication* **8**, (2016).
91. Chouhan, D., Dey, N., Bhardwaj, N. & Mandal, B. B. Emerging and innovative approaches for wound healing and skin regeneration: Current status and advances. *Biomaterials* **216**, 119267 (2019).
92. Vaughan, M. B. *et al.* A reproducible laser-wounded skin equivalent model to study the effects of aging in vitro. *Rejuvenation Res.* **7**, 99–110 (2004).
93. Oberringer, M., Meins, C., Bubel, M. & Pohlemann, T. A new in vitro wound model based on the co-culture of human dermal microvascular endothelial cells and human dermal fibroblasts. *Biol. Cell* **99**, 197–207 (2007).
94. Iljas, J. D. *et al.* A human skin equivalent burn model to study the effect of a nanocrystalline silver dressing on wound healing. *Burns* **47**, 417–429 (2021).
95. Falanga, V. *et al.* Wounding of bioengineered skin: Cellular and molecular aspects after injury. *J. Invest. Dermatol.* **119**, 653–660 (2002).
96. Geer, D. J., Swartz, D. D. & Andreadis, S. T. Fibrin promotes migration in a three-dimensional in vitro model of wound regeneration. *Tissue Eng.* **8**, 787–798 (2002).
97. Xie, Y. *et al.* Development of a three-dimensional human skin equivalent wound model for investigating novel wound healing therapies. *Tissue Eng.*

- *Part C Methods* **16**, 1111–1123 (2010).

98. Biglari, S. *et al.* Simulating Inflammation in a Wound Microenvironment Using a Dermal Wound-on-a-Chip Model. *Adv. Healthc. Mater.* **8**, 1801307 (2019).
99. Tefft, J. B., Chen, C. S. & Eyckmans, J. Reconstituting the dynamics of endothelial cells and fibroblasts in wound closure Reconstituting the dynamics of endothelial cells and fibroblasts in wound closure. **016102**, (2021).
100. Shabestani Monfared, G., Ertl, P. & Rothbauer, M. An on-chip wound healing assay fabricated by xurography for evaluation of dermal fibroblast cell migration and wound closure. *Sci. Reports 2020 101* **10**, 1–14 (2020).
101. Sakar, M. S. *et al.* Cellular forces and matrix assembly coordinate fibrous tissue repair. *Nat. Commun.* **7**, (2016).
102. Wufuer, M. *et al.* Skin-on-a-chip model simulating inflammation, edema and drug-based treatment. *Sci. Rep.* **6**, 1–12 (2016).
103. Lombardi, B., Casale, C., Imparato, G., Urciuolo, F. & Netti, P. A. Spatiotemporal Evolution of the Wound Repairing Process in a 3D Human Dermis Equivalent. *Adv. Healthc. Mater.* **6**, 1–11 (2017).
104. Casale, C. *et al.* Engineering a human skin equivalent to study dermis remodelling and epidermis senescence in vitro after UVA exposure. *J. Tissue Eng. Regen. Med.* **12**, 1658–1669 (2018).
105. Selman, M. & Pardo, A. Fibroageing: An ageing pathological feature driven by dysregulated extracellular matrix-cell mechanobiology. *Ageing Res. Rev.* **70**, (2021).
106. Imparato, G., Urciuolo, F., Casale, C. & Netti, P. A. The role of microscaffold properties in controlling the collagen assembly in 3D dermis equivalent using modular tissue engineering. *Biomaterials* **34**, 7851–7861 (2013).
107. Gioiella, F., Urciuolo, F., Imparato, G., Brancato, V. & Netti, P. A. An Engineered Breast Cancer Model on a Chip to Replicate ECM-Activation In Vitro during Tumor Progression. *Adv. Healthc. Mater.* **5**, 3074–3084 (2016).

108. Yousuf, Y., Amini-Nik, S. & Jeschke, M. G. *Overall perspective on the clinical importance of skin models*. *Skin Tissue Models* (Elsevier Inc., 2018). doi:10.1016/B978-0-12-810545-0.00002-4.

109. Pastar, I. *et al. Preclinical models for wound-healing studies*. *Skin Tissue Models* (Elsevier Inc., 2017). doi:10.1016/B978-0-12-810545-0.00010-3.

110. Suttho, D. *et al.* 3D modeling of keloid scars in vitro by cell and tissue engineering. *Arch. Dermatol. Res.* **309**, 55–62 (2017).

111. Fan, C. *et al.* Application of "macromolecular crowding" in vitro to investigate the naphthoquinones shikonin, naphthazarin and related analogues for the treatment of dermal scars. *Chem. Biol. Interact.* **310**, 108747 (2019).

112. Fan, C. *et al.* In vitro model of human cutaneous hypertrophic scarring using macromolecular crowding. *J. Vis. Exp.* **2020**, 1–8 (2020).

113. Xu, Q., Norman, J. T., Shrivastav, S., Lucio-Cazana, J. & Kopp, J. B. In vitro models of TGF-β-induced fibrosis suitable for high-throughput screening of antifibrotic agents. *Am. J. Physiol. - Ren. Physiol.* **293**, (2007).

114. Alsharabasy, A. M. & Pandit, A. Protocol for in vitro skin fibrosis model to screen the biological effects of antifibrotic compounds. *STAR Protoc.* **2**, 100387 (2021).

115. Todd, C. *et al.* Co-culture of human melanocytes and keratinocytes in a skin equivalent model: effect of ultraviolet radiation. *Arch. Dermatol. Res.* **285**, 455–459 (1993).

116. Li, L., Fukunaga-Kalabis, M. & Herlyn, M. The Three-Dimensional Human Skin Reconstruct Model: a Tool to Study Normal Skin and Melanoma Progression. *J. Vis. Exp.* (2011) doi:10.3791/2937.

117. Kosten, I. J., Spiekstra, S. W., de Gruijl, T. D. & Gibbs, S. MUTZ-3 derived Langerhans cells in human skin equivalents show differential migration and phenotypic plasticity after allergen or irritant exposure. *Toxicol. Appl. Pharmacol.* **287**, 35–42 (2015).

118. Ouwehand, K., Scheper, R. J., De Gruijl, T. D. & Gibbs, S. Epidermis-to-dermis migration of immature Langerhans cells upon topical irritant

exposure is dependent on CCL2 and CCL5. *Eur. J. Immunol.* **40**, 2026–2034 (2010).

119. Chau, D. Y. S., Johnson, C., Macneil, S., Haycock, J. W. & Ghaemmaghami, A. M. The development of a 3D immunocompetent model of human skin. *Biofabrication* **5**, 035011 (2013).
120. Kühbacher, A. *et al.* Central role for dermal fibroblasts in skin model protection against candida albicans. *J. Infect. Dis.* **215**, 1742–1752 (2017).
121. Lorthois, I., Simard, M., Morin, S. & Pouliot, R. Infiltration of T cells into a three-dimensional psoriatic skin model mimics pathological key features. *Int. J. Mol. Sci.* **20**, (2019).
122. Shin, J. U. *et al.* Recapitulating T cell infiltration in 3D psoriatic skin models for patient-specific drug testing. *Sci. Reports 2020 101* **10**, 1–12 (2020).
123. Linde, N., Gutschalk, C. M., Hoffmann, C., Yilmaz, D. & Mueller, M. M. Integrating macrophages into organotypic co-cultures: A 3D in vitro model to study tumor-associated macrophages. *PLoS One* **7**, (2012).
124. Bechetoille, N. *et al.* A new organotypic model containing dermal-type macrophages. *Exp. Dermatol.* **20**, 1035–1037 (2011).
125. Claire E. Witherel, Kimheak Sao, Becky K. Brisson, Biao Han, Susan W. Volk, Ryan J. Petrie, Lin Han, and K. L. S. Regulation of extracellular matrix assembly and structure by hybrid M1/M2 macrophages. *Biomaterials* **269**, 1–23 (2021).
126. Sapudom, J. *et al.* 3D in vitro M2 macrophage model to mimic modulation of tissue repair. *npj Regen. Med.* **6**, 1–13 (2021).
127. Wang, X. F. *et al.* Potential effect of non-thermal plasma for the inhibition of scar formation: a preliminary report. *Sci. Rep.* **10**, 1–10 (2020).
128. Kubinova, S. *et al.* Non-thermal air plasma promotes the healing of acute skin wounds in rats. *Sci. Rep.* **7**, 1–11 (2017).
129. Deal, H. E., Brown, A. C. & Daniele, M. A. Microphysiological systems for the modeling of wound healing and evaluation of pro-healing therapies. *J. Mater. Chem. B* **8**, 7062–7075 (2020).
130. Zhang, M., Li, H., Ma, H. & Qin, J. A simple microfluidic strategy for cell

migration assay in an in vitro wound-healing model. *Wound Repair Regen.* **21**, 897–903 (2013).

131. Poujade, M. *et al.* Collective migration of an epithelial monolayer in response to a model wound. *Proc. Natl. Acad. Sci. U. S. A.* **104**, 15988–15993 (2007).
132. Gao, A. X., Tian, Y. L., Shi, Z. Z. & Yu, L. A cost-effective microdevice bridges microfluidic and conventional in vitro scratch / wound-healing assay for personalized therapy validation. *Biochip J.* **10**, 56–64 (2016).
133. Go, H., Tian, T. & Rhee, S. W. Fabrication of Microfluidic Chip for Investigation of Wound Healing Processes. *BioChip J. 2018 122* **12**, 146–153 (2018).
134. Nie, F. Q. *et al.* On-chip cell migration assay using microfluidic channels. *Biomaterials* **28**, 4017–4022 (2007).
135. Lin, J. Y., Lo, K. Y. & Sun, Y. S. A microfluidics-based wound-healing assay for studying the effects of shear stresses, wound widths, and chemicals on the wound-healing process. *Sci. Rep.* **9**, 1–11 (2019).
136. Conant, C. G., Nevill, J. T., Schwartz, M. & Ionescu-Zanetti, C. Wound Healing Assays in Well Plate—Coupled Microfluidic Devices with Controlled Parallel Flow. *J. Lab. Autom.* **15**, 52–57 (2010).
137. Wei, Y. *et al.* A Tubing-Free Microfluidic Wound Healing Assay Enabling the Quantification of Vascular Smooth Muscle Cell Migration. *Sci. Rep.* **5**, 1–11 (2015).
138. Conde, A. J., Salvatierra, E., Podhajcer, O., Fraigi, L. & Madrid, R. E. Wound healing assay in a low-cost microfluidic platform. *J. Phys. Conf. Ser.* **477**, (2013).
139. Lee, I., Kim, D., Park, G. L., Jeon, T. J. & Kim, S. M. Investigation of wound healing process guided by nano-scale topographic patterns integrated within a microfluidic system. *PLoS One* **13**, 1–16 (2018).
140. Murrell, M., Kamm, R. & Matsudaira, P. Tension, free space, and cell damage in a microfluidic wound healing assay. *PLoS One* **6**, (2011).
141. Jeong, G. S. *et al.* Microfluidic assay of endothelial cell migration in 3D

interpenetrating polymer semi-network HA-Collagen hydrogel. *Biomed. Microdevices* **13**, 717–723 (2011).

142. Shih, H. C. *et al.* Microfluidic Collective Cell Migration Assay for Study of Endothelial Cell Proliferation and Migration under Combinations of Oxygen Gradients, Tensions, and Drug Treatments. *Sci. Rep.* **9**, 1–10 (2019).
143. Sticker, D., Lechner, S., Jungreuthmayer, C., Zanghellini, J. & Ertl, P. Microfluidic Migration and Wound Healing Assay Based on Mechanically Induced Injuries of Defined and Highly Reproducible Areas. *Anal. Chem.* **89**, 2326–2333 (2017).
144. Shaner, S. *et al.* Bioelectronic microfluidic wound healing: a platform for investigating direct current stimulation of injured cell collectives. *Lab Chip* **23**, 1531–1546 (2023).
145. Biglari, S. *et al.* Simulating Inflammation in a Wound Microenvironment Using a Dermal Wound-on-a-Chip Model. **1801307**, 1–12 (2019).
146. Gonzalez, A. C. D. O., Andrade, Z. D. A., Costa, T. F. & Medrado, A. R. A. P. Wound healing - A literature review. *An. Bras. Dermatol.* **91**, 614–620 (2016).
147. Mercandetti, M. & Cohen, A. J. Wound Healing and Repair. *Medscape* https://emedicine.medscape.com/article/1298129-overview?icd=login_success_email_match_norm#a5 (2021).
148. Urciuolo, F., Casale, C., Imparato, G. & Netti, P. A. Bioengineered skin substitutes: The role of extracellular matrix and vascularization in the healing of deep wounds. *J. Clin. Med.* **8**, (2019).
149. Vedula, S. R. K., Ravasio, A., Lim, C. T. & Ladou, B. Collective cell migration: A mechanistic perspective. *Physiology* **28**, 370–379 (2013).
150. Jain, S. *et al.* The role of single-cell mechanical behaviour and polarity in driving collective cell migration. *Nat. Phys.* **16**, 802–809 (2020).
151. Darby, I. A., Laverdet, B., Bonté, F. & Desmoulière, A. Fibroblasts and myofibroblasts in wound healing. *Clin. Cosmet. Investig. Dermatol.* **7**, 301–311 (2014).
152. Tseng, Q. *et al.* Spatial organization of the extracellular matrix regulates

cell-cell junction positioning. *Proc. Natl. Acad. Sci. U. S. A.* **109**, 1506–1511 (2012).

153. Staneva, R. *et al.* Cancer cells in the tumor core exhibit spatially coordinated migration patterns. *J. Cell Sci.* **132**, 1–9 (2019).

154. Wu, M. & Ben Amar, M. Growth and remodelling for profound circular wounds in skin. *Biomech. Model. Mechanobiol.* **14**, 357–370 (2015).

155. Bowden, L. G., Byrne, H. M., Maini, P. K. & Moulton, D. E. A morphoelastic model for dermal wound closure. *Biomech. Model. Mechanobiol.* **15**, 663–681 (2016).

156. M, U. Speed of fibroblast in healing wound. https://bionumbers.hms.harvard.edu/bionumber.aspx?id=106806 doi:106806.

157. Hartman, C. D., Isenberg, B. C., Chua, S. G. & Wong, J. Y. Extracellular matrix type modulates cell migration on mechanical gradients. *Exp. Cell Res.* **359**, 361–366 (2017).

158. Walker, J. L., Bleaken, B. M., Romisher, A. R., Alnwibit, A. A. & Menko, A. S. In wound repair vimentin mediates the transition of mesenchymal leader cells to a myofibroblast phenotype. *Mol. Biol. Cell* **29**, 1555–1570 (2018).

159. Van Zuijlen, P. P. M. *et al.* Collagen morphology in human skin and scar tissue: No adaptations in response to mechanical loading at joints. *Burns* **29**, 423–431 (2003).

160. CALIN, M. A., COMAN, T. & CALIN, M. R. THE EFFECT OF LOW LEVEL LASER THERAPY ON SURGICAL WOUND HEALING. *Rom. Reports Phys.* **62**, 617–627 (2010).

161. Wojciak-Stothard, B., Denver, M., Mishra, M. & Brown, R. A. Adhesion, orientation, and movement of cells cultured on ultrathin fibronectin fibers. *Vitr. Cell. Dev. Biol. - Anim.* **33**, 110–117 (1997).

162. Rodrigues, M., Kosaric, N., Bonham, C. A. & Gurtner, G. C. Wound healing: A cellular perspective. *Physiol. Rev.* **99**, 665–706 (2019).

163. Alhajj, M., Bansal, P. & Goyal, A. Physiology, Granulation Tissue.

StatPearls (2020).

164. McDougall, S., Dallon, J., Sherratt, J. & Maini, P. Fibroblast migration and collagen deposition during dermal wound healing: Mathematical modelling and clinical implications. *Philos. Trans. R. Soc. A Math. Phys. Eng. Sci.* **364**, 1385–1405 (2006).
165. Mirza, R., DiPietro, L. A. & Koh, T. J. Selective and specific macrophage ablation is detrimental to wound healing in mice. *Am. J. Pathol.* **175**, 2454–2462 (2009).
166. Desmouliere, A., Redard, M., Darby, I. & Gabbiani, G. Apoptosis mediates the decrease in cellularity during the transition between granulation tissue and scar. *Am. J. Pathol.* **146**, 56–66 (1995).
167. Midwood, K. S. & Orend, G. The role of tenascin-C in tissue injury and tumorigenesis. *Journal of Cell Communication and Signaling* vol. 3 287–310 at https://doi.org/10.1007/s12079-009-0075-1 (2009).
168. Cho, C. Y. & Lo, J. S. DRESSING THE PART. *Dermatol. Clin.* **16**, 25–47 (1998).
169. Marshall, C. D. *et al.* Cutaneous Scarring: Basic Science, Current Treatments, and Future Directions. *Adv. Wound Care* **7**, 29–45 (2018).
170. Masanovic, M. G. & Téot, L. Textbook on Scar Management. *Textb. Scar Manag.* 117–122 (2020) doi:10.1007/978-3-030-44766-3.
171. Parry, I., Walker, K., Niszczak, J., Palmieri, T. & Greenhalgh, D. Methods and tools used for the measurement of burn scar contracture. *J. Burn Care Res.* **31**, 888–903 (2010).
172. Hardy, M. A. The biology of scar formation. *Phys. Ther.* **69**, 1014–1024 (1989).
173. Wynn, T. A. Cellular and molecular mechanisms of fibrosis. *J. Pathol.* **214**, 199–210 (2008).
174. Plantier, L. *et al.* Physiology of the lung in idiopathic pulmonary fibrosis. *Eur. Respir. Rev.* **27**, 1–14 (2018).
175. Friedman, S. L. Mechanisms of disease: Mechanisms of hepatic fibrosis and therapeutic implications. *Nat. Clin. Pract. Gastroenterol. Hepatol.* **1**, 98–

105 (2004).

176. Dhar, D., Baglieri, J., Kisseleva, T. & Brenner, D. A. Mechanisms of liver fibrosis and its role in liver cancer. *Exp. Biol. Med.* **245**, 96–108 (2020).

177. Rybinski, B., Franco-Barraza, J. & Cukierman, E. The wound healing, chronic fibrosis, and cancer progression triad. *Physiol. Genomics* **46**, 223–244 (2014).

178. Simon, F. *et al.* Enhanced secretion of TIMP-1 by human hypertrophic scar keratinocytes could contribute to fibrosis. *Burns* **38**, 421–427 (2012).

179. Daniels, J. T. *et al.* Matrix metalloproteinase inhibition modulates fibroblast-mediated matrix contraction and collagen production in vitro. *Investig. Ophthalmol. Vis. Sci.* **44**, 1104–1110 (2003).

180. Montesano, R. & Orci, L. Transforming growth factor beta stimulates collagen-matrix contraction by fibroblasts: implications for wound healing. *Proc. Natl. Acad. Sci. U. S. A.* **85**, 4894–4897 (1988).

181. Bell, E., Ivarsson, B. & Merrill, C. Production of a tissue-like structure by contraction of collagen lattices by human fibroblasts of different proliferative potential in vitro. *Proc. Natl. Acad. Sci. U. S. A.* **76**, 1274–1278 (1979).

182. Sharma, J. R., Lebeko, M., Kidzeru, E. B., Khumalo, N. P. & Bayat, A. In Vitro and Ex Vivo Models for Functional Testing of Therapeutic Anti-scarring Drug Targets in Keloids. *Adv. Wound Care* **8**, 655–670 (2019).

183. Ud-Din, S. *et al.* A Double-Blind, Randomized Trial Shows the Role of Zonal Priming and Direct Topical Application of Epigallocatechin-3-Gallate in the Modulation of Cutaneous Scarring in Human Skin. *J. Invest. Dermatol.* **139**, 1680-1690.e16 (2019).

184. Tan, K. T., McGrouther, D. A., Day, A. J., Milner, C. M. & Bayat, A. Characterization of hyaluronan and TSG-6 in skin scarring: Differential distribution in keloid scars, normal scars and unscarred skin. *J. Eur. Acad. Dermatology Venereol.* **25**, 317–327 (2011).

185. Syed, F. *et al.* Fibroblasts from the growing margin of keloid scars produce higher levels of collagen i and III compared with intralesional and

extralesional sites: Clinical implications for lesional site-directed therapy. *Br. J. Dermatol.* **164**, 83–96 (2011).

186. Kieran, I. *et al.* Interleukin-10 reduces scar formation in both animal and human cutaneous wounds: Results of two preclinical and phase II randomized control studies. *Wound Repair Regen.* **21**, 428–436 (2013).

187. Basson, R., Baguneid, M., Foden, P., Al Kredly, R. & Bayat, A. Functional Testing of a Skin Topical Formulation in Vivo: Objective and Quantitative Evaluation in Human Skin Scarring Using a Double-Blind Volunteer Study with Sequential Punch Biopsies. *Adv. Wound Care* **8**, 208–219 (2019).

188. Ud-Din, S. *et al.* Objective assessment of dermal fibrosis in cutaneous scarring, using optical coherence tomography, high-frequency ultrasound and immunohistomorphometry of human skin. *Br. J. Dermatol.* **181**, 722–732 (2019).

189. Mendoza-Garcia, J., Sebastian, A., Alonso-Rasgado, T. & Bayat, A. Ex vivo evaluation of the effect of photodynamic therapy on skin scars and striae distensae. *Photodermatol. Photoimmunol. Photomed.* **31**, 239–251 (2015).

190. Bagabir, R., Syed, F., Paus, R. & Bayat, A. Long-term organ culture of keloid disease tissue. *Exp. Dermatol.* **21**, 376–381 (2012).

191. Li, Y. *et al.* Adipose tissue-derived stem cells suppress hypertrophic scar fibrosis via the p38/MAPK signaling pathway. *Stem Cell Res. Ther.* **7**, 1–16 (2016).

192. Syed, F., Bagabir, R. A., Paus, R. & Bayat, A. Ex vivo evaluation of antifibrotic compounds in skin scarring: EGCG and silencing of PAI-1 independently inhibit growth and induce keloid shrinkage. *Lab. Investig.* **93**, 946–960 (2013).

193. Abaci, H. E. *et al.* Tissue engineering of human hair follicles using a biomimetic developmental approach. *Nat. Commun.* **9**, 1–11 (2018).

194. Hesketh, M., Sahin, K. B., West, Z. E. & Murray, R. Z. Macrophage phenotypes regulate scar formation and chronic wound healing. *Int. J. Mol. Sci.* **18**, 1–10 (2017).

195. Chen, S. *et al.* Macrophages in immunoregulation and therapeutics. *Signal*

Transduct. Target. Ther. **8**, (2023).

196. Lis-López, L., Bauset, C., Seco-Cervera, M. & Cosín-Roger, J. Is the macrophage phenotype determinant for fibrosis development? *Biomedicines* **9**, 1–30 (2021).
197. Frangogiannis, N. G. Transforming growth factor–ß in tissue fibrosis. *J. Exp. Med.* **217**, 1–16 (2020).
198. Chanput, W., Mes, J. J. & Wichers, H. J. THP-1 cell line: An in vitro cell model for immune modulation approach. *Int. Immunopharmacol.* **23**, 37–45 (2014).
199. Genin, M., Clement, F., Fattaccioli, A., Raes, M. & Michiels, C. M1 and M2 macrophages derived from THP-1 cells differentially modulate the response of cancer cells to etoposide. *BMC Cancer* **15**, 1–14 (2015).
200. Madhvi, A., Mishra, H., Leisching, G. R., Mahlobo, P. Z. & Baker, B. Comparison of human monocyte derived macrophages and THP1-like macrophages as in vitro models for M. tuberculosis infection. *Comp. Immunol. Microbiol. Infect. Dis.* **67**, 101355 (2019).
201. Bosshart, H. & Heinzelmann, M. THP-1 cells as a model for human monocytes. *Ann. Transl. Med.* **4**, 4–7 (2016).
202. Yuming Liu, Adib Keikhosravi, Guneet S. Mehta, Cole R. Drifka, and K. W. E. Methods for Quantifying Fibrillar Collagen Alignment Yuming. *Methods Mol Biol.* **1627**, 429–451 (2017).
203. Bredfeldt, J. S. *et al.* Computational segmentation of collagen fibers from second-harmonic generation images of breast cancer. *J. Biomed. Opt.* **19**, 016007 (2014).
204. Clemons, T. D. *et al.* Coherency image analysis to quantify collagen architecture: Implications in scar assessment. *RSC Adv.* **8**, 9661–9669 (2018).
205. Nesbitt, S., Scott, W., Macione, J. & Kotha, S. Collagen fibrils in skin orient in the direction of applied uniaxial load in proportion to stress while exhibiting differential strains around hair follicles. *Materials (Basel).* **8**, 1841–1857 (2015).

206. Sendín-Martín, M. *et al.* Quantitative collagen analysis using second harmonic generation images for the detection of basal cell carcinoma with ex vivo multiphoton microscopy. *Exp. Dermatol.* **32**, 392–402 (2023).
207. Jiang, D. *et al.* Injury triggers fascia fibroblast collective cell migration to drive scar formation through N-cadherin. *Nat. Commun.* **11**, (2020).
208. Chen, K. *et al.* Pullulan-Collagen hydrogel wound dressing promotes dermal remodelling and wound healing compared to commercially available collagen dressings. *Wound Repair Regen.* **30**, 397–408 (2022).
209. Lin, D. C., Shreiber, D. I., Dimitriadis, E. K. & Horkay, F. Spherical indentation of soft matter beyond the Hertzian regime: Numerical and experimental validation of hyperelastic models. *Biomech. Model. Mechanobiol.* **8**, 345–358 (2009).
210. Cha, B. H. *et al.* Integrin-Mediated Interactions Control Macrophage Polarization in 3D Hydrogels. *Adv. Healthc. Mater.* **6**, 1–12 (2017).
211. Pfisterer, K., Shaw, L. E., Symmank, D. & Weninger, W. The Extracellular Matrix in Skin Inflammation and Infection. *Frontiers in Cell and Developmental Biology* vol. 9 at https://doi.org/10.3389/fcell.2021.682414 (2021).
212. Kasprzycka, M., Hammarström, C. & Haraldsen, G. Tenascins in fibrotic disorders—from bench to bedside. *Cell Adhes. Migr.* **9**, 83–89 (2015).
213. Verhaegen, P. D. *et al.* Adaptation of the dermal collagen structure of human skin and scar tissue in response to stretch: An experimental study. *Wound Repair Regen.* **20**, 658–666 (2012).
214. Hassanshahi, A. *et al.* Macrophage-Mediated Inflammation in Skin Wound Healing. *Cells* **11**, (2022).
215. Bhattacharyya, S., Midwood, K. S. & Varga, J. Tenascin-C in fibrosis in multiple organs: Translational implications. *Semin. Cell Dev. Biol.* **128**, 130–136 (2022).
216. Vasse, G. F. *et al.* Macrophage–stroma interactions in fibrosis: biochemical, biophysical, and cellular perspectives. *J. Pathol.* **254**, 344–357 (2021).
217. Moretti, L., Stalfort, J., Barker, T. H. & Abebayehu, D. The interplay of

fibroblasts, the extracellular matrix, and inflammation in scar formation. *J. Biol. Chem.* **298**, 101530 (2022).

218. Shi, J. H. *et al.* Protection against TGF-β1-induced fibrosis effects of IL-10 on dermal fibroblasts and its potential therapeutics for the reduction of skin scarring. *Arch. Dermatol. Res.* **305**, 341–352 (2013).

219. Sapudom, J. *et al.* Collagen Fibril Orientation Instructs Fibroblast Differentiation Via Cell Contractility. *Adv. Sci.* **10**, 1–14 (2023).